January 2010

The Role of Aerobic Glycolysis in the Resting Human Brain

Sanjeev Vaishnavi
Washington University in St. Louis

WASHINGTON UNIVERSITY

Division of Biology and Biomedical Sciences

Neurosciences

Dissertation Examination Committee:
Marcus E. Raichle, Chair
Mark A. Mintun
Joel Perlmutter
Larry Snyder
W. Thomas Thach
David Van Essen

THE ROLE OF AEROBIC GLYCOLYSIS IN THE RESTING HUMAN BRAIN

by

Sanjeev Neil Vaishnavi

A dissertation presented to the
Graduate School of Arts and Sciences
of Washington University in
partial fulfillment of the
requirements for the degree
of Doctor of Philosophy

May 2010

Saint Louis, Missouri

ABSTRACT OF THE DISSERTATION

The Role of Aerobic Glycolysis in the Resting Human Brain

by

Sanjeev Neil Vaishnavi

Doctor of Philosophy in Biology and Biomedical Sciences
(Neurosciences)

Washington University in St. Louis, 2010

Professor Marcus E. Raichle, Chairperson

The human brain accounts for 2% of total body weight, though it consumes 20% of the body's energy supply. Most of this energy is provided by the complete oxidation of glucose to carbon dioxide and water, though some fraction of glucose undergoes aerobic glycolysis without concomitant oxidative phosphorylation. Elevation in neuronal activity increases aerobic glycolysis due to the disproportionate increase in blood flow and glucose utilization greater than oxygen consumption. Since aerobic glycolysis produces significantly less energy than complete oxidation of glucose, its role in cellular activities has been overlooked, though its presence in the resting brain has been known for several decades. In this thesis, we investigate three aspects of resting aerobic glycolysis using positron emission tomography. First, we characterize the regional distribution of aerobic glycolysis in the awake, eyes closed human brain. We show that brain regions with high levels of functional activity in the resting state, including the default network and prefrontal cortex, have elevated aerobic glycolysis. In addition, we show that aerobic glycolysis is modulated by prior task performance. Performance of a complex visuomotor rotation learning task increases aerobic glycolysis in premotor

cortex for several hours following task completion. Further, we show that regional brain

metabolism is correlated to neurotransmitter receptor density. Aerobic glycolysis is

highest in regions with a balanced density of excitatory and inhibitory receptors. Taken

together, these results demonstrate the functional significance of resting aerobic

glycolysis and its modulation by transient functional activity. These data provide

supporting evidence for the synaptic homeostasis hypothesis, indicating elevation in brain

metabolism, specifically aerobic glycolysis, during wakefulness associated with

alterations in synaptic strength and receptor density.

Acknowledgements

There are numerous people who contributed to the success of this work. First, I would like to thank Marc Raichle for his outstanding mentorship that has allowed me to develop as a scientist and to think independently. I have appreciated the significant creative freedom to take my project in unexpected directions ranging from normal human physiology to sleep, depression, blindness, traumatic brain injury, and Alzheimer's disease. Second, I would like to thank Andrei Vlassenko for his guidance in positron emission tomography research and the countless hours of 'discussions' that taught me the tenets of good experimental design and the accurate and deliberate interpretation of metabolic data. There are numerous other mentors and collaborators that I have to thank for their help over the past several years. I would especially like to thank Yvette Sheline, Mark Mintun, Linda Larson-Prior, Avi Snyder, Lice Ghilardi, and Giulio Tononi for their help and guidance.

Finally, I thank my parents Vijay and Kirti Vaishnavi, my brother Sandeep, Deepti, and Shivum Vaishnavi for their unending support and guidance.

Table of Contents

Contents

List of Figures

List of Tables

Chapter 1: Introduction

> *"As long as our brain is a mystery,*
> *the universe, the reflection of the structure*
> *of the brain, will also be a mystery."*
> -Santiago Ramon y Cajal
> <u>Charlas de Cafe</u>

Much of what we know about neuronal activity is obtained indirectly by the effect of brain cells on cerebral energy utilization. Increased neuronal activity results in an elevation in cerebral blood flow (CBF), glucose (CMRGlu), and oxygen ($CMRO_2$) utilization to supply the cells with metabolites for energy consumption as well as to remove waste products. The metabolic response to cellular activity, though, is not homogenous. Transient increases in cerebral blood flow and glucose utilization are disproportionate to the corresponding changes in oxygen consumption. The disproportionate increase in cerebral blood flow results in an excess of oxyhemoglobin in regions of neuronal activity, a physiological marker that can be detected using magnetic resonance imaging (MRI). In addition to this discrepancy, cerebral glucose utilization also increases disproportionately to oxygen consumption. This finding is counterintuitive as the primary utility of glucose is to provide energy to cells via its complete oxidation to carbon dioxide and water. But for several decades, researchers have found that some fraction of glucose does not undergo complete oxidative metabolism, resulting in the presence of aerobic glycolysis in the brain (Raichle, Posner et al. 1970; Blomqvist, Seitz et al. 1994; Madsen, Hasselbalch et al. 1995). Aerobic glycolysis is defined as glycolysis occurring in the presence of oxygen but in excess of that required for oxidative

phosphorylation. The primary goal of this research is to begin to understand the possible roles for aerobic glycolysis in normal neuronal function.

The remainder of this chapter will provide relevant background information to understand the tenets of this thesis. (I) First, we will briefly overview the cellular physiology of aerobic glycolysis. (II) Next, we will discuss how brain metabolism changes during and following learning. (III) Then we will present an overview of the synaptic homeostasis hypothesis as one possible explanation for learning related changes in brain metabolism. (IV) Finally, this chapter concludes with a brief preview of the set of experiments included in this thesis.

Cellular physiology of aerobic glycolysis

Functional neuroimaging techniques detect local changes in energy utilization and blood flow. But what cellular processes are responsible for these alterations? Early experimental work by Schwartz and colleagues provided important technical insights (Schwartz, Smith et al. 1979). In their experiments they measured regional glucose metabolism in rats using 2-deoxy-glucose (2DG) autoradiography (Sokoloff 1977). This technique detects the trapped 2DG in cells following the initial phosphorylation of glucose as the first step of glycolysis (a similar approach as that taken with positron emission tomography as discussed later). Rats were exposed to an osmotic load to stimulate cell bodies in the paraventricular nucleus of the hypothalamus. These neurons were stimulated by the osmotic load and in turn transmitted the signal to their axon terminals in the pituitary gland. Since the cell body and axon terminals are separated

spatially by a large distance, the site of energy consumption could be directly assessed. They found that glucose metabolism, as measured by 2DG uptake, was significantly increased in the axon terminals located near the posterior pituitary, and not measurably increased in the cell body itself. These data indicate that functional imaging techniques primarily detect the input and output of neurons, namely activity at the neuronal synapse. This is also the case for functional MRI (Logothetis, Pauls et al. 2001; Logothetis 2003). Estimates of the cost of brain activity indicate that 60-80% of the energetic cost is associated with synaptic activity and fluctuations in membrane potential (Attwell and Laughlin 2001; Attwell and Iadecola 2002).   Though measurement of glucose metabolism does not allow for the detection of particular subcellular processes, these techniques do allow for the in vivo assessment of synaptic activity.

The initial work with 2DG imaging has subsequently been expanded from animal models to humans using positron emission tomography (PET). Using PET, blood flow, glucose and oxygen consumption can be detected noninvasively, providing an indirect measure of neuronal activity and allowing for experimental manipulation of behavioral state. While glucose metabolism is measured with radiolabeled fluoro-deoxyglucose, blood flow is measured with labeled H_2O and oxygen metabolism with labeled O_2 (also requiring measurement of cerebral blood volume with labeled carbon monoxide to account for any oxygen bound to hemoglobin and not removed by brain cells). Collection of metabolic data from various modalities provides additional cellular specificity to the observed neuronal response, allowing for the quantification of aerobic glycolysis.

Initial positron emission tomography (PET) studies in humans were used to identify functionally specialized cortical regions. For example, in a classic early experimental paradigm, human subjects were asked to view a flickering black and white checkerboard stimulus while being scanned via PET. As a result blood flow and glucose utilization in visual cortex significantly increased compared to a baseline state (visual fixation or rest). This approach revealed an apparent coupling between blood flow and glucose utilization in regions of increased neuronal activity. But what happens to oxygen consumption in these locations? Surprisingly, oxygen consumption was only slightly increased compared to the baseline state (~5%), significantly less than glucose consumption or blood flow measures (~50%) (Fox, Raichle et al. 1988; Blomqvist, Seitz et al. 1994). This finding stimulated research into the possible functional role of aerobic glycolysis.

Traditionally, it has been assumed that the energy needed for brain function is entirely provided by the complete oxidation of glucose to carbon dioxide to water. Both glycolysis and oxidative phosphorylation produce energy in the form of ATP, but differing amounts. Glycolysis produces 2 net ATP while oxidative phosphorylation produces ~32 net ATP. In this context, oxidative phosphorylation is much more efficient in producing energy. However, cells may utilize glycolysis preferentially in several circumstances, especially during rapid increases in neuronal activity.

First, glycolysis may be advantageous as it can be performed extremely rapidly and does not require the presence of oxygen. Since glycolysis can produce pyruvate much faster than it can be oxidized, ATP can be rapidly produced and the resultant pyruvate can be converted to lactate and removed as a waste product with cerebral blood

flow (Cerdan, Rodrigues et al. 2006). Also aerobic glycolysis occurs within the cytosol and does not require mitochondrial function, providing rapid energy to subcellular locations such as the postsynaptic density (Wu, Aoki et al. 1997).

In addition, glycolytic intermediates provide carbon fragments necessary for production of DNA and RNA via the pentose phosphate shunt (Gaitonde, Jones et al. 1987). Some fraction, estimated to be 5-10% of glucose consumed, may be used for anabolism and not directly for energy production. In this context, aerobic glycolysis may provide precursors for cellular and synaptic remodeling. Although the contribution of glycolysis to energy metabolism may be relatively small compared to oxidative phosphorylation, its contribution may have significant strategic importance.

The cellular role of glycolysis has been most clearly elucidated in investigation of the astrocyte (Pellerin and Magistretti 1994; Pellerin and Magistretti 1996; Kasischke, Vishwasrao et al. 2004). Glycolysis is increased in astrocytes due to the uptake of glutamate from the synaptic cleft along with Na^+ in a co-transport mechanism. The intracellular glutamate is converted to glutamine and the increased intracellular Na^+ is removed by increased activity of Na^+/K^+ ATPase. Both these processes require hydrolysis of ATP, which appears to occur by glycolysis alone in the astrocyte (Voutsinos-Porche, Bonvento et al. 2003; Magistretti and Chatton 2005).

Aerobic glycolysis also appears to partially regulate the blood-flow response to an increase in cellular activity. Increases in the plasma lactate/pyruvate ratio (reflecting increased aerobic glycolysis) augment the blood flow response to neuronal activity (Mintun, Vlassenko et al. 2004; Vlassenko, Rundle et al. 2006). Since there is a near equilibrium in the ratio of lactate/pyruvate and cytosolic $NADH/NAD^+$, these results

indicate that NADH may sense the circulatory needs of the cell in response to its level of aerobic glycolysis. This mechanism may be essential for neurovascular coupling, consistent with recent evidence that astrocytes mediate the vascular response to neuronal activity (Petzold, Albeanu et al. 2008).

So far we have discussed several roles for aerobic glycolysis in cellular activity: 1) To provide energy for Na^+/K^+ ATPase in astrocytes (for removal of glutamate from the synaptic cleft); 2) To provide intermediates for the pentose phosphate shunt for anabolism in neurons; 3) To regulate the vascular response to neuronal activity by modulation of the $NADH/NAD^+$ ratio.

While we have some indications of the possible cellular roles of aerobic glycolysis, we do not know its distribution in the resting human brain. Are particular cortical regions primarily glycolytic? Or does aerobic glycolysis simply recapitulate glucose metabolism, reflecting ~10% of the fate of glucose throughout the brain? The brain continues to have a high metabolic rate at rest and regional elevations in aerobic glycolysis may indicate functionally relevant networks important for normal brain function. We seek to answer these questions in Chapter 2.

Given a particular resting distribution of aerobic glycolysis, how is this modulated by prior neuronal activity? Does the bioenergetic response to neuronal stimulation change over time?

A sudden increase in neuronal activity is followed by a rapid increase in aerobic glycolysis as well as an increase in oxidative phosphorylation if the activity persists. This activity appears to be spatially and temporally segregated with aerobic glycolysis

within the astrocyte and oxidative metabolism within neurons (Kasischke, Vishwasrao et al. 2004), though this remains somewhat controversial (Gjedde and Marrett 2001).

Acutely, during short periods (~5 minutes) of neuronal activity early positron emission tomography experiments did not find any changes in energy requirements (Fox and Raichle 1986). Other studies have found conflicting results, though. Continuous passive visual stimulation with a flickering checkerboard results in a rapid increase in blood flow of 39% along with an increase in oxygen consumption of 6%. Following 25 minutes of continuous stimulation, though, oxygen consumption increases 14% from the initial 6% above control state, and blood flow declines to 24% from the initial value of 39% above control state. Following completion of stimulation, all measurements return to their control levels (Vlassenko, Rundle et al. 2006).

The role of glycolysis, though, has not been studied in as much detail. Work from Madsen and colleagues provide some insight (Madsen, Hasselbalch et al. 1995). They measured cerebral blood flow, oxygen, and glucose utilization using the Kety-Schmidt technique using arterial and venous blood sampling (Hatazawa, Ito et al. 1988). They asked subjects to perform the cognitively demanding Wisconsin card sorting task and measured glycolysis at regular intervals during and following completion of the task. During the 20 minute task performance, blood flow and glucose utilization rose immediately and remained elevated while oxygen consumption did not change significantly. Surprisingly these alterations in brain metabolism were maintained following task completion. As long as they continued measurements (40 minutes following task completion) though blood flow had returned to its original baseline, the level of aerobic glycolysis remained elevated. These results confirm that aerobic

glycolysis increases during task performance as previously reported, but also demonstrates its persistence in the resting state following completion of task performance.

If the findings of Madsen and colleague accurately reflect changes in resting cerebral metabolism, is there any other corroborating evidence for changes in cerebral aerobic glycolysis and brain activity following task completion?

Following a period of wakefulness, whole brain glucose utilization increases by almost 20% (Boyle, Scott et al. 1994). PET studies performed in the early morning after a period of sleep reveals a significant reduction in cerebral glucose utilization, though the causative factors and regional cerebral distribution of this decrease remains unclear. Consistent with this finding, though, is a comparable 20% decrease in cerebral blood flow following a night of sleep (Braun, Balkin et al. 1997). Though these two studies were performed in separate groups of subjects, taken together, these data suggest that some activity during wakefulness results in a significant increase in brain glucose utilization, though no similar changes in oxygen consumption have been found. Animal studies have confirmed this finding, with a significant increase in glucose utilization following a period of wakefulness that is attenuated following a period of sleep (Vyazovskiy, Cirelli et al. 2008). These changes in metabolism are paralleled by an increase in GluR1 AMPA receptors during wakefulness that likewise decrease during sleep, suggesting net synaptic potentiation during wakefulness (Vyazovskiy, Cirelli et al. 2008). Taken together, these disparate pieces of evidence suggest that synaptic potentiation, possibly associated with learning, may induce increases in aerobic glycolysis in the resting brain following task completion. This theory is partially the

focus of this thesis. Before we discuss the resultant experiments, we must review the evidence that changes in synaptic density and strength may be associated with learning.

Changes in brain metabolism following learning

The human brain is constantly changing as novel stimuli are presented and behaviors are learned. The brain stores this information in the form of new neuronal connections and remodeling of existing neuronal synapses. But how do these changes in synaptic strength cause measurable changes in brain metabolism?

Many studies have shown learning induced alterations in brain structure and connectivity using imaging techniques including fMRI, PET, structural and volumetric techniques (Simpson, Snyder et al. 2001; Ungerleider, Doyon et al. 2002; Zach, Kanarek et al. 2005). These changes in brain structure and function represent acute and long-term changes in cellular activity, though a complete understanding of the time course and extent of these changes remains to be elucidated.

Short-term changes in brain physiology are often detected as altered patterns of brain metabolism during the performance of a task. For example, practice of a verb generation task results in changes in the functional anatomy of regions necessary for task performance over time (Raichle, Fiez et al. 1994). Areas initially utilized for naïve task performance including anterior cingulate and left prefrontal cortex reduced their activity (measured as alterations in cerebral blood flow) following repeated practice. Similarly, practice of a maze tracing task in humans results in alterations in the brain regions needed

for accurate task performance (van Mier, Tempel et al. 1998). There are several possible explanations for these changes.

The site of neuronal plasticity is predominantly the synapse (Martin, Grimwood et al. 2000). This location is also the site of greatest energy utilization in the brain reflecting fluctuations in membrane potentials due to neuronal signaling (Magistretti and Pellerin 1999). So a change in energy metabolism may reflect local alterations in the efficacy of neurotransmission. Following learning an individual presynaptic neuron is able to more easily induce a postsynaptic action potential, altering the energy requirements of both cells as well as the release of glutamate into the synaptic cleft.

One well characterized cellular mechanism of learning is long-term potentiation (LTP) (Bashir, Alford et al. 1991). LTP causes alterations in synaptic strength and the efficacy of synaptic transmission. In the initial phases of learning, increased glutamate is released presynaptically to cause more potent postsynaptic receptor activation. Following repeated synaptic potentiation, the synapse is structurally and functionally modified. This occurs via transcription and translation of new postsynaptic receptors as well as insertion of already translated receptors into the postsynaptic membrane (Frick, Magee et al. 2004). In addition, the binding potential of glutamate to the postsynaptic receptor is altered by modification of the structural conformation of receptors via phosphorylation. LTP alters the ultrastructure of the synapse causing an increase in the apposition zones, larger postsynaptic densities (PSD), and enlarged spine profiles (Buchs and Muller 1996). These changes in cellular neurophysiology induced by learning remain following task completion.

An increase in the strength of a particular synaptic connection requires increased energy utilization. This energy may be provided by elevated aerobic glycolysis, due to the role of glycolysis in providing intermediates for synaptic remodeling and DNA and RNA production via the pentose phosphate shunt. Or conversely, synapses that are strengthened by the learning process could increase their spontaneous glutamate flux (Mao, Hamzei-Sichani et al. 2001), also requiring increased aerobic glycolysis. Since aerobic glycolysis supplies the postsynaptic density with energy (Wu, Aoki et al. 1997; Sheng and Hoogenraad 2007) an alteration in synaptic structure could also cause a subsequent increase in aerobic glycolysis. A complete understanding of the metabolic consequences of learning at a cellular level remains elusive, though.

Learning related alterations in brain activity may also extend beyond acute task performance. Recent studies have revealed a replay of spatial memories in hippocampal-parietal circuits during post-learning sleep in both rats and humans (Kudrimoti, Barnes et al. 1999; Louie and Wilson 2001; Ribeiro, Gervasoni et al. 2004). Task performance tends to improve following sleep in a variety of working and procedural memory tasks (Marshall, Helgadottir et al. 2006; Orban, Rauchs et al. 2006), suggesting that brain activity is somehow modulated after task completion.

Synaptic Homeostasis Hypothesis

One intriguing explanation for the role of ongoing aerobic glycolysis in the resting brain is provided by the synaptic homeostasis hypothesis. This hypothesis suggests that ongoing neuronal activity is associated with significant metabolic and

functional costs to the brain in the form of increased synaptic density and energy utilization (Tononi and Cirelli 2003). The four components of this hypothesis include:

> "1. Wakefulness is associated with synaptic potentiation in several cortical circuits;
>
> 2. Synaptic potentiation is tied to the homeostatic regulation of slow-wave activity;
>
> 3. Slow-wave activity is associated with synaptic downscaling;
>
> 4. Synaptic downscaling is tied to the beneficial effects of sleep on performance. (Tononi and Cirelli 2003; Tononi and Cirelli 2006)"

This hypothesis suggests that wakefulness is associated with increases in synaptic strength in cortical circuits that were previously activated. Neuronal activity leads to net synaptic potentiation, reflecting increased efficacy of neurotransmission and increased density of synaptic connections (Vyazovskiy, Cirelli et al. 2008). These new and modified synapses likely have an energetic cost, as discussed earlier. Increased glutamatergic neurotransmission is associated with alterations in aerobic glycolysis. It remains unknown whether this synaptic potentiation is a global or local phenomenon. There is some evidence for global changes in gene expression during wakefulness, with an increase in genes associated with energy metabolism, growth factors, synaptic proteins, neurotransmitter receptors, and transcription factors (Cirelli and Tononi 2000). During sleep, these genes decrease their expression, consistent with the hypothesis. Evidence cited above from the limited human studies suggests that learning induces changes in cortical metabolism following completion of a learning task though its regional distribution has not been investigated.

Overview of dissertation

To investigate the role of aerobic glycolysis in the resting human brain and to test our hypothesis that sustained, task-specific regional increases in resting brain metabolism follow learning, we present the following data. In Chapter 2, we examine the distribution of aerobic glycolysis in the human brain during eyes-closed rest. Previous experiments have only assessed global levels of aerobic glycolysis without regard for its local distribution. We hypothesize that cortical networks known to have high levels of functional activity in the eyes-closed state, including the default network, would also have elevated aerobic glycolysis. In Chapter 3, we test the core hypothesis of this thesis, that aerobic glycolysis is elevated regionally in eyes-closed rest following completion of a learning task. We utilize a visuomotor rotation task that has previously been shown to induce increased slow-wave activity in post-learning sleep in regions involved in task performance. In Chapter 4, we compare our resting metabolic data with neurotransmitter receptor density data obtained in a separate group of subjects postmortem via autoradiography. We hypothesize that cortical regions with high levels of aerobic glycolysis would also have high levels of excitatory receptor density. Finally, in Chapter 5 we provide our interpretations of these data and discuss implications for normal physiology, learning, and disease pathophysiology.

Chapter 2: Regional distribution of aerobic glycolysis in the human brain

Abstract

Transient regional increases in brain activity associated with task performance result in elevated glucose metabolism greater than the corresponding increase in oxygen consumption (aerobic glycolysis). Aerobic glycolysis is also present in the resting adult brain but neither its regional pattern nor its mission is known. We studied the distribution of aerobic glycolysis in the resting human brain using positron emission tomography to measure glucose and oxygen utilization in 33 healthy young adults. The default system and dorsolateral prefrontal cortex bilaterally showed metabolic rates significantly above the brain mean and had high levels of aerobic glycolysis. However, sensory cortices, particularly primary visual cortex, while also exhibiting equally high metabolic rates, did not exhibit elevated glycolysis. The cerebellum, whose energy consumption is close to the brain mean, had the lowest levels of aerobic glycolysis. Our data demonstrates heterogenic distribution of aerobic glycolysis in the human brain and indicate that the most pronounced elevation in aerobic glycolysis occurs in regions characterized by high functional activity at the resting state.

Introduction

The human brain accounts for 2% of total body weight but 20% of total energy metabolism (Sokoloff 1977). Estimates are that 60-80% of this ongoing energy consumption is devoted to signaling associated with the input and output of neurons (Attwell and Laughlin 2001). In the mature brain, the major source of this energy is the oxidation of glucose to carbon dioxide and water (Siesjo and Plum 1971). However, following transient increases in neural activity, glucose utilization increases more than oxygen consumption (Fox, Raichle et al. 1988; Madsen, Hasselbalch et al. 1995) . Because this metabolic response occurs in the presence of adequate oxygen it is usually referred to as aerobic glycolysis to differentiate it from glycolysis occurring as the result of ischemia or hypoxia.

The phenomenon of increased levels of aerobic glycolysis following transient increases in neural activity has stimulated research on the mechanism by which glutamate is moved with sodium into astrocytes from the synapse. Research to date strongly implicates membrane-bound, astrocyte Na^+/K^+ ATPase which relies exclusively on glycolysis for the energy needed to pump the accumulated sodium from the astrocyte (Pellerin and Magistretti 1994; Pellerin and Magistretti 1996). Largely unexplored is the possibility that Na^+/K^+ ATPase elsewhere (e.g., in dendrites) might also be relying on aerobic glycolysis (Wu, Aoki et al. 1997).

Aerobic glycolysis is also present at rest. During the past three decades researchers have repeatedly demonstrated that the resting whole brain molar ratio of oxygen consumed to glucose utilized (the so-called oxygen-to-glucose index or OGI) is

less than 6, which indicates that some glucose is used for purposes other than providing substrate for oxidative phosphorylation (Raichle, Posner et al. 1970; Powers, Videen et al. 2007). Presently, we have no information on how the products of glycolysis are allocated among several possible pathways. For example, it is not known to what extent aerobic glycolysis via the pentose phosphate pathway serves as a source of carbon fragments and reducing equivalents for the synthesis of RNA, DNA and membrane replication.

The experiments reported herein seek to initiate an expansion of our understanding of the role of glycolysis in the resting activity of the adult human brain by determining whether regional variations in glycolysis exist and how these regional variations might relate to regional variations in overall brain energy consumption. We were particularly interested to determine whether areas thought to play a major role in spontaneous or intrinsic activity (e.g., the brain's default system (Raichle, MacLeod et al. 2001; Buckner, Andrews-Hanna et al. 2008)) have increased levels of glycolysis in the resting state.

Methods

Participants

Thirty-three healthy, right-handed neurologically normal participants (19 women) aged 20 to 33 years (mean 25.4 ± 2.6) were recruited from the Washington University community. Subjects were excluded if they had contraindications to MRI, history of mental illness, possible pregnancy, or medication use that could interfere with brain

function. All experiments were approved by the Human Research Protection Office (HRPO) and Radioactive Drug Research Committee (RDRC) at Washington University in St. Louis. Written informed consent was provided by all participants.

Image Acquisition

Structural MRI: MRI scans were obtained in all subjects to guide anatomical localization. High-resolution structural images were acquired using a 3D sagittal T1-weighted MPRAGE on a Siemens (Siemens, Erlangen, Germany) 3T Allegra [TE=3.93ms, TR=1900ms, TI=1100ms, flip angle=20°, 256x256 acquisition matrix, 160 slices, 1x1x1 mm voxels] or 1.5T Sonata scanner [TE=3.93ms, TR=1900ms, TI=1100ms, flip angle =15°, 224x256 acquisition matrix, 160 slices, 1x1x1 mm voxels].

Resting fMRI scanning: Twenty normal right-handed subjects (out of 33 PET subjects) also underwent resting state fMRI scanning similar to Fox et al., 2005 (Fox, Snyder et al. 2005). Two 7.5 minute scans (194 frames) were performed during visual fixation on a crosshair. All imaging was performed on a 3T Siemens Allegra scanner (Erlangen, Germany). Functional data were collected by using a gradient echo, echo-planar sequence sensitive to BOLD contrast [echo time (TE) = 25 ms, flip angle = 90°, 4 x 4 x 4-mm isotropic voxels, volume repetition time (TR) = 2.16 s]. Whole brain coverage was obtained with 32 contiguous slices. The first four frames of each run were not included in data analysis. Additional fMRI processing details are given below.

PET Scanning: Studies were performed using a Siemens model 961 ECAT EXACT HR 47 PET scanner (Siemens/CTI, Knoxville, TN) with 47 slices encompassing an axial field of view of 15cm. Transverse resolution was 3.8-5.0 mm FWHM and axial resolution was

4.7-5.7 mm full width at half maximum (FWHM). Attenuation data was obtained using ^{68}Ge-^{68}Ga rotating rod sources to enable quantitative reconstruction of subsequent emission scans. Emission data were obtained in the 2D mode (inter-slice septa extended). All PET data was reconstructed using a ramp filter (approximately 6mm FWHM) and then blurred to 12 mm FWHM. Subject head movement during scanning was restricted by a thermoplastic mask. All PET images were acquired in the eyes-closed waking state. No specific instructions were given regarding cognitive activity during scanning other than to remain awake.

All subjects underwent a single PET session including one FDG scan (to measure CMRGlu) and either one (13 subjects) or two (20 subjects) replicate sets of three ^{15}O scans to measure CBV, CBF, and CMRO$_2$, respectively.   In subjects with two replicates of ^{15}O scans, CBV, CBF, and CMRO$_2$, values were averaged for data analysis.

PET Measurement of Glucose Metabolism: ^{18}F-fluorodeoxygluse (FDG) uptake and trapping was used to image CMRGlu(Fox, Raichle et al. 1988). Measurements of CMRGlu were performed after slow intravenous injection of 5mCi of [^{18}F]FDG. Dynamic acquisition of PET emission data continued for 60 minutes with 25 5-sec frames, 9 20-sec frames, 10 1-min frames, and 9 5-min frames. Venous samples for plasma glucose determination were obtained just before and at the mid-point of the scan.

[^{15}O]tracer PET scans: 120 second dynamic scans comprised of 2 second frames that began with tracer injection (or inhalation) (Raichle, Martin et al. 1983; Mintun, Raichle et al. 1984). With this method, the optimum 40 second scan was created from summation of the appropriate frames. By reconstructing all frames and then creating a whole brain

time-activity curve, the onset of activity in the brain could be judged exactly. **CBF Scan:** Distribution of CBF was measured with a 40-sec emission image (derived from a 120 second dynamic scan) after rapid injection of 50 mCi [^{15}O]water in saline (Raichle, Martin et al. 1983). **CBV Scan:** Distribution of CBV was measured with a 5-min emission scan beginning 2 min after brief inhalation of 75mCi of [^{15}O]carbon monoxide in room air (Martin, Powers et al. 1987). **CMRO$_2$ Scan:** Distribution of CMRO$_2$ was measured with a 40-sec emission scan (derived from a 120 second dynamic scan) after brief inhalation of 60 mCi of [^{15}O]oxygen in room air (Mintun, Raichle et al. 1984).

Image Analysis

While previous studies have focused on task-related alterations in regional metabolism, we were interested in the relationship between metabolic measurements during the resting state. Specifically, the ratio between CMRO$_2$ and CMRGlu, known as the oxygen-to-glucose index (OGI), can be used as a measure of aerobic glycolysis. Measurements of OGI in humans using invasive measurements of cerebral arterial and venous blood (Kety-Schmidt technique) have estimated a global ratio of ~5.3-5.5. Thus, ~5.5 molecules of oxygen are metabolized for each molecule of glucose. Theoretically, this ratio would be six if all glucose were completely oxidized according to the following formula:

$$C_6H_{12}O_6 + 6O_2 \rightarrow 6CO_2 + 6H_2O \quad\quad\quad\quad (1)$$

Some fraction of glucose, estimated to be 10%, is only partially oxidized. This regional mismatch between glucose and oxygen metabolism represents glucose that undergoes aerobic glycolysis. Our objective was to image regional variations in the $CMRO_2/CMRGlu$ ratio in a manner independent from whole brain measures. This objective differs somewhat from the originally described PET methodology (Mintun, Raichle et al. 1984), in which absolute metabolic rates, e.g., $CMRO_2$, in units of ml/min/100g tissue, were determined. Absolute metabolic rates can be of interest, but, in practice, are rarely measured with variability less than about 10%. The principal source of measurement error is the limited precision achievable in determining the arterial input function. Accordingly, we modified the original quantitative methodology to image regional variations in which we fix rather than measure global (absolute) metabolic rates. This approach is analogous to that done for CBF (Mintun, Fox et al. 1989). A derivation of the present method follows.

A short PET collection (e.g. 40 sec) begun soon after inhalation of $[^{15}O]O_2$ provides a PET_{O2} image in which activity is nearly proportional to oxygen utilization except that metabolized O_2 also appears in the blood compartment as $[^{15}O]H_2O$. However, the blood compartment can be directly visualized as labeled hemoglobin in a PET_{CO} image (Martin, Powers et al. 1987). Thus, the blood-compartment-corrected, relative oxygen utilization image is obtained as

$$CMRO_2 \propto PET_{O2} - \alpha \cdot PET_{CO} \qquad (2)$$

where α is a multiplicative factor that represents the proportionality between blood volume and tracer activity. From the original CMRO$_2$ equations (Mintun, Raichle et al. 1984) this factor is a global constant based on measured blood activity values. Eqn (2) is the numerator of the oxygen extraction fraction equation (Mintun, Raichle et al. 1984)

$$OEF = (PET_{O2} - \alpha \cdot PET_{CO}) / (\beta \cdot PET_{H2O}) \qquad\qquad (3)$$

where PET_{H2O} is activity in a short (e.g., 40 sec) acquisition scan after a bolus injection of [^{15}O]H$_2$O. The β term is a global multiplicative factor that represents the proportionality between CBF and tracer uptake. The near-linear relationship between CBF and the tracer uptake in a 40 second acquisition [^{15}O]H$_2$O image has been well documented (e.g. (Raichle, Martin et al. 1983)). In the original method, α and β were calculated using information obtained by arterial blood sampling. However, small errors in the measurement of the blood activity used in the calculation of α leads to over or underestimations of this vascular contribution, which in turn, leads to high variation in the calculated regional CMRO$_2$. This effect is especially prominent in regions of high blood volume. The present method exploits the sensitivity of the OEF image to errors in α by incorporating the observation that OEF is highly uniform over the brain compared with other metabolic profiles (Raichle, MacLeod et al. 2001). Thus, we estimated α by finding the value that minimizes OEF image variability over the brain. Concurrently, β was adjusted to obtain a whole-brain mean OEF of 0.4. It should be noted, however, that computed CMRO$_2$ is nearly independent of the value assigned to β (Mintun, Raichle et

al. 1984). Following estimation of α and β, we calculated $CMRO_2$ according to equation (2).

General PET Data Analysis:

Preprocessing: For each subject, measures of CBF, CBV, $CMRO_2$, and CMRGlu were aligned to each other and then to the subject's MPRAGE. The re-aligned data was then transformed to Talairach space (Lancaster, Glass et al. 1995) using in-house software and scaled to a whole-brain mean of one (local-to-global ratio (Raichle, MacLeod et al. 2001)).

Oxygen-to-glucose index (OGI): OGI was computed by a voxelwise division of $CMRO_2$ by CMRGlu to compute a local-to-global OGI. For comparison to traditional OGI measures, this ratio was scaled by 5.323 (Raichle, Posner et al. 1970).

Glycolytic Index: In order to quantitatively assess aerobic glycolysis, we performed a linear regression of CMRGlu on $CMRO_2$. The residuals were scaled by 1000 to produce the glycolytic index (GI). GI represents glucose consumption above or below that predicted by oxygen consumption.

PET statistics: To combine results across subjects, we computed a general linear model (GLM) which contained metabolic data for $CMRO_2$, CMRGlu, CBF, CBV, OEF, OGI, and GI for each subject. We performed groupwise random effects analysis (one sample t-test; n=33) to determine regions with significant deviations in their metabolic values from the whole brain mean. Images were thresholded at a $Z>4.4$ ($p<0.0001$, cluster >99, corrected for multiple comparisons).

Surface mapping: Volumetric statistical results were projected onto the cortical surface of the PALS B12 (population-average landmark and surface-based) atlas by multifiducial mapping (Van Essen 2005). Surface mapping was performed using Caret v5.512 [http://brainmap.wustl.edu/caret].

Brodmann Regions: Brodmann regions were extracted from the PALS B12 atlas (Caret v5.512). Values for $CMRO_2$, CMRGlu, CBF, CBV, OEF, OGI, and GI were extracted for each Brodmann region in the brain (41 regions for each hemisphere) from the general linear model (GLM) computed for each subject. Comparison of metabolic values between different Brodmann regions involved paired groupwise *t*-tests (n=33, two-tailed, α =0.05).

Correlations: Pearson product-moment correlations between metabolic values were performed over cortical Brodmann regions. Correlations were weighted by the size (number of voxels) of the Brodmann regions utilized. Weighted correlation across Brodmann regions is equivalent to voxelwise computation of the standard Pearson product-moment correlation after assigning to every voxel within a Brodmann region the value of its regional mean. Significance of correlations was computed using α=.05 and 80 degrees of freedom (df). Statistical analysis was performed using SPSS for Windows v16.0 (SPSS Inc., Chicago, IL).

Subcortical regions: As Caret does not provide subcortical parcellations, regions of bilateral caudate, putamen, globus pallidus, and thalamus were manually drawn on our representative atlas MPRAGE using Analyze v6.1 (Mayo, Rochester, MN).

General fMRI data analysis:

Preprocessing: BOLD processing included compensation of systematic, slice-dependent time shifts, systemic odd-even slice intensity differences, and rigid body correction for interframe head motion within and across BOLD runs. Each BOLD run was intensity scaled to a whole brain mode of 1000. Atlas registration was performed by affine transforms connecting the first BOLD run frame with the T1W and T2W structural images. Our atlas template includes MPRAGE data from 12 normal individuals from a Siemens Allegra 3T scanner and was made to conform to the 1988 Talairach and Tournoux atlas (Lancaster, Glass et al. 1995).

Low-frequency BOLD fluctuation correlations: Data was temporally band-pass filtered (f<0.08) and spatially smoothed (6mm FWHM). Sources of spurious variance and their temporal derivatives were removed from this data through linear regression (see (Fox, Snyder et al. 2005)). Nuisance regressors included signals averaged over ventricle, white matter, and whole brain ROIs as well as measures of head movement. Correlation maps were produced by extracting the BOLD time course from the seed region and computing the Pearson's r between that time course and that of every other voxel in the brain. Distributed seed regions were comprised of 6-mm-radius spheres centered on previously published foci. Default system spheres were placed in medial prefrontal cortex (MPF, [-1, 47, -4]), posterior cingulate/precuneus (PCC, [-5, -49, 40]), lateral parietal cortex (LP, [-45, -67, 36]). Cognitive control system spheres were placed bilaterally in dorsolateral prefrontal cortex (DLPFC, [-34, 51, 12]; [24, 50, 13]) and anterior parietal cortex (aIPL, [-43, -55, 42]; [48, -47, 42]).

BOLD correlation mapping: To combine results across subjects and compute statistical significance, correlation coefficients were converted to a normal distribution by Fischer's

z transformation. Fischer z-maps were combined across subjects using a random-effects analysis (one sample t-test, N=20). To prepare for comparison to PET data, the default and control system maps were resampled to 2mm cubic voxels and thresholded at Z>3.0 (p<0.01, cluster > 17 voxels, corrected for multiple comparisons (Forman, Cohen et al. 1995)).

Conjunction Analysis: A conjunction analysis was performed to qualitatively compare regions with elevated aerobic glycolysis measured via PET and the default and cognitive control systems delineated by correlation mapping. Z-score maps of aerobic glycolysis were thresholded at a Z>4.4 (p<0.0001, cluster > 99 voxels, corrected for multiple comparisons). The conjunction image (Figure 2.3d) was computed by identifying voxels showing significantly elevated aerobic glycolysis *and* being within either default *or* control systems (conjunction = GI significantly high Λ [voxel $\in$ default system $\mathbf{V}$ voxel $\in$ cognitive control system]).

Results

Measures of resting oxygen and glucose metabolism

Relative metabolic rates for oxygen ($CMRO_2$) and glucose (CMRGlu) were imaged with positron emission tomography (PET) in 33 normal right handed adults in the resting awake state. Regional CMRGlu was measured using [^{18}F]-fluorodeoxyglucose (FDG). Regional $CMRO_2$ was measured using a total of three scans involving the administration of [^{15}O]H$_2$0 (water), [^{15}O]CO (carbon monoxide) and [^{15}O]O$_2$ (oxygen). In each individual, regional $CMRO_2$ and CMRGlu were scaled to a whole brain mean of one (local-to-global ratio; see Methods). The individual results were averaged over

subjects in Talairach atlas space. The obtained mean regional distributions of $CMRO_2$ and CMRGlu were similar to previously reported results obtained using quantitative measurements in normal subjects (Phelps, Huang et al. 1979; Raichle, MacLeod et al. 2001). Glucose and oxygen metabolism both were greatest in cortical gray matter and comparatively less in white matter. The highest local-to-global ratios of $CMRO_2$ and CMRGlu were in primary visual cortex (1.35) and posterior cingulate/precuneus (1.34), respectively (Figure 2.1). While the distributions of $CMRO_2$ and CMRGlu exhibited regional variation across the brain, these two measures were highly correlated over all (r=0.869, p<0.001). As well, both $CMRO_2$ (r=0.822, p<0.001) and CMRGlu (r=0.869, p<0.001) were highly correlated with cerebral blood flow (CBF).

Resting aerobic glycolysis

We used two approaches to assess aerobic glycolysis. First, an oxygen-to-glucose index (OGI) image (Figure 2.4) was computed for each individual by voxelwise division of relative $CMRO_2$ by relative CMRGlu; the resulting quotient image was scaled to obtain a whole brain molar ratio of 5.323 based upon a prior quantitative human PET study (Raichle, Posner et al. 1970). Lower OGI values represent higher levels of aerobic glycolysis. While the OGI is a straightforward measure based on well-established metabolic principles, OGI images may be noisy in areas of low metabolism because they involve voxelwise division.

To overcome this limitation, we defined a novel measure of aerobic glycolysis in the brain: the glycolytic index (GI). The GI is obtained by linear regression of CMRGlu on $CMRO_2$ (Figure 2.2) and exhibiting the residuals scaled by 1000. Positive GI values represent locally increased CMRGlu relative to the line of regression, i.e., excess aerobic

glycolysis. Likewise, negative GI values represent less glycolysis than that predicted by the line of regression.

Following computation of GI maps for each subject, significance was assessed at the population level by voxelwise *t*-tests against the null hypothesis of uniformly proportional glucose:oxygen metabolism, i.e., no deviation from the line of regression. The *t*-maps were converted to equi-probable Z-maps and thresholded at p<0.0001 (Z>4.4, cluster >99 voxels) according to previously described methodology (Forman, Cohen et al. 1995; McAvoy, Ollinger et al. 2001). Regions with significantly elevated aerobic glycolysis were found bilaterally in prefrontal cortex, lateral parietal cortex, the posterior cingulate/precuneus, lateral temporal gyrus, gyrus rectus, and the caudate nuclei (Table 2.1). In contrast, significantly low glycolysis was found bilaterally in the inferior temporal gyrus and throughout the cerebellum.

The acquired PET data provided the opportunity to compute statistics at the regional level and to examine correlations between multiple metabolic measures. Correlations were computed over regions corresponding to Brodmann areas defined using Caret software (Van Essen 2005) on relative metabolic measures averaged over subjects. Thus, GI was significantly correlated (weighted Pearson's product-moment correlation, 80df; see Methods) with OGI (r= -0.986, p<0.001), CBF (r=0.501, p<0.001), $CMRO_2$ (r=0.243, p<0.05) and CMRGlu (r=0.690, p<0.001). While the glycolytic index overall tended to scale with various metabolic rates, there were significant regional deviations particularly in primary sensory cortices. For example, while primary visual cortex (V1 or BA 17) showed the highest $CMRO_2$ in the cerebral cortex, its level of aerobic glycolysis was at the brain mean. Moreover, GI was significantly lower in V1 as compared to BA

46 in dorsolateral prefrontal cortex (DLPFC) (p<0.001; paired *t*-test, n=33; see Methods) as well as the posterior midline component of the default system (BA 23, p<0.001; paired *t*-test, n=33). The cerebellum, as whole, showed low levels of CMRGlu (0.89) but relatively high $CMRO_2$ (1.04). Thus, the mean cerebellar GI was strongly negative (p<0.0001; n=33; H_o: cerebellar GI = 0), indicating much lower aerobic glycolysis than expected for this region given its $CMRO_2$. Data for all Brodmann regions are listed in Table 2.3 and 2.4. Data for selected subcortical regions (illustrated in Figure 2.5) are listed in Table 2.5.

Oxygen extraction fraction

The oxygen extraction fraction (OEF) reflects the $CMRO_2$-to-CBF ratio (see Equation (3) in Methods). Because of the strong correlation between $CMRO_2$ and CBF (r=0.822; Table 2.2) presumably based on the constant need of the brain for oxygen, it is easy to anticipate a uniform OEF across the brain uncorrelated with either CBF or $CMRO_2$. This was not observed (Figure 2.6). Rather, a significant OEF-$CMRO_2$ correlation was found (r=0.637) indicating that approximately 40% of the regional variation in OEF can be attributed to $CMRO_2$ and not CBF (r=0.086). This arises, in part, because of a striking elevation of the OEF in visual cortices (Figure 2.6), an observation previously noted by us and others (Raichle, MacLeod et al. 2001). If aerobic glycolysis and oxidative phosphorylation are regarded, to some extent, as competing fates of glucose, one might expect a negative OEF-GI correlation. Such a relation was found, but it was weak (r=-0.223). Thus, the present data demonstrate a substantial, regionally independent variation in OEF, GI and CBF indicating not only regional variations in metabolic profiles but also complex relationships between CBF and the brain's metabolic requirements.

The default and cognitive control systems

Examination of the GI map (Figure 2.3a) suggested a correspondence between regions showing higher than average glycolysis and two distributed systems previously defined on the basis of functional neuroimaging studies, specifically, the default and cognitive control systems. The default system is comprised of brain regions that reliably reduce activity during the performance of goal-directed tasks (Raichle, MacLeod et al. 2001). More recently, the default system has been delineated by analysis of the blood oxygen level dependent (BOLD) functional magnetic resonance imaging (fMRI) signal acquired in the resting state (Fox, Snyder et al. 2005; Damoiseaux, Rombouts et al. 2006). Similarly, the cognitive control system includes a set of regions recruited by the performance of complicated cognitive tasks (Braver and Barch 2006) and has also been delineated on the basis of resting BOLD imaging (Dosenbach, Fair et al. 2008; Vincent, Kahn et al. 2008). We performed resting BOLD correlation mapping (Fox, Snyder et al. 2005) in a subset (N=20) of the present subjects. The default system was mapped by correlation against the signal averaged over three nodes (posterior cingulate [-5 -49 40], left lateral parietal [-45 -67 36], and medial prefrontal [-1 47 -4] cortex). Similarly, the cognitive control system was mapped using a distributed seed region placed bilaterally in prefrontal [-34, 51, 12], [24, 50, 13] and anterior parietal [-43, -55, 42], [48, -47, 42] cortex. Regions of significant BOLD correlations (p<0.01, random effects analysis; Z>3.0, cluster>17) within the default and control systems are shown in Figures 2.3b and 2.3c, respectively. Figure 2.3d shows the overlap between regions of elevated aerobic glycolysis and a mask computed as above threshold in either the default or control systems. These two distributed systems together account for most cortical areas showing high levels of aerobic glycolysis at rest.

Discussion

The highest levels of aerobic glycolysis appear to reside within two cortical systems, the default system (Raichle, MacLeod et al. 2001) (Figure 2.3b) and areas in frontal and parietal cortex that have been associated with task control processes (Dosenbach, Fair et al. 2008) and working memory (Braver and Barch 2006) (Figure 2.3c). However, the distribution of aerobic glycolysis within these two systems is not uniform. Within the default system the highest area of aerobic glycolysis is in the lateral parietal lobes followed by the dorsal medial prefrontal cortex, posterior cingulate and medial precuneus. The hippocampal formation, a component of the default system (Vincent, Snyder et al. 2006), has a level of aerobic glycolysis significantly below the brain mean (Table 2.6; Figure 2.7). In the other system the highest level of aerobic glycolysis resides in DLPFC (Table 2.7; Figure 2.8).

The level of aerobic glycolysis does not follow the overall metabolic rate of the tissue in a simple fashion. While both CMRGlu and $CMRO_2$ are correlated with aerobic glycolysis, aerobic glycolysis, as assessed by the GI, is much more variable in relation to $CMRO_2$ (r=0.243) than CMRGlu (r=0.690) when surveyed broadly across the brain (Tables 2.2-2.4). Sensory regions such as V1 (BA17) have high metabolic rates with $CMRO_2$ (1.35) and CMRGlu (1.30) both significantly elevated above the brain mean, although their level of aerobic glycolysis is at the brain mean. In contrast, though DLPFC and posterior cingulate have $CMRO_2$ and CMRGlu comparable to V1, their level of aerobic glycolysis is significantly elevated above the brain mean. These results point to regional differences in the manner in which blood flow is coupled to oxygen consumption and glucose utilization.

In contrast to many areas of the cerebral cortex, the cerebellum as a whole appears to have a level of aerobic glycolysis well below the brain mean despite the presence of numerous cells that exhibit elevated resting firing rates (Gruol and Franklin 1987). While a full explanation for the low level of aerobic glycolysis in the cerebellum is not presently at hand several factors should be considered in seeking an explanation.

Most of the synaptic connections and, hence, most of this ongoing activity in the cerebellum is GABAergic rather than glutamatergic (Huang, Di Cristo et al. 2007). A known contributor to aerobic glycolysis in the brain is the cycling of glutamate by astrocytes (Chatton, Pellerin et al. 2003). In vitro studies of cerebellar astrocytes (Bergersen, Magistretti et al. 2005) reveal their similarity to the astrocytes of the cerebral cortex in responding to glutamate but not GABA with a burst of glycolysis. But, the ratio of neurons to glia is much higher in the cerebellum (~6:1) (Ghandour, Vincendon et al. 1980) than in the cerebral cortex (1:1.5) (Pelvig, Pakkenberg et al. 2007) possibly reflecting the preponderance of GABAergic synapses. This leads us to posit that the low level of aerobic glycolysis in the cerebellum reflects a much reduced role of excitatory neurotransmission and, hence, less aerobic glycolysis in the astrocytes.

However, the level of aerobic glycolysis within the cerebellum does not preclude transient task-related alterations in the fMRI BOLD signal (a putative correlate to aerobic glycolysis driven by increased glutamatergic neurotransmission (Raichle and Mintun 2006)); nor a decrease in CBF and CMRGlu greater than $CMRO_2$ when excitatory input to the cerebellum from the cerebral cortex is reduced due to a cerebral hemisphere stroke (so-called cross cerebellar diaschisis (Shamoto and Chugani 1997)).

One factor responsible for ongoing aerobic glycolysis in the brain is likely to be the need to support membrane-bound, ATP-dependent processes. Best characterized in this regard is the process whereby glutamate is removed from the synapse into astrocytes along with sodium. The sodium is returned to the extracellular fluid by Na^+/K^+-ATPase. The energy needed for the pumping action of Na^+/K^+-ATPase is derived from aerobic glycolysis (Pellerin and Magistretti 1996; Magistretti and Chatton 2005). The use of aerobic glycolysis by Na^+/K^+-ATPase is not unique to the astrocyte. It fuels Na^+/K^+-ATPase in all cells that possess this membrane-bound pump (Pellerin and Magistretti 1996) including neurons (Wu, Aoki et al. 1997).

The use of aerobic glycolysis as an energy source may seem surprising because it is inefficient: glycolysis produces a net 2 ATP versus 32 ATP for complete oxidation to carbon dioxide and water. However, it produces ATP at a rate much faster than oxidative phosphorylation making it uniquely suited to accommodate small, rapidly changing requirements in energy for Na^+/K^+-ATPase. In this regard it is probably not fortuitous that brain glycogen, a ready source of glucose, resides exclusively in astrocytes (Brown 2004) .

A more extended view of the role of aerobic glycolysis has emerged from the observation that glycolytic enzymes are found in the postsynaptic density or PSD (Wu, Aoki et al. 1997), a very dynamic protein complex containing various glutamate receptor complexes concentrated at the site of contact with the presynaptic terminal (Kennedy and Ehlers 2006). While Na^+/K^+-ATPase is likely a consumer of glycolytically-generated ATP at the PSD it has been posited that some of this ATP may also be used to fuel protein synthesis (Wu, Aoki et al. 1997).

A further role for aerobic glycolysis in the PSD has been suggested by the finding of a selective co-localization of MCT2, the neuronal monocarboxylate transporter used to move lactate, with AMPA receptor GluR2/3 (Bergersen, Magistretti et al. 2005). This associates aerobic glycolysis with AMPA receptor trafficking and its role in synaptic plasticity raising the possibility that among the causes of high levels of aerobic glycolysis may be anabolic processes that require glycolysis for the cycling of cell components in the service of processes involved in memory and learning. The presence of MCT2 in the PSD provides a means of moving the lactate resulting from aerobic glycolysis to the extracellular fluid where it may be further utilized or removed from the brain.

Glucose makes important contributions to anabolic processes in all organs of the body providing needed intermediates for cellular proliferation including NADPH, nucleotides for DNA replication, and intermediates for fatty acid synthesis (Gaitonde, Jones et al. 1987; DeBerardinis, Mancuso et al. 2007) largely by way of the pentose phosphate pathway (PPP). In the adult brain it is estimated that 5-10% of the glucose consumed may enter the PPP. Several lines of research provide a perspective from which to evaluate its potential significance. These include brain development and the sleep-wake cycle in adults.

In the developing nervous system, aerobic glycolysis appears to play a substantial role, consistent with its potential to provide the building blocks for cell development and proliferation. In a study of 9 normal infants (age range 1-12 months) under general anesthesia, Settergren and colleagues measured $CMRO_2$ and CMRGlu (Settergren, Lindblad et al. 1976). Their data indicate that fully 35% of the glucose consumed is utilized outside of oxidative phosphorylation compared to 10% in the adult. Combining

much more limited data from two studies of preterm infants (Altman, Perlman et al. 1993; Powers, Rosenbaum et al. 1998) indicates that, prior to birth, glycolysis may account for over 90% of the glucose consumed. Unfortunately, we do not know how aerobic glycolysis is apportioned among its several potential roles.

The developmental trajectory of CMRGlu in the human brain has been best characterized in the work of Chugani and colleagues (Chugani, Phelps et al. 1987). They studied a cohort of 29 children ranging in age from 5 days to 15 years. Measurements were performed with ^{18}F-fluoro-deoxyglucose and PET. At birth, values were approximately 70% of adult values. By 2 years of age the CMRGlu had risen to adult values but continued to rise through years 3 to 4 achieving levels almost twice that of the adult. These very high levels were maintained until approximately age 9 when they were observed to commence a slow decline to adult levels. As they point out, this temporal profile of CMRGlu in the human brain corresponds rather well to an initial overproduction neuropil components followed by an elimination of excessive cells and their processes.

Missing from these important data (Chugani, Phelps et al. 1987) are measures of the level of aerobic glycolysis across development. One can only speculate from other data (Altman, Perlman et al. 1993; Powers, Rosenbaum et al. 1998) that, in the newborn, it is a much higher fraction of the CMRGlu than in the adult. Is the dramatic increase in the CMRGlu during the years in which the brain is rapidly developing primarily accounted for by an increase in aerobic glycolysis? Surprisingly, we do not know the answer. Of particular importance would be information on the amount of glucose entering the PPP because of the critical role it plays in synthetic processes in the brain. It

is reasonable to posit that a major factor driving the increase of glucose consumption in the developing brain are the demands associated with synthesizing an expanding neuropil. Future research must focus on these critical gaps in our knowledge.

If, indeed, aerobic glycolysis plays a critical role in the synthesis of brain constituents in the developing brain, is there any remnant of that role in the adult brain to account for some of its ongoing aerobic glycolysis? Much interest as well as controversy has surrounded the possibility that new neurons are produced in the adult brain (Gage, Kempermann et al. 1998). Regardless of the resolution of that controversy such cells are few in number and have been primarily found in the hippocampus, an area of the brain we find to have a low level of aerobic glycolysis (see Table 2.6).

However, to focus on the creation of new cells as a possible requirement for ongoing aerobic glycolysis in the adult brain overlooks the fact that 'old' cells are continually being updated and remodeled. As Eve Marder has pointed out "…neurons can live for up to 100 years" yet "…the ion channels and receptors that underlie electrical signaling and synaptic transmission turn over in the membrane in minutes, hours, days or weeks" (Marder and Goaillard 2006) These dynamic processes undoubtedly call upon the brain's anabolic machinery to which aerobic glycolysis is known to contribute significantly. While evidence for the participation of aerobic glycolysis in ongoing anabolic activity in the adult brain is limited and, to some extent inferential (see above), it is complemented by studies of the sleep-wake cycle in adult humans.

One attractive hypothesis associates wakefulness with synaptic potentiation and sleep with synaptic depression (Tononi and Cirelli 2003), a cycle that facilitates learning

and memory through experience while preserving long-term synaptic balance. With regard to the metabolic accompaniments of this cycle, evidence exists that learning a difficult task is accompanied not only by the expected increase in aerobic glycolysis during task performance but also a persistence of aerobic glycolysis long after the task has been completed (Madsen, Hasselbalch et al. 1995). Set in the context of a day's wakeful experiences, this is consistent with the observation that CMRGlu, $CMRO_2$ (Boyle, Scott et al. 1994) and CBF (Boyle, Scott et al. 1994; Braun, Balkin et al. 1997) all increase over a period of wakefulness but CMRGlu disproportionately so. As a result the level of aerobic glycolysis rises significantly during wakefulness (Boyle, Scott et al. 1994), returning to normal levels with sleep (Vyazovskiy, Cirelli et al. 2008). One interpretation of these observations is that synaptic potentiation is associated with ongoing anabolic activity at synapses supported by increased aerobic glycolysis. Sleep-induced synaptic depression (Vyazovskiy, Cirelli et al. 2008) reverses this process with an attendant reduction in aerobic glycolysis. A clear test of this hypothesis would be the demonstration that the wakefulness-induced increase in aerobic glycolysis is accounted for by increased activity of the PPP.

We have assessed regional differences in resting $CMRO_2$, CMRGlu and aerobic glycolysis in a manner independent of whole brain quantitative measures. This strategy (see Methods) differs somewhat from that originally described by us (Raichle, Martin et al. 1983; Mintun, Raichle et al. 1984; Martin, Powers et al. 1987; Fox, Raichle et al. 1988) in which absolute rates for CMRGlu and $CMRO_2$ were determined. The primary advantage of the present strategy is its improved accuracy in determining the regional variations in $CMRO_2$ and CMRGlu. This is due to the elimination of rapid arterial blood

sampling for the determination of an arterial input function for quantitative measurements of $CMRO_2$ and CMRGlu. Arterial blood sampling of rapidly time-varying radioactivity is an inherently noisy measurement which would have significantly compromised our ability to accurately assess levels of metabolism regionally. Because our primary interest was in regional variations in our measurements and not absolute values we elected to forego arterial blood sampling in this study.

The level of aerobic glycolysis is normally obtained from the molar ratio of $CMRO_2$ to CMRGlu. This ratio, known as the oxygen-glucose index or OGI, is 6 when all of the glucose consumed by the brain is oxidized to carbon dioxide and water. In the present study we have assessed variations in the OGI in two ways. First, we have calculated regional variations in the OGI by assuming a mean value for the whole brain of 5.323 (Raichle, Posner et al. 1970). Second, we have estimated the levels of aerobic glycolysis in the brain from the residuals of a regression of local-to-global ratios of $CMRO_2$ as a function of CMRGlu (Figure 2.2). This provided us with a glycolytic index or GI. This approach has three advantages: first, it is not based on an assumed whole-brain average value of the OGI; second, it is more intuitive in that it varies directly with the level of aerobic glycolysis in contrast with the OGI which varies inversely; and, third, it is less sensitive to noise from $CMRO_2$ measurements. The OGI and GI approaches were well correlated (r= -0.986).

$CMRO_2$ and CMRGlu each varied greatly across the brain (Figure 2.1) but were highly correlated (r=0.869) over regions (Table 2.2). These findings are consistent with a regional relationship between $CMRO_2$ and CMRGlu which has been assumed for many years despite the almost total lack of directly supporting data in vivo. Cerebral blood

37

flow (CBF; Figure 2.1) exhibited an almost identical variability and, as expected, was highly correlated with both $CMRO_2$ (r=0.822) and CMRGlu (r=0.869). These highly correlated relationships among CBF, $CMRO_2$ and CMRGlu have often led investigators to assume, we believe incorrectly, that they are equivalent in providing an assessment of the regional variability in brain energy metabolism. Because of the relative ease of measuring CBF and CMRGlu as compared to $CMRO_2$, the former two have been the most commonly used in this regard. For a more complete assessment of the brain's metabolic activity and aerobic glycolysis in particular, however, knowledge of the ratio of $CMRO_2$ to CMRGlu is required as demonstrated in the data we report here.

Summing up, the significant finding of the present study is that ongoing aerobic glycolysis in the adult human brain is not uniformly distributed. The high levels of ongoing aerobic glycolysis in systems associated with self-referential processing and memory, both working and episodic, suggests that anabolic processes, for which aerobic glycolysis is known to play a critical role, may well be particularly active in these systems. Moving forward, research on brain metabolism must distinguish between the roles of aerobic glycolysis and oxidative phosphorylation with particular attention to the unique contributions of the former in energizing membrane bound processes and providing critical building blocks for cellular constituents which, even in the adult nervous system, may be turning over rapidly to accommodate memory and learning. Understanding these relationships more thoroughly will not only advance our understanding of brain function but will also enlighten us with regard to diseases of the nervous system such as Alzheimer's disease (Li, Nowotny et al. 2004) and Huntington's disease (Powers, Videen et al. 2007) in which alterations of glycolysis have been

implicated in their pathophysiology. With regard to Alzheimer's disease, we note that the distribution of pathology in this condition remarkably falls within the brain's regions of high resting glycolysis (Buckner, Snyder et al. 2005).
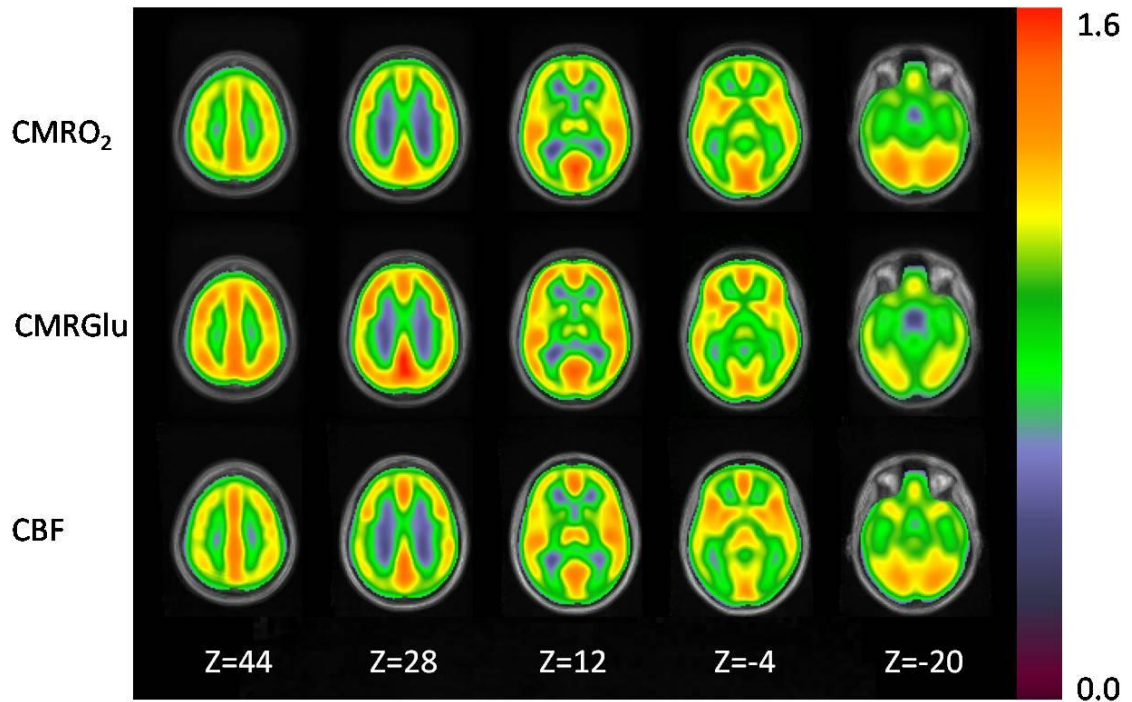
Figure 2.1: Global maps of cerebral blood flow and metabolism.

Average maps of oxygen consumption (Upper; $CMRO_2$), glucose consumption (Middle; CMRGlu), and cerebral flood flow (Lower; CBF) were computed using data collected in the eyes-closed awake state and averaged across 33 subjects. Because we were interested in regional changes, the whole brain mean was set to 1.0. Note the large deviations in oxygen and glucose consumption across the brain, most prominently between gray and white matter. Despite regional variations, $CMRO_2$, CMRGlu and CBF generally are matched across most of the brain.
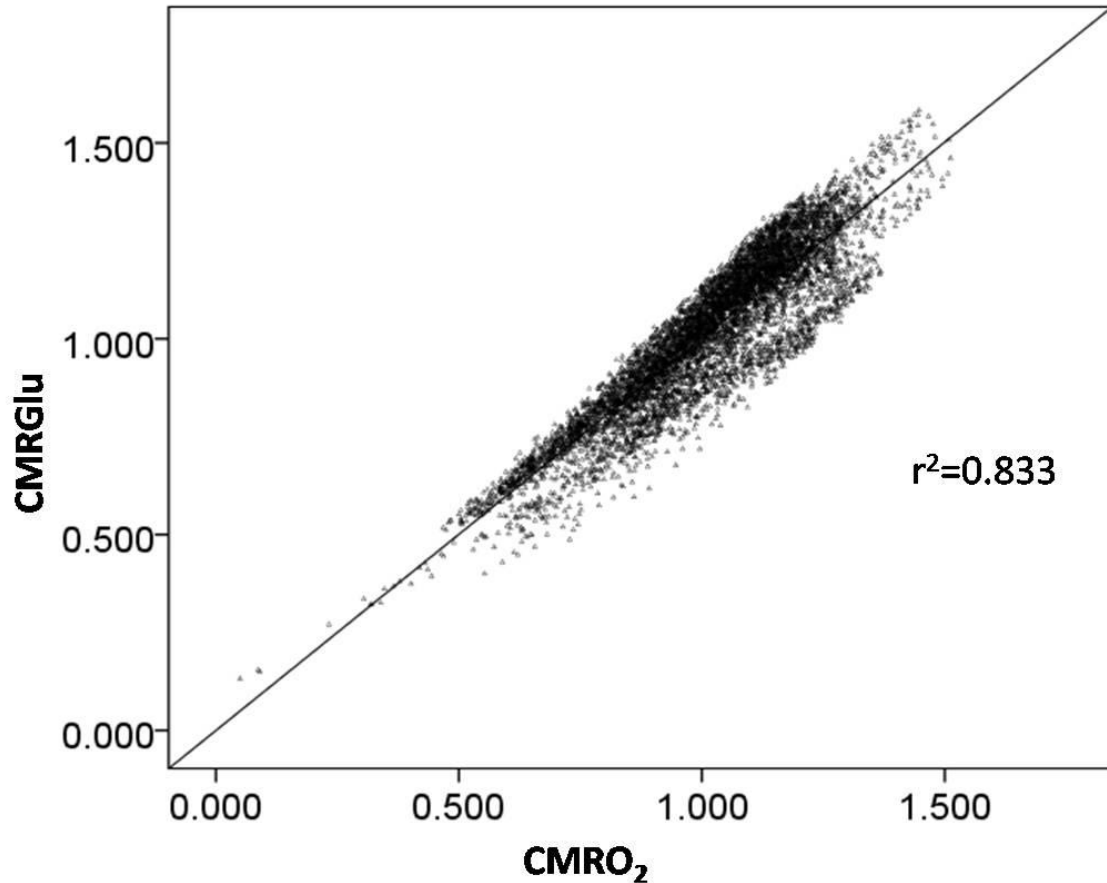
Figure 2.2: Voxelwise linear regression of glucose consumption (CMRGlu) on oxygen consumption (CMRO2).

For illustration purposes, data from group average CMRGlu and $CMRO_2$ is shown here. However, regression was performed individually for each subject to compute individual glycolytic index maps. Although CMRGlu and $CMRO_2$ were highly correlated (r=0.913), voxel clusters that systematically deviate from the line of regression are evident. In particular, the cluster below the line of regression corresponds to regions of significantly low GI, found predominantly in the cerebellum and inferior temporal cortex.
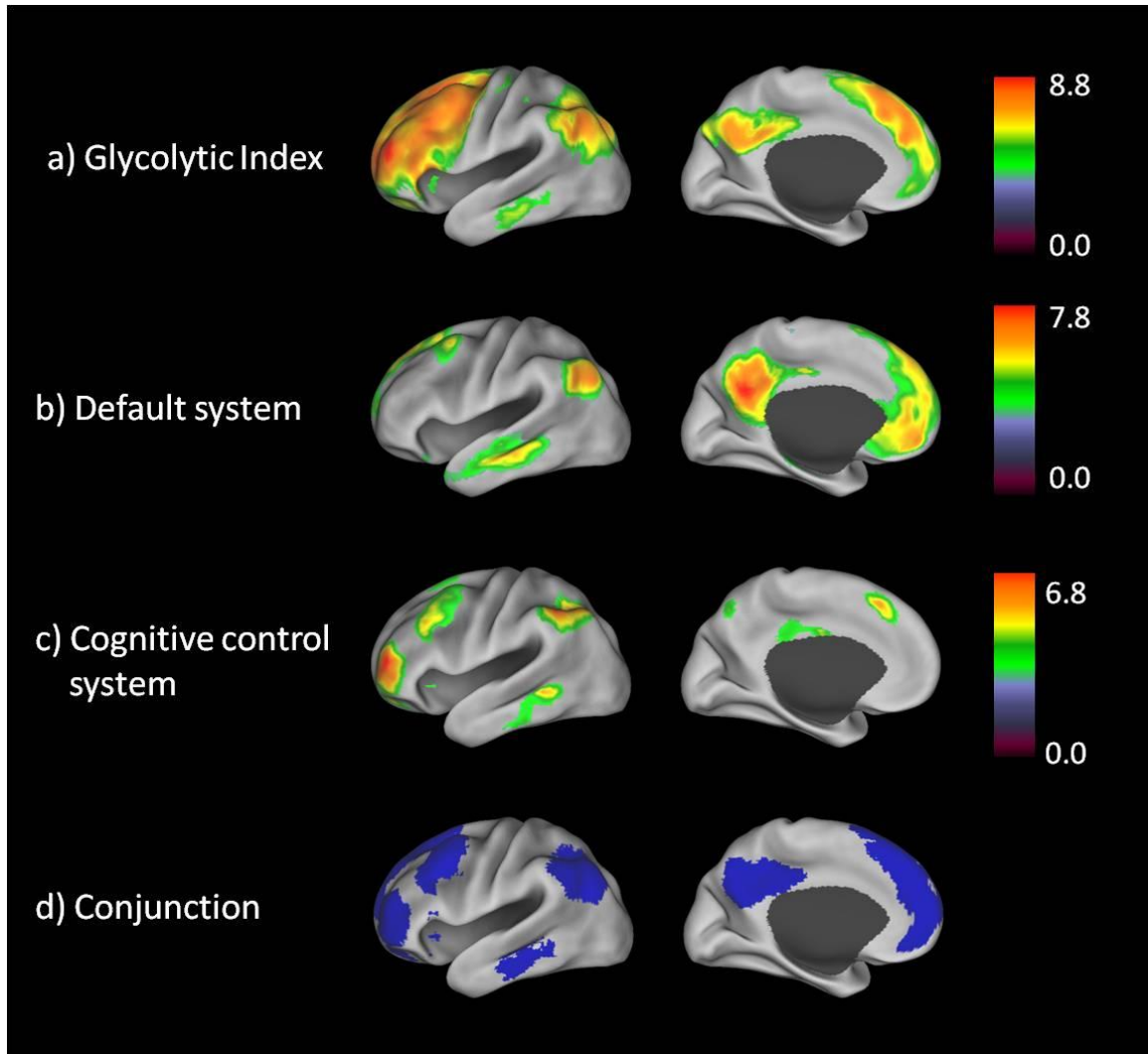
Figure 2.3: Conjunction analysis between resting aerobic glycolysis (Glycolytic Index; GI) and BOLD correlation maps of the default and cognitive control systems.

(**a**): Regions with elevated aerobic glycolysis (n=33, groupwise t-test, Z>4.4, p<0.0001, cluster >99, corrected for multiple comparisons). (**b**): Default system as delineated by BOLD correlation mapping (n=20, groupwise t-test, Z>3.0, p<0.01, cluster >17, corrected for multiple comparisons). (**c**): Cognitive control system defined as in (b). (**d**): Intersection of voxels showing significantly elevated GI and membership in either the default or cognitive control systems.

Regions	Z-score	Coordinates	Volume (cm^3)	GI	OGI	CMRO$_2$	CMRGlu	CBF	CBV	OEF
Prefrontal Cortex	9.30	[41 13 34]	271.36	102.74±18.92	4.61±0.11	1.07±0.02	1.18±0.02	1.10±0.02	1.05±0.11	0.98±0.01
L Lateral Parietal	9.06	[-41 -61 36]	33.17	85.55±22.35	4.70±0.16	1.10±0.02	1.19±0.03	1.06±0.03	0.64±0.14	1.04±0.02
R Lateral Parietal	8.16	[47 -57 40]	30.38	82.37±26.97	4.71±0.16	1.11±0.03	1.19±0.03	1.08±0.03	0.60±0.10	1.03±0.02
Posterior Cingulate	8.03	[1 -59 24]	29.97	107.55±29.18	4.73±0.16	1.30±0.04	1.39±0.04	1.27±0.03	1.21±0.21	1.02±0.02
Gyrus rectus	7.25	[31 27 -14]	4.51	75.15±32.94	4.76±0.22	1.02±0.04	1.08±0.05	1.03±0.05	1.09±0.16	0.99±0.03
R Lateral Temporal	6.30	[61 -35 -8]	6.85	66.45±35.03	4.75±0.20	1.10±0.04	1.16±0.05	1.06±0.04	0.90±0.25	1.03±0.03
L Lateral Temporal	6.01	[-57 -31 -18]	5.26	64.88±34.36	4.71±0.24	1.02±0.06	1.09±0.06	1.00±0.05	1.49±0.50	1.02±0.05
R Caudate	5.95	[7 9 8]	1.34	78.45±56.24	4.47±0.32	0.84±0.09	0.94±0.11	0.86±0.10	1.06±0.21	0.98±0.07
L Caudate	5.65	[-11 5 16]	1.09	79.08±61.48	4.55±0.39	0.94±0.10	1.04±0.09	0.95±0.09	1.05±0.15	0.99±0.05
L Inferior Temporal	-8.00	[1 -11 -24]	26.89	-94.52±22.88	5.67±0.28	0.92±0.04	0.83±0.03	0.99±0.04	1.24±0.16	0.94±0.03
R Inferior Temporal	-8.18	[33 5 -18]	32.86	-101.59±21.21	5.70±0.22	0.93±0.03	0.83±0.03	1.00±0.03	1.16±0.14	0.93±0.03
Cerebellum	-8.98	[1 -61 -22]	259.42	-143.46±25.05	5.94±0.23	1.04±0.03	0.89±0.03	1.06±0.03	1.08±0.12	0.98±0.02

Table 2.1: Regions with elevated aerobic glycolysis.

Aerobic glycolysis (Glycolytic Index; GI) significantly (p<0.0001) different from the line of regression (n=33, groupwise *t*-test, Z>4.4, cluster >99, corrected for multiple comparisons) under the assumption of a homogenous normal bivariate distribution of CMRO$_2$ and CMRGlu. Data are shown as mean ± SD. Coordinates represent peak GI Z-score location in the Talairach system. GI, glycolytic index; CMRO$_2$, cerebral metabolic rate of oxygen; CMRGlu, cerebral metabolic rate of glucose; CBF, cerebral blood flow; CBV, cerebral blood volume; OEF, oxygen extraction fraction.

43

Correlations	GI	OGI	CMRO$_2$	CMRGlu	CBF	CBV	OEF
GI	1	-0.986[a]	0.243[c]	0.690[a]	0.501[a]	0.072	-0.223[c]
OGI		1	-0.119	-0.591[a]	-0.384[a]	-0.115	0.280[b]
CMRO$_2$			1	0.869[a]	0.822[a]	-0.385[a]	0.637[a]
CMRGlu				1	0.869[a]	-0.249[c]	0.361[a]
CBF					1	-0.065	0.086
CBV						1	-0.593[a]
OEF							1

Table 2.2: Correlations over Brodmann regions between metabolic variables.

GI, glycolytic index; OGI, oxygen-to-glucose index; CMRO$_2$, cerebral metabolic rate of oxygen; CMRGlu, cerebral metabolic rate of glucose; GI, glycolytic index; CBF, cerebral blood flow; CBV, cerebral blood volume; OEF, oxygen extraction fraction. [a]$p<0.001$; [b]$p<0.01$, [c]$p<0.05$.
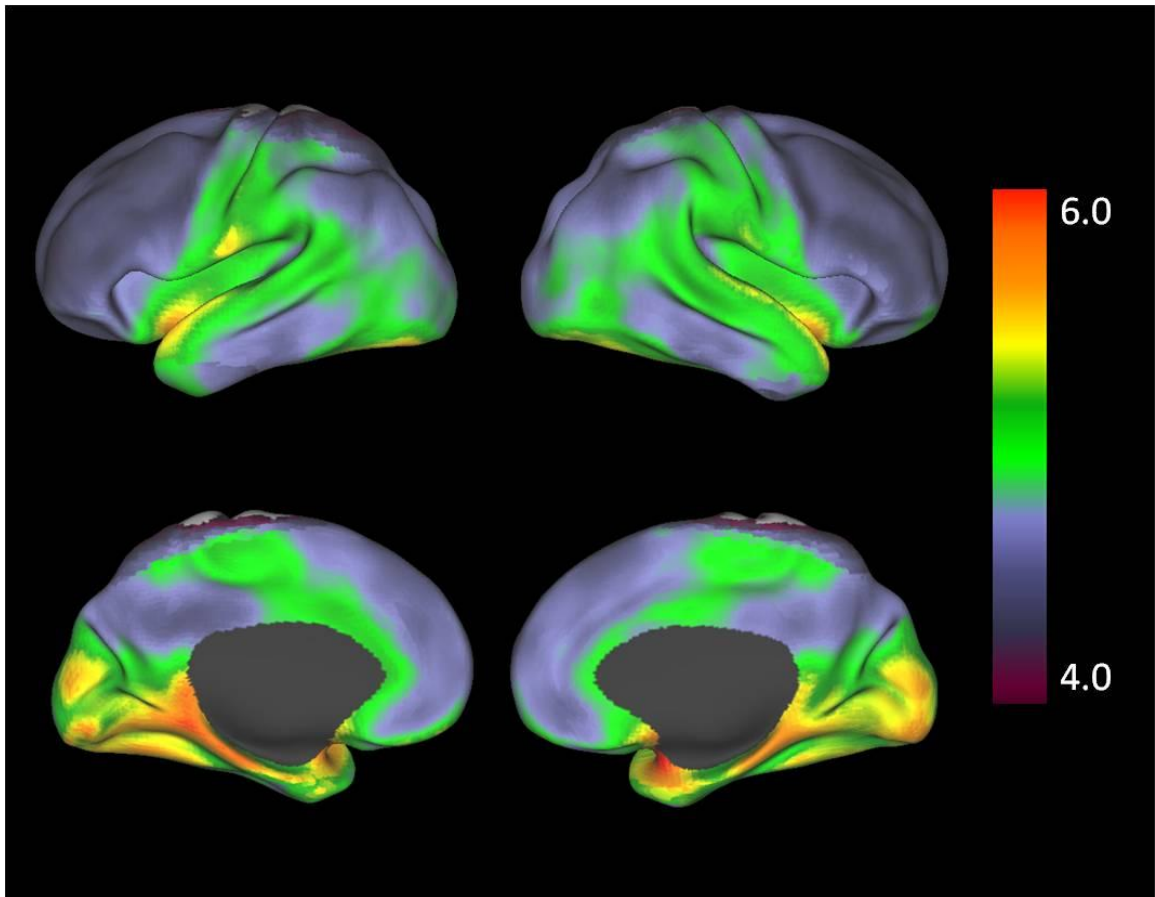
Figure 2.4: Average map of the oxygen-to-glucose index.

The whole brain mean is set to a molar ratio of 5.323 as derived from Raichle et al., 1970. Lower OGI values represent regions with higher levels of aerobic glycolysis. These regions include medial and dorsolateral prefrontal cortex, posterior cingulate, and lateral parietal lobes. Regions with high OGI values include the cerebellum (not shown).
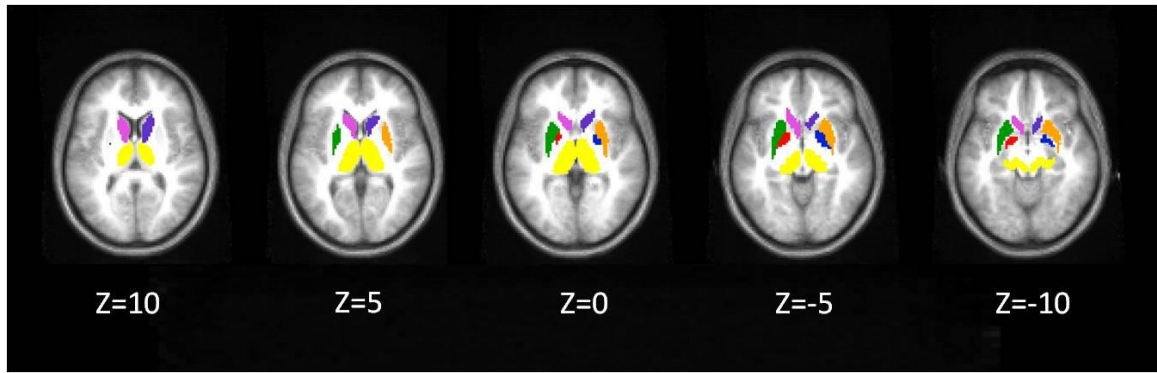
Figure 2.5: Subcortical regions of interest.

Regions were manually defined on our representative Talairach atlas.
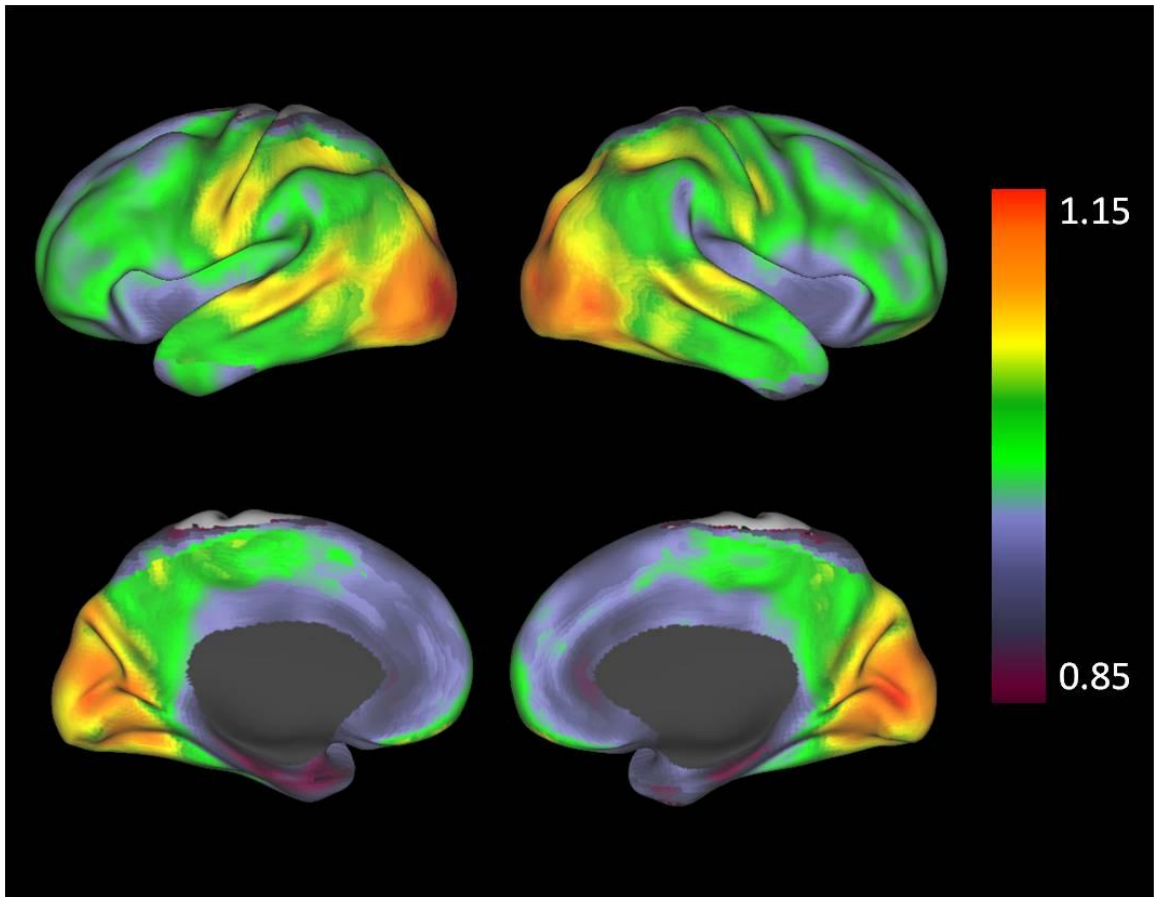
Figure 2.6: Average map of the oxygen extraction fraction.

The whole brain mean is set to 1.0. Note high OEF in occipital cortex, and especially primary visual cortex.
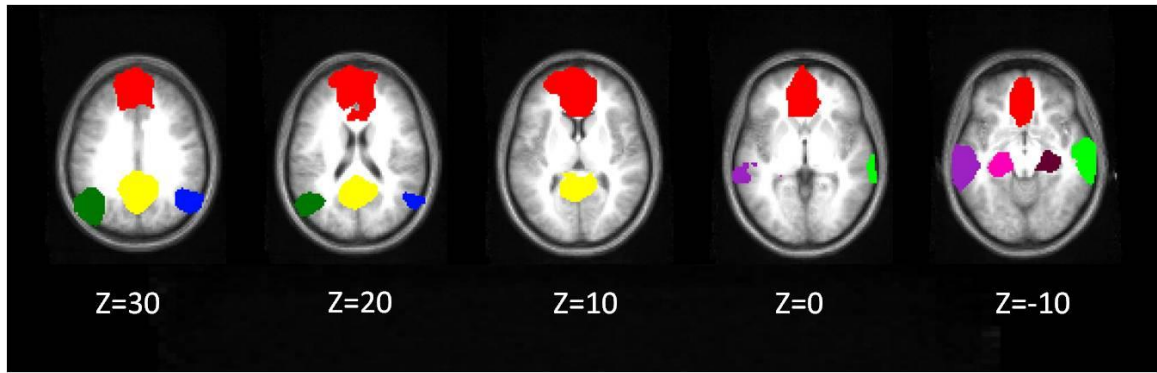
Figure 2.7: Default system regions of interest.

Regions were identified by resting state BOLD correlation mapping (n=20, Z>3.0, p<0.01, cluster >17, corrected for multiple comparisons). Correlations were computed between all voxels in the brain and the signal averaged within a distributed seed region comprised of three 6mm radius spheres placed in medial prefrontal cortex (MPF, [-1, 47, -4]), posterior cingulate/precuneus (PCC, [-5, -49, 40]), and lateral parietal cortex (LP, [-45, -67, 36]).
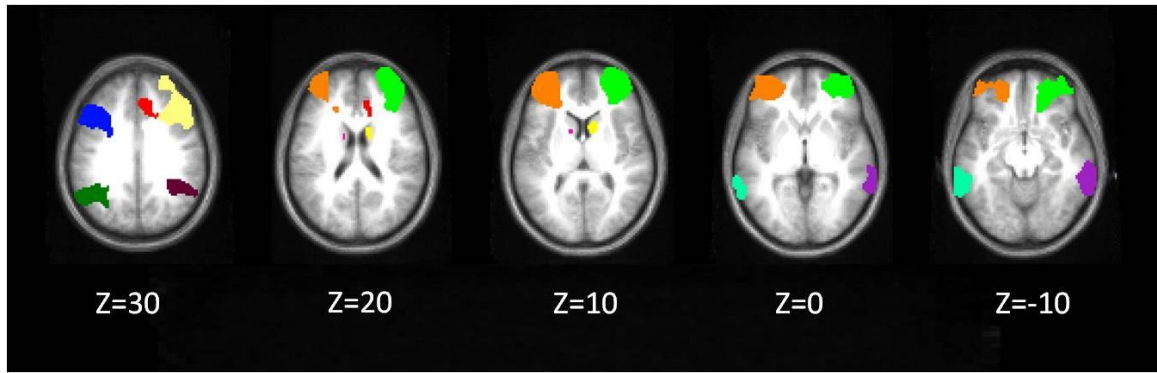
Figure 2.8: Cognitive control system regions of interest.

Regions were identified by resting state BOLD correlation mapping. The distributed seed region was comprised of four 6mm radius spheres placed bilaterally in dorsolateral prefrontal cortex (DLPFC,[-34, 51, 12], [24, 50, 13]) and anterior parietal cortex (aIPL, [-43, -55, 42], [48, -47, 42]).

Left Hemisphere	Volume (cm³)	GI	OGI	CMRO$_2$	CMRGlu	CBF	CBV	OEF
BA1	5.27	5.67±37.66	5.00±0.27	1.02±0.06	1.03±0.06	0.99±0.05	0.86±0.25	1.03±0.02
BA2	5.90	18.82±31.65	5.00±0.21	1.09±0.04	1.11±0.03	1.04±0.04	0.89±0.23	1.05±0.02
BA3	3.69	25.76±34.70	4.95±0.21	1.08±0.05	1.11±0.05	1.04±0.04	0.95±0.18	1.04±0.02
BA4	14.79	31.55±23.85	4.95±0.16	1.09±0.04	1.11±0.04	1.06±0.04	1.12±0.29	1.02±0.02
BA5	3.49	16.33±38.92	5.00±0.27	1.14±0.06	1.15±0.05	1.10±0.05	0.96±0.43	1.03±0.04
BA6	11.80	93.29±31.18	4.68±0.16	1.11±0.03	1.20±0.04	1.12±0.03	1.14±0.22	0.99±0.02
BA7	11.23	80.41±30.98	4.74±0.16	1.18±0.03	1.25±0.03	1.14±0.03	0.70±0.21	1.04±0.02
BA8	6.65	113.46±28.78	4.52±0.16	1.07±0.04	1.18±0.04	1.12±0.04	1.17±0.36	0.95±0.03
BA9	8.63	113.10±37.41	4.58±0.16	1.08±0.03	1.19±0.04	1.11±0.04	1.04±0.18	0.97±0.03
BA10	8.66	107.58±37.48	4.63±0.16	1.11±0.03	1.22±0.05	1.13±0.03	0.98±0.14	0.99±0.02
BA11	10.38	48.05±45.12	4.84±0.27	1.04±0.04	1.09±0.05	1.05±0.05	1.10±0.15	0.99±0.04
BA17	5.89	-23.09±52.50	5.27±0.21	1.35±0.06	1.30±0.07	1.23±0.06	0.95±0.24	1.10±0.03
BA18	11.32	-5.25±42.14	5.11±0.27	1.18±0.05	1.16±0.05	1.09±0.05	0.77±0.12	1.09±0.03
BA19	16.21	13.04±36.40	5.06±0.21	1.14±0.03	1.15±0.05	1.05±0.03	0.82±0.15	1.09±0.03
BA20	8.70	-33.79±25.66	5.16±0.21	0.93±0.05	0.91±0.05	0.95±0.05	1.21±0.20	0.97±0.03
BA21	4.10	26.41±31.66	4.84±0.21	0.94±0.05	0.98±0.06	0.93±0.05	1.39±0.31	1.02±0.04
BA22	12.50	23.91±28.99	4.95±0.21	1.13±0.04	1.15±0.04	1.09±0.04	1.15±0.19	1.04±0.02
BA23	2.53	114.90±56.36	4.63±0.21	1.22±0.07	1.33±0.11	1.23±0.07	1.67±0.60	0.99±0.03
BA24	6.46	19.67±35.60	4.95±0.21	1.03±0.07	1.05±0.07	1.09±0.07	1.18±0.25	0.94±0.03
BA25	0.89	-37.89±58.49	5.27±0.37	1.09±0.08	1.05±0.08	1.17±0.09	1.24±0.29	0.93±0.06
BA26	0.17	-41.83±77.93	5.32±0.48	0.93±0.11	0.90±0.14	0.96±0.11	1.55±0.72	0.98±0.07
BA27	0.62	-106.52±60.63	5.70±0.48	0.99±0.06	0.89±0.07	1.08±0.05	1.19±0.26	0.92±0.04
BA28	1.06	-65.73±63.44	5.38±0.48	0.94±0.06	0.88±0.05	1.04±0.05	1.07±0.13	0.90±0.04
BA29	0.29	-37.14±85.71	5.32±0.48	1.04±0.11	1.01±0.14	1.05±0.10	1.61±0.68	1.00±0.06
BA30	0.68	7.34±69.17	5.11±0.32	1.20±0.09	1.20±0.11	1.17±0.09	1.66±0.60	1.03±0.05
BA31	3.31	99.65±49.57	4.74±0.21	1.26±0.04	1.34±0.05	1.24±0.04	1.43±0.42	1.02±0.03
BA32	4.86	79.07±31.75	4.74±0.21	1.13±0.04	1.21±0.05	1.20±0.04	1.10±0.24	0.95±0.03
BA33	0.94	-14.95±36.04	5.11±0.32	0.90±0.08	0.90±0.07	0.98±0.09	1.15±0.18	0.93±0.05
BA35	0.54	-118.80±66.21	5.75±0.48	1.02±0.07	0.90±0.08	1.07±0.05	1.24±0.31	0.96±0.04
BA36	2.03	-85.38±47.11	5.54±0.43	0.89±0.05	0.82±0.04	1.00±0.05	1.15±0.17	0.89±0.04
BA37	8.12	-30.60±36.93	5.22±0.27	1.15±0.05	1.11±0.04	1.10±0.05	1.15±0.31	1.05±0.03
BA38	6.19	-58.43±27.13	5.32±0.21	0.96±0.04	0.91±0.04	1.00±0.05	1.12±0.25	0.96±0.04
BA39	5.41	65.91±30.41	4.79±0.21	1.17±0.03	1.23±0.04	1.12±0.04	0.70±0.14	1.05±0.02
BA40	6.20	32.81±29.24	4.90±0.21	1.12±0.04	1.15±0.05	1.11±0.04	0.80±0.15	1.01±0.04
BA41	1.80	-2.06±43.44	5.11±0.27	1.10±0.08	1.09±0.08	1.10±0.08	0.97±0.15	1.00±0.03
BA42	3.18	40.71±47.61	4.90±0.27	1.16±0.07	1.19±0.06	1.15±0.08	0.98±0.17	1.01±0.03
BA43	2.06	-29.03±45.97	5.22±0.32	1.13±0.04	1.09±0.06	1.09±0.05	1.06±0.14	1.04±0.04
BA44	3.19	116.19±52.34	4.63±0.21	1.18±0.05	1.29±0.06	1.19±0.06	1.04±0.13	0.99±0.03
BA45	1.76	124.67±47.59	4.58±0.27	1.14±0.06	1.27±0.06	1.15±0.06	1.07±0.17	0.99±0.04
BA46	3.70	137.20±51.07	4.52±0.21	1.16±0.04	1.29±0.06	1.17±0.05	1.02±0.18	0.99±0.04
BA47	1.06	94.47±65.54	4.68±0.32	1.12±0.06	1.21±0.08	1.13±0.07	1.15±0.19	1.00±0.05

Table 2.3: Metabolism (mean ± SD) for each Brodmann region in the left hemisphere.

Regions from Caret atlas. GI, glycolytic index; OGI, oxygen-to-glucose index; CMRO$_2$, cerebral metabolic rate of oxygen; CMRGlu, cerebral metabolic rate of glucose; CBF, cerebral blood flow; CBV, cerebral blood volume; OEF, oxygen extraction fraction

Right Hemisphere	Volume (cm³)	GI	OGI	CMRO₂	CMRGlu	CBF	CBV	OEF
BA1	4.42	21.87±32.84	4.95±0.21	1.04±0.06	1.06±0.07	1.03±0.06	0.83±0.25	1.01±0.03
BA2	5.31	28.19±32.02	4.95±0.21	1.12±0.03	1.14±0.04	1.08±0.04	0.85±0.25	1.03±0.03
BA3	3.47	30.01±38.45	4.95±0.21	1.10±0.04	1.13±0.06	1.07±0.05	0.97±0.19	1.03±0.03
BA4	13.96	34.61±29.10	4.90±0.21	1.08±0.04	1.11±0.04	1.08±0.05	1.07±0.29	1.01±0.03
BA5	3.37	14.22±41.88	5.00±0.27	1.14±0.06	1.15±0.05	1.12±0.05	0.85±0.31	1.02±0.04
BA6	11.50	86.61±27.34	4.68±0.16	1.13±0.03	1.21±0.03	1.14±0.03	1.18±0.27	0.99±0.02
BA7	10.54	74.28±33.47	4.79±0.21	1.18±0.04	1.25±0.04	1.14±0.03	0.66±0.18	1.04±0.03
BA8	6.10	113.08±41.46	4.58±0.16	1.07±0.04	1.18±0.05	1.12±0.04	1.29±0.50	0.95±0.03
BA9	8.06	113.66±35.10	4.58±0.16	1.08±0.04	1.20±0.05	1.11±0.03	1.09±0.24	0.97±0.03
BA10	8.74	102.76±39.08	4.63±0.21	1.09±0.04	1.19±0.05	1.10±0.04	1.00±0.15	0.99±0.02
BA11	11.22	55.17±44.56	4.84±0.27	1.04±0.03	1.09±0.05	1.04±0.04	1.05±0.12	1.00±0.03
BA17	5.78	-33.69±60.77	5.32±0.37	1.35±0.07	1.29±0.06	1.22±0.06	0.88±0.21	1.11±0.04
BA18	11.06	-4.46±59.09	5.16±0.37	1.20±0.04	1.19±0.06	1.11±0.04	0.73±0.12	1.09±0.03
BA19	16.79	18.93±35.74	5.00±0.27	1.12±0.03	1.13±0.04	1.04±0.03	0.71±0.09	1.08±0.03
BA20	9.45	-26.06±31.16	5.11±0.21	0.93±0.04	0.91±0.04	0.95±0.04	1.28±0.28	0.98±0.03
BA21	4.84	40.57±32.89	4.84±0.21	0.98±0.05	1.03±0.05	0.97±0.05	1.16±0.26	1.02±0.03
BA22	12.89	19.68±29.82	5.00±0.21	1.13±0.03	1.15±0.04	1.09±0.03	1.02±0.12	1.04±0.02
BA23	2.48	95.65±61.33	4.74±0.27	1.24±0.08	1.32±0.10	1.24±0.07	1.48±0.59	1.00±0.03
BA24	6.59	36.66±37.02	4.90±0.21	1.04±0.06	1.08±0.07	1.11±0.07	1.14±0.32	0.94±0.03
BA25	1.45	-34.04±60.35	5.22±0.37	1.07±0.06	1.03±0.06	1.15±0.08	1.18±0.23	0.93±0.04
BA26	0.17	-43.11±52.00	5.22±0.43	0.87±0.13	0.84±0.13	0.91±0.11	1.21±0.55	0.96±0.06
BA27	0.55	-85.86±72.82	5.54±0.53	0.99±0.08	0.91±0.06	1.06±0.07	1.00±0.15	0.93±0.06
BA28	0.94	-62.64±54.79	5.38±0.37	0.94±0.06	0.88±0.04	1.04±0.05	1.06±0.32	0.90±0.04
BA29	0.30	-48.28±61.80	5.32±0.43	1.00±0.13	0.96±0.11	1.01±0.11	1.31±0.59	1.00±0.05
BA30	0.81	4.80±60.40	5.06±0.32	1.14±0.12	1.14±0.12	1.11±0.10	1.23±0.40	1.03±0.04
BA31	3.34	92.19±41.56	4.79±0.21	1.27±0.05	1.34±0.05	1.25±0.04	1.29±0.33	1.02±0.03
BA32	5.53	68.35±31.35	4.74±0.21	1.07±0.04	1.14±0.04	1.12±0.04	1.11±0.32	0.96±0.02
BA33	0.86	8.51±51.10	4.95±0.37	0.90±0.08	0.92±0.08	0.98±0.08	1.04±0.22	0.92±0.04
BA35	0.52	-84.98±67.28	5.54±0.48	1.02±0.09	0.94±0.07	1.06±0.07	1.02±0.16	0.96±0.05
BA36	1.91	-88.14±42.45	5.54±0.37	0.90±0.04	0.83±0.03	0.99±0.04	1.07±0.17	0.91±0.04
BA37	9.13	-12.76±28.33	5.11±0.21	1.14±0.05	1.12±0.04	1.09±0.05	1.06±0.25	1.05±0.02
BA38	6.94	-55.31±32.35	5.32±0.27	0.97±0.03	0.92±0.04	1.01±0.04	1.08±0.13	0.97±0.03
BA39	5.10	65.06±38.42	4.84±0.21	1.19±0.04	1.25±0.05	1.14±0.06	0.63±0.11	1.04±0.03
BA40	5.50	32.75±39.47	4.95±0.21	1.14±0.04	1.17±0.04	1.15±0.04	0.73±0.17	1.00±0.04
BA41	1.82	5.48±35.69	5.00±0.27	1.07±0.07	1.08±0.07	1.11±0.07	1.01±0.15	0.97±0.04
BA42	3.32	40.58±37.08	4.90±0.21	1.21±0.05	1.24±0.05	1.22±0.06	0.98±0.08	0.99±0.03
BA43	2.15	-8.03±50.87	5.11±0.27	1.08±0.05	1.06±0.05	1.06±0.05	1.08±0.17	1.01±0.04
BA44	2.91	122.43±35.08	4.63±0.16	1.20±0.04	1.32±0.05	1.21±0.05	1.08±0.17	0.99±0.03
BA45	1.96	118.96±52.51	4.58±0.27	1.09±0.07	1.20±0.08	1.10±0.06	1.07±0.12	0.99±0.04
BA46	3.90	141.55±39.14	4.52±0.16	1.15±0.05	1.29±0.05	1.16±0.05	1.03±0.16	0.99±0.03
BA47	1.22	103.28±53.71	4.63±0.27	1.04±0.07	1.14±0.08	1.05±0.07	1.11±0.17	1.00±0.04

Table 2.4: Metabolism (mean ± SD) for each Brodmann region in the right hemisphere.

Regions from Caret atlas. GI, glycolytic index; OGI, oxygen-to-glucose index; CMRO₂, cerebral metabolic rate of oxygen; CMRGlu, cerebral metabolic rate of glucose; CBF, cerebral blood flow; CBV, cerebral blood volume; OEF, oxygen extraction fraction

Subcortical Regions	Volume (cm^3)	GI	OGI	CMRO$_2$	CMRGlu	CBF	CBV	OEF
R caudate	4.82	35.69±43.38	4.79±0.27	0.89±0.06	0.95±0.07	0.91±0.07	0.98±0.21	0.99±0.04
L caudate	5.40	29.97±43.48	4.79±0.32	0.90±0.07	0.95±0.07	0.91±0.08	1.06±0.15	0.99±0.04
L putamen	4.37	28.12±58.43	5.00±0.27	1.21±0.05	1.23±0.07	1.19±0.04	0.97±0.14	1.02±0.04
R putamen	4.53	-2.34±51.24	5.11±0.27	1.24±0.06	1.22±0.07	1.20±0.05	0.90±0.10	1.03±0.04
L globus pallidus	1.20	-30.94±66.09	5.27±0.37	1.10±0.06	1.06±0.07	1.08±0.06	1.12±0.23	1.02±0.05
Thalamus	17.63	-56.65±51.00	5.38±0.32	1.06±0.05	1.00±0.05	1.16±0.06	1.17±0.16	0.92±0.02
R globus pallidus	1.32	-73.86±71.36	5.48±0.43	1.11±0.07	1.03±0.08	1.07±0.06	0.98±0.15	1.04±0.05

Table 2.5: Metabolism (mean ± SD) for selected subcortical regions.

Regions were manually defined on our representative Talairach atlas (see Figure 2.5). Note elevated glycolysis in bilateral caudate, and low glycolysis in bilateral globus pallidus and thalamus. Abbreviations as in Table 2.3.

Default system	Volume (cm^3)	GI	OGI	CMRO$_2$	CMRGlu	CBF	CBV	OEF
R lateral parietal	15.90	90.70±38.82	4.66±0.22	1.05±0.05	1.14±0.06	1.03±0.04	0.55±0.08	1.02±0.03
L lateral parietal	22.21	84.15±26.01	4.69±0.19	1.03±0.04	1.11±0.05	1.01±0.04	0.60±0.12	1.02±0.03
MPFC	137.97	77.05±20.35	4.70±0.13	1.02±0.02	1.10±0.03	1.06±0.02	1.08±0.12	0.96±0.02
PCC	39.75	65.12±28.07	4.85±0.14	1.18±0.05	1.23±0.06	1.17±0.04	1.38±0.21	1.01±0.02
R Lateral temporal	15.90	35.14±32.10	4.91±0.24	1.00±0.05	1.04±0.04	0.98±0.04	1.05±0.14	1.03±0.04
L Lateral temporal	22.21	31.54±24.65	4.92±0.21	1.01±0.03	1.03±0.03	0.98±0.03	1.17±0.18	1.03±0.03
R hippocampal formation	3.44	-75.57±54.05	5.45±0.38	0.92±0.05	0.85±0.04	1.02±0.05	1.03±0.28	0.89±0.03
L hippocampal formation	5.21	-84.61±51.22	5.52±0.39	0.94±0.05	0.86±0.05	1.04±0.03	1.07±0.14	0.90±0.04

Table 2.6: Metabolism (mean ± SD) within default system.

Regions identified by resting state BOLD correlation mapping. Note high levels of glycolysis in all regions except bilateral hippocampal formation. MPFC, medial prefrontal cortex; PCC, posterior cingulate; additional abbreviations as in Table 2.3.

Control system	Volume (cm^3)	GI	OGI	CMRO$_2$	CMRGlu	CBF	CBV	OEF
L DLPFC	23.27	120.15±36.98	4.52±0.16	1.01±0.04	1.13±0.04	1.03±0.04	0.98±0.13	0.98±0.02
R DLPFC	32.71	119.36±27.27	4.56±0.13	1.06±0.03	1.18±0.04	1.08±0.03	1.02±0.21	0.98±0.02
L anterior PFC	23.63	98.96±32.91	4.58±0.18	0.98±0.03	1.09±0.04	0.99±0.03	0.95±0.11	1.00±0.03
Dorsal ACC	16.77	97.13±36.76	4.66±0.18	1.11±0.03	1.21±0.04	1.17±0.04	1.28±0.36	0.96±0.02
R anterior PFC	29.33	94.52±31.23	4.64±0.17	1.01±0.02	1.11±0.03	1.01±0.03	0.96±0.10	1.00±0.02
L lateral parietal	25.00	82.09±30.80	4.72±0.20	1.03±0.04	1.11±0.05	1.01±0.04	0.65±0.16	1.02±0.02
R lateral parietal	26.02	76.22±27.94	4.72±0.16	1.06±0.04	1.13±0.04	1.04±0.03	0.61±0.11	1.02±0.03
L caudate	0.20	74.26±68.03	4.59±0.44	0.94±0.10	1.04±0.09	0.95±0.08	1.04±0.18	0.99±0.05
R caudate	1.41	62.57±59.31	4.63±0.35	0.89±0.08	0.98±0.10	0.90±0.08	0.99±0.22	0.99±0.05
R lateral temporal	9.32	55.50±38.00	4.79±0.24	1.02±0.05	1.07±0.06	0.98±0.04	0.84±0.24	1.03±0.03
L lateral temporal	9.47	43.98±34.03	4.79±0.24	0.93±0.06	0.98±0.07	0.90±0.05	1.13±0.26	1.02±0.05

Table 2.7: Metabolism (mean ± SD) within cognitive control system.

Regions identified by resting state BOLD correlation mapping. Note high levels of glycolysis in all regions, including bilateral caudate nuclei. DLPFC, dorsolateral prefrontal cortex; PFC, prefrontal cortex; ACC, anterior cingulate cortex; additional abbreviations as in Table 2.3.

Chapter 3: Resting brain metabolism is modified by task performance: metabolic plasticity of the brain

Abstract

Neuronal activity results in a regional increase in glucose metabolism greater than the corresponding increase in oxygen consumption, resulting in elevated aerobic glycolysis. It has been assumed that short-term increases in neuronal activity are associated with only transient alterations in brain metabolism, though learning induces rapid brain plasticity and alters the metabolic response to task performance. In order to investigate the effect of visuomotor rotation learning on resting cerebral metabolism we performed functional MRI (fMRI) during motor task performance (28 subjects) as well as positron emission tomography (PET) (18 subjects) and fMRI (40 subjects) during eyes-closed rest both before and after completion of task performance. The relative distribution of aerobic glycolysis across the resting brain was determined using a combination of cerebral blood flow, glucose and oxygen utilization measures derived from positron emission tomography. Brain regions involved in task performance, as determined from the fMRI study, including left lateral premotor cortex, had elevated aerobic glycolysis in the resting state several hours following task completion, though no other changes in cerebral metabolism or spontaneous BOLD correlations were found. These data provide supporting evidence to the synaptic homeostasis hypothesis, which suggests that learning causes changes in cellular neurophysiology that increase regional metabolic demands long after transient neuronal activation.

Introduction

In the normal 'resting' brain, its metabolic needs are supported by the nearly complete (>90%) oxidation of glucose to carbon dioxide and water producing approximately 36 moles of ATP per mole of glucose consumed (Siesjo 1978). During transient task conditions, when brain activity increases or decreases, blood flow and glucose consumption, as measured in humans with PET, faithfully follow (Raichle, Posner et al. 1970; Madsen, Hasselbalch et al. 1995). These changes are, surprisingly, not associated with proportionate changes in oxygen consumption (Fox, Raichle et al. 1988; Blomqvist, Seitz et al. 1994). Consequently, increases in regional brain activity are associated with increases in regional aerobic glycolysis, glycolysis occurring in the presence of oxygen but in excess of that required for oxidative phosphorylation (Fox, Raichle et al. 1988; Raichle and Mintun 2006). Since aerobic glycolysis produces significantly less energy than complete oxidation of glucose, its role in cellular activities has been overlooked, though its presence in the resting brain has been known for several decades (Raichle, Posner et al. 1970; Magistretti and Pellerin 1999).

Aerobic glycolysis may have an important role in providing energy and needed metabolic intermediates for long-term potentiation (LTP) and learning. Aerobic glycolysis in the normal brain is largely confined to the astrocytes where it is used to provide the energy needed to remove the excitatory neurotransmitter glutamate from synapses and convert it to glutamine (Pellerin and Magistretti 1994; Chatton, Pellerin et al. 2003). Since the largest fraction of the brain's energy budget is related to glutamate cycling (Sibson, Dhankhar et al. 1997; Attwell and Iadecola 2002), aerobic glycolysis may be uniquely positioned to provide energy for synaptic activity and be associated with

synaptic strength. Since learning and long term potentiation (Bashir, Alford et al. 1991; Richter-Levin, Canevari et al. 1995; Buchs and Muller 1996) lead to increases in neuronal firing and synaptic efficacy and increased synaptic glutamate flux then aerobic glycolysis may be important for the removal of this glutamate from the synaptic cleft (Pellerin and Magistretti 1994; Pellerin and Magistretti 1996).

In addition, aerobic glycolysis may provide an important window into neuronal changes related to memory. Glutamate and its interactions with the NMDA receptor have been at the center of discussions of the cellular basis of memory for some time (Sibson, Dhankhar et al. 1998; Lynch 2004). Recent evidence would suggest that the induction of long term potentiation or LTP is accompanied by a local increase in dendritic excitability that is dependent upon the activation of NMDA receptors (Martin, Grimwood et al. 2000; Frick, Magee et al. 2004). In addition, LTP induces an increase in synaptic proteins and alters the ultrastructure of the postsynaptic density (Buchs and Muller 1996; Wu, Aoki et al. 1997). This change in dendritic excitability and synaptic structure may be locally expressed by changes in brain glycolysis.

There are several pieces of indirect evidence that would be compatible with such a hypothesis. First, the short-term metabolic changes we observe with imaging tasks are largely related to events in axon terminals and dendrites (Schwartz, Smith et al. 1979; Lauritzen 2001; Lauritzen and Gold 2003; Logothetis 2003; Raichle 2006). Presumably, these same locations are the sites of sustained synaptic plasticity. Second, as just discussed, these transient changes are associated with disproportionate increases in aerobic glycolysis over oxidative phosphorylation. However, the changes induced by long-term potentiation continue after task completion as synaptic strength increases and

57

new synapses are formed. Performance of a demanding cognitive task such as the Wisconsin card sorting task (Madsen, Hasselbalch et al. 1995) but not a passive visual perception task is followed by a persistent increase in global aerobic glycolysis upto forty minutes following task completion, though its regional distribution has not been investigated. Other studies have found that a full day of wakefulness is associated with a 20% global increase in blood flow and glucose utilization when compared with measurements made shortly after awakening in the morning (Boyle, Scott et al. 1994; Braun, Balkin et al. 1997; Mintun, Vlassenko et al. 2002; Vyazovskiy, Cirelli et al. 2008). These changes are specific to activities performed during wakefulness, presumably related to experiential learning and neuronal plasticity. While it is presently unknown whether this rather remarkable increase in blood flow and glucose utilization over the waking part of the day is associated with an increase in glycolysis, this seems more likely than an increase in oxidative phosphorylation simply because a significant additional increase in oxidative phosphorylation of this magnitude would be energetically awkward. From these observations one might reasonably posit that experience-induced changes in synaptic activity would be reflected in persistent local changes in aerobic glycolysis. While evidence for this assertion is presently very modest it is, nevertheless, consistent.

Taken together these observations cause us to entertain the hypothesis that novel experiences during wakefulness are associated with persistent glutamate mediated increases in excitatory synaptic activity, expressed as a disproportionate increase in aerobic glycolysis within task relevant circuits. To test this hypothesis we performed positron emission tomography (PET) to measure resting aerobic glycolysis both before

58

and after completion of a rotational learning task (Ghilardi, Ghez et al. 2000; Huber, Ghilardi et al. 2004). In order to control for effects of kinematic alterations and circadian rhythm, we utilized a parallel control group who performed the identical motor task without rotational perturbation. We also used task-related fMRI to determine the regions involved acutely during task performance and resting BOLD correlation analysis to determine whether brain regions involved in task performance altered their functional connectivity following learning.

Methods

Participants

Fifty-eight healthy, right-handed neurologically normal participants were recruited from the Washington University community for one of three experiments: 1) a functional MRI (fMRI) study involving an implicit motor learning task; 2) a positron emission tomography (PET) experiment performed during the eyes closed awake state; 3) a resting fMRI study performed in the eyes closed awake state. Twenty-eight healthy, right-handed subjects (14 women) aged 18 to 28 (mean 24.4 ± 2.0) participated in the fMRI study. Eighteen healthy, right-handed participants (9 women) aged 20 to 29 years (mean 25.5 ± 1.8) participated in the PET study. Fifty-eight subjects participated in the resting fMRI study (28 subjects from Experiment 1; 18 subjects from Experiment 2). Subjects were excluded if they had contraindications to MRI, history of mental illness, possible pregnancy, or medication use that could interfere with brain function. All experiments were approved by the Human Research Protection Office (HRPO) as well as

the Radioactive Drug Research Committee (RDRC) for the PET sessions at Washington University in St. Louis. Written informed consent was provided by all participants.

Motor Learning Task

The motor learning task was an out-and-back reaching movement task (eTT, Verona, Italy) that was performed using a MRI compatible stylus and digitizing tablet (Mag Design and Engineering, Sunnyvale, CA). The characteristics of this task have been described in detail previously (Ghilardi, Ghez et al. 2000; Krakauer, Pine et al. 2000; Ghilardi, Eidelberg et al. 2003; Huber, Ghilardi et al. 2004). Subjects viewed a computer monitor that displayed a central fixation point and eight surrounding circles and on-screen cursor that was controlled by a hand-held stylus. When one of the eight surrounding circles changed color from white to black (at 0.93Hz), subjects were instructed to move the cursor from the central fixation point to that circle and back to the central fixation point as quickly and accurately as possible. Each of the surrounding circles was presented in a pseudo-random order. Stimuli blocks included 264 such out-and-back movements. Subjects were randomized into two groups: an implicit rotation learning group (ROT) and a motor control (CON). Rotation learning (ROT) subjects performed the task with a stepwise 15 degree visuomotor rotation. The initial stimulus block (block 1) involved no perturbation in the ROT condition. Subsequent blocks involved the mismatch between movement on the digitizing tablet and the movement of the onscreen cursor; cursor movement was rotated 15 degrees counterclockwise causing the subjects to compensate with a 15 degree clockwise movement. Following the initial completion of a 15 degree visuomotor rotation, ROT subjects performed stepwise 15 degree rotation for 3 additional blocks until subjects had adapted to 60 degree visuomotor

rotation. Fifteen degree increments were chosen because this allows for implicit learning without conscious awareness (Ghilardi, Ghez et al. 2000). Motor control (CON) subjects performed this task without any perturbation (Figure 3.1).

Experiment 1: fMRI

Experimental Design

Subjects performed one fMRI session that consisted of nine BOLD runs. In the first two runs (pre-learning), all subjects performed the motor learning task with no perturbation. In the next five runs subjects were assigned to either the CON or ROT group and performed the task as described previously while in the scanner. Following completion of learning, the CON group underwent two final runs with no visuomotor rotation (CON) and the ROT group performed the two final runs with sixty degrees of visuomotor rotation (ROT). fMRI data was collected in block design format with two movements per TR interval (2.16s). In each of the eight-minute pre- and post-learning runs, three task blocks included performance of 32 movements (16 frames) interleaved with visual fixation (12 frames). For the motor learning task subjects performed 5 runs with one block per run for a total of 264 movements/run (1320 movements). T1- and T2-images were collected for alignment.

Image Acquisition

Structural MRI: MRI studies were performed on the Siemens 3T Allegra (Erlangen, Germany). Imaging sessions began with acquisition of a three orthogonal slice scout scan, followed by a coarse 3D sagittal T1-weighted MPRAGE acquisition for slice pre-

registration [TE=3.93ms, TR=722ms, TI=380ms, flip angle=8°, 128x128 acquisition matrix, 1 acquisition, 80 slices, 2x2x2 mm voxels]. High-resolution structural images were acquired using a 3D sagittal T1-weighted MPRAGE acquisition optimized for high contrast-to-noise ratio and resolution [TE=3.93ms, TR=1.9s, 256x256 acquisition matrix, 1 acquisition, 160 slices, 1x1x1 mm voxels]. High-resolution 2D multislice oblique axial spin density/T2-weighted fast spin echo (TSE) structural images were acquired using slice tilts and positions computed by slice pre-registration [TE=98ms, TR=2.1s].

fMRI Scanning: The functional images were collected in serial runs of an asymmetric spin-echo echo-planar sequence (same as that used in the BOLD contrast) (TR=2.16s, TE=25ms). One acquisition consisted of 39 transverse slices and 4mm^3 isotropic voxels. All subjects completed 2 fMRI runs, each 200 frames (8 minutes) in duration both before and after learning task performance. During each run, sets of 39 contiguous 4mm thick, axial images were acquired parallel to the anterior-posterior commissural plane (4 x 4 mm in plane resolution). MR data was reconstructed in images and normalized by: 1) scaling whole-brain signal intensity to a fixed value; and 2) removing the linear slope on a voxel-by-voxel basis to counteract signal drift. Between-subjects analyses will be conducted following transformation of data to a common atlas space and blurring images with an 8mm FWHM Gaussian filter. Registration to a Talairach atlas template was achieved by computing linear (affine) transforms connecting the fMRI run first frame (averaged over all runs after cross-run realignment) with a T2 and T1-weighted structural image.

General fMRI Data Analysis

fMRI preprocessing steps included compensation of systematic, slice-dependent

time shifts, elimination of systematic odd-even slice intensity differences due to interleaved acquisition, and rigid body correction for interframe head motion within and across runs. Each fMRI run was intensity scaled to a yield a whole brain mode value of 1000 (not counting the first four frames). Atlas registration was achieved by computing affine transforms connecting the fMRI run first frame (averaged over all runs after crossrun realignment) with the T2 and average T1-weighted structural images. Our atlas representative template includes MP-RAGE data from 12 normal individuals and was made to conform to the 1988 Talairach atlas. To prepare the BOLD data for the present main analyses, each fMRI run was transformed to atlas space and resampled to 3 mm cubic voxels. For each participant, a General Linear Model (GLM) was used to estimate hemodynamic model-independent event related responses over 35-seconds (16 frames).

Statistics: Two ANOVA analyses were performed. First, ANOVA was performed to determine regions with increased activity across groups (ROT and CON combined) and states (pre and post combined) during motor task performance (main effect of time). Images were thresholded at $Z>3.0$, $p<0.01$, cluster size >17, Monte Carlo corrected. Second, ANOVA was performed to compare pre- and post-learning in both CON and ROT groups. A mixed-effects model was used to determine the (pre x post) X (ROT x CON) interaction. Images were thresholded at $Z>3.0$, $p<0.01$, cluster size >17, Monte Carlo corrected.

Experiment 2: PET

Experimental Design

Subjects performed two positron emission tomography (PET) sessions during eyes-closed rest in a single day, one immediately before (pre-task) and one immediately after completion of the motor task (post-task) mentioned above. Motor task performed between the PET sessions took place outside the PET scanner.

Image Acquisition

Structural MRI: MRI scans were obtained in all subjects to guide anatomical localization. High-resolution structural images were acquired using a 3D sagittal T1-weighted MPRAGE on a Siemens (Siemens, Erlangen, Germany) 3T Allegra [TE=3.93ms, TR=1900ms, TI=1100ms, flip angle=20°, 256x256 acquisition matrix, 160 slices, 1x1x1 mm voxels].

PET Scanning: All subjects underwent two duplicate PET session that each included one [^{18}F]-fluorodeoxyglucose (FDG) scan to measure resting glucose utilization (CMRGlu) and two replicate sets of three ^{15}O scans: [^{15}O]-H_2O to measure cerebral blood flow and of [^{15}O]-CO and [^{15}O]-O_2 to measure cerebral oxygen utilization (CMRO$_2$). The two replicates of ^{15}O scans within a scanning session were averaged for data analysis. All PET images were acquired in the eyes-closed waking state. No specific instructions were given regarding cognitive activity during scanning other than to remain awake.

Studies were performed using a Siemens model 961 ECAT EXACT HR 47 PET scanner (Siemens/CTI, Knoxville, TN) with 47 slices encompassing an axial field of view of 15cm. Transverse resolution was 3.8-5.0 mm FWHM and axial resolution was 4.7-5.7 mm full width at half maximum (FWHM). Attenuation data was obtained using ^{68}Ge-

[68]Ga rotating rod sources to enable quantitative reconstruction of subsequent emission scans. Emission data were obtained in the 2D mode (inter-slice septa extended). All PET data was reconstructed using a ramp filter (approximately 6mm FWHM) and then blurred to 12 mm FWHM. Subject head movement during scanning was restricted by a thermoplastic mask.

PET Measurement of Glucose Metabolism: [18F]-fluorodeoxygluse (FDG) uptake and trapping was used to image CMRGlu(Fox, Raichle et al. 1988). Measurements of CMRGlu were performed after slow intravenous injection of 5mCi of [18F]-FDG. Dynamic acquisition of PET emission data continued for 60 minutes with 25 5-sec frames, 9 20-sec frames, 10 1-min frames, and 9 5-min frames. Venous samples for plasma glucose determination were obtained just before and at the mid-point of the scan. The two scanning sessions were approximately 5 hours apart. In order to account for any residual radioactivity from the initial FDG scan, an additional 10 minute background scan was performed before the second FDG scan.

[15O]tracer PET scans: 120 second dynamic scans comprised of 2 second frames that began with tracer injection (or inhalation) (Raichle, Martin et al. 1983; Mintun, Raichle et al. 1984). With this method, the optimum 40 second scan was created from summation of the appropriate frames. By reconstructing all frames and then creating a whole brain time-activity curve, the onset of activity in the brain could be judged exactly. **CBF Scan:** Distribution of CBF was measured with a 40-sec emission image (derived from a 120 second dynamic scan) after rapid injection of 50 mCi [15O]water in saline (Raichle, Martin et al. 1983). **CBV Scan:** Distribution of CBV was measured with a 5-min emission scan beginning 2 min after brief inhalation of 75mCi of [15O]carbon monoxide

in room air (Martin, Powers et al. 1987). **CMRO$_2$ Scan:** Distribution of CMRO$_2$ was measured with a 40-sec emission scan (derived from a 120 second dynamic scan) after brief inhalation of 60 mCi of [^{15}O]oxygen in room air (Mintun, Raichle et al. 1984).

General PET Data Analysis:

Preprocessing: For each subject, measures of CBF, CBV, CMRO$_2$, and CMRGlu were aligned to each other and then to the subject's MPRAGE. The re-aligned data was then transformed to Talairach space (Lancaster, Glass et al. 1995) using in-house software and scaled to a whole-brain mean of one (local-to-global ratio (Raichle, MacLeod et al. 2001)).

Glycolytic Index: In order to quantitatively assess aerobic glycolysis, we performed a linear regression of CMRGlu on CMRO$_2$. The residuals were scaled by 1000 to produce the glycolytic index (GI). GI represents glucose consumption above or below that predicted by oxygen consumption.

PET statistics: To combine results across subjects, we computed a general linear model (GLM) which contained metabolic data for CMRO$_2$, CMRGlu, CBF, and GI for each subject in both pre- and post-task PET sessions. We performed a groupwise mixed-effects analysis (repeated measures t-test; n=18) to determine any regions that showed preferential changes in either ROT or CON groups between pre- and post-task resting states. All analyses were performed on a voxelwise basis. Images were thresholded at Z>4.4 (p<0.00001, cluster > 99).

Surface mapping: Volumetric statistical results were projected onto the cortical surface of the PALS B12 (population-average landmark and surface-based) atlas by multifiducial

mapping (Van Essen 2005). Surface mapping was performed using Caret v5.512 [http://brainmap.wustl.edu/caret].

<u>Conjunction Analysis</u>

A conjunction analysis was performed to qualitatively compare regions with increased activity during motor task performance (Experiment 1), altered activity during visuomotor rotation task performance measured using fMRI (Experiment 1), elevated aerobic glycolysis measured via PET (Experiment 2).

Experiment 3: Resting fMRI

<u>Experimental Design</u>

Two groups of subjects were included in this analysis (total N=58). Forty subjects (28 subjects from Experiment 1; 26 subjects ROT, 14 subjects CON) performed two resting fMRI sessions during eyes-closed rest in a single day, one immediately before (pre-task) and one immediately after completion of the motor task (post-task) mentioned above. Motor task performed between the resting fMRI sessions took within the MR scanner. In addition, eighteen subjects (from Experiment 2) performed a single resting fMRI session during eyes-closed rest on separate day from the PET experiment.

<u>Image Acquisition</u>

Structural MRI: MRI scans were obtained in all subjects to guide anatomical localization. High-resolution structural images were acquired using a 3D sagittal T1-weighted MPRAGE on a Siemens (Siemens, Erlangen, Germany) 3T Allegra

[TE=3.93ms, TR=1900ms, TI=1100ms, flip angle=20°, 256x256 acquisition matrix, 160 slices, 1x1x1 mm voxels].

Resting fMRI scanning: Forty normal right-handed subjects also underwent resting state fMRI scanning similar to Fox et al., 2005 (Fox, Snyder et al. 2005). Two 7.5 minute scans (194 frames) were performed during visual fixation on a crosshair. All imaging was performed on a 3T Siemens Allegra scanner (Erlangen, Germany). Functional data were collected by using a gradient echo, echo-planar sequence sensitive to BOLD contrast [echo time (TE) = 25 ms, flip angle = 90°, 4 x 4 x 4-mm isotropic voxels, volume repetition time (TR) = 2.16 s]. Whole brain coverage was obtained with 32 contiguous slices. The first four frames of each run were not included in data analysis. Additional fMRI processing details are given below.

<u>General resting fMRI Data Analysis</u>

Preprocessing: BOLD processing included compensation of systematic, slice-dependent time shifts, systemic odd-even slice intensity differences, and rigid body correction for interframe head motion within and across BOLD runs. Each BOLD run was intensity scaled to a whole brain mode of 1000. Atlas registration was performed by affine transforms connecting the first BOLD run frame with the T1W and T2W structural images. Our atlas template includes MPRAGE data from 12 normal individuals from a Siemens Allegra 3T scanner and was made to conform to the 1988 Talairach and Tournoux atlas according to the method described by Lancaster et al (Lancaster, Glass et al. 1995).

Low-frequency BOLD fluctuation correlations: Data was temporally band-pass filtered (f<0.08) and spatially smoothed (6mm FWHM). Sources of spurious variance and their temporal derivatives were removed from this data through linear regression (see (Fox, Snyder et al. 2005)). Nuisance regressors included signals averaged over ventricle, white matter, and whole brain ROIs as well as measures of head movement. Correlation maps were produced by extracting the BOLD time course from the seed region and computing the Pearson's r between that time course and that of every other voxel in the brain. The seed region was comprised of a 6-mm-radius spheres centered on left lateral premotor cortex [-55 3 10] (see experiment 2 PET results).

BOLD correlation mapping: To combine results across subjects and compute statistical significance, correlation coefficients were converted to a normal distribution by Fischer's z transformation. Fischer z-maps were combined across subjects using a random-effects analysis (one sample *t*-test; N=18 from Experiment 2) and thresholded at Z>3.0 (p<0.01, cluster size > 17 voxels, corrected for multiple comparisons (Forman, Cohen et al. 1995)). In addition, we performed a groupwise mixed-effects analysis (repeated measures t-test; n=40 from Experiment 1 and 3) to determine any regions that showed preferential changes in either ROT or CON groups between pre- and post-task resting states. All analyses were performed on a voxelwise basis. Images were thresholded at Z>3.0 (p<0.01, cluster size > 17).

Results

Experiment 1: fMRI

Regions that show an increase in activity during performance of the motor task

We first performed an ANOVA across twenty-eight subjects to identify brain regions with significantly elevated BOLD signal during performance of the motor task (utilizing runs 1-2 and 8-9 combining ROT and CON groups) (N=28; Z>3.0, cluster >17, monte carlo corrected). Peak foci were located in left motor, left premotor/supplementary motor, visual cortex, and right parietal cortex, consistent with performance of a visuomotor task (Figure 3.2).

Regions that show altered activity following visuomotor rotation

We then analyzed changes in rotation learning (ROT) and motor control task (CON) BOLD signal over time to identify brain regions that show differential activity due to visuomotor learning. We identified group differences (ROT x CON) in brain regions with altered timecourses in post-learning (runs 8-9) compared to pre-learning (runs 1-2) (task x time x group ANOVA; Z>3.0; cluster >17; monte carlo corrected). Peak foci were located in left premotor (BA6/BA44), bilateral angular gyrus (BA40), right medial prefrontal (BA10), and left lateral temporal cortex (Figure 3.3).

Experiment 2: PET

Behavioral performance

Subjects performed either a rotation learning (ROT) or motor control (CON) task. Both groups of subjects performed the same number of movements (1320), either with or without visuomotor rotation. Rotation learning subjects significantly decreased directional error during task performance (p<0.01) (Figure 3.4). In contrast, directional

error was unchanged in CON subjects (p>0.05). Subjects learned approximately 80% of the imposed visuomotor rotation at each stage of learning, similar to previous studies using this task (Ghilardi, Ghez et al. 2000; Huber, Ghilardi et al. 2004).

Measures of resting oxygen and glucose metabolism

Relative metabolic rates for blood flow (CBF), oxygen ($CMRO_2$), and glucose (CMRGlu) were imaged with positron emission tomography (PET) in both rotation learning (ROT; n=9) and motor control (CON; n=9) groups in the resting awake state. In each individual, regional CBF, $CMRO_2$ and CMRGlu were scaled to a whole brain mean of one (local-to-global ratio; see Methods). The individual results were averaged over subjects in Talairach atlas space. The obtained mean regional distributions of $CMRO_2$ and CMRGlu were similar to previously reported results obtained using quantitative measurements in normal subjects (Phelps, Huang et al. 1979; Raichle, MacLeod et al. 2001). Of note, the regional distribution of metabolic variables was not significantly different in the pre-task state between the two groups (Figure 3.5).

Measures of resting aerobic glycolysis (GI)

The glycolytic index (GI) is obtained by linear regression of CMRGlu on $CMRO_2$ and exhibiting the residuals scaled by 1000. Positive GI values represent locally increased CMRGlu relative to the line of regression, i.e., excess aerobic glycolysis. Likewise, negative GI values represent less aerobic glycolysis than that predicted by the line of regression.

Following computation of GI maps for each subject, significance was assessed at the population level by voxelwise *t*-tests against the null hypothesis of uniformly

proportional glucose:oxygen metabolism, i.e., no deviation from the line of regression. The *t*-maps were converted to equi-probable Z-maps and thresholded at p<0.00001 (Z>4.4, cluster >99 voxels) according to previously described methodology (Forman, Cohen et al. 1995; McAvoy, Ollinger et al. 2001). Regions with significantly elevated aerobic glycolysis were found bilaterally in prefrontal cortex, lateral parietal cortex, and the posterior cingulate/precuneus (Figure 3.6). In contrast, significantly low aerobic glycolysis was found bilaterally in the inferior temporal gyrus and throughout the cerebellum.

Effect of task performance on brain metabolism

In order to compare resting state metabolism before and after task performance, significance was assessed at the population level by a voxelwise repeated measures t-test against the null hypothesis of uniformly proportional changes in CBF, CMRO2, CMRGlu, and GI in both ROT and CON groups between pre- and post-task states. The t-maps were converted to equi-probable Z-maps and thresholded at p<0.0001 (N=18, Z>4.4, cluster >99 voxels) according to previously described methodology (Forman, Cohen et al. 1995; McAvoy, Ollinger et al. 2001). Following visuomotor rotation task performance, regional aerobic glycolysis was differentially increased during eyes-closed rest for several hours following task completion in left lateral premotor cortex (BA6) [-55 3 10] (Z=5.15, p<0.0001, cluster size = 124 voxels) while no changes in CBF, CMRO2, or CMRGlu were observed. (Figure 3.7)

Conjunction analysis

We then performed a conjunction analysis to assess the degree of overlap between the regions involved in motor task performance (Experiment 1A), regions altered in visuomotor rotation (Experiment 1B), and regions with increased aerobic glycolysis in the resting state (Experiment 2). We found significant overlap between left lateral premotor regions involved in rotation learning and altered resting state aerobic glycolysis (Figure 3.8).

Experiment 3: resting fMRI

Correlation mapping of the blood oxygen level dependent (BOLD) functional magnetic resonance imaging (fMRI) signal acquired in the resting state (Fox, Snyder et al. 2005) has been used to identify brain regions that have similar spontaneous BOLD fluctuations and are 'functionally connected'.

We performed two sets of analyses. First, we performed a random effects analysis (one-sample t-test, N=18 from Experiment 2) to determine regions with correlated spontaneous BOLD fluctuations to the premotor cortex region [-55 3 10] found with altered aerobic glycolysis in Experiment 2 in the same group of individuals. Regions of significant BOLD correlations (p<0.01, random effects analysis; Z>3.0, cluster>17) to the left premotor cortex are shown in Figure 3.9. We found correlations between left premotor cortex and bilateral motor and premotor cortex, supplementary motor cortex, and bilateral parietal lobe.

In addition, we performed a repeated measures t-test comparing pre- and post-learning spontaneous BOLD correlations to the same premotor cortex region defined above. This analysis was performed on 40 subjects with pre- and post-task fMRI data (26

subjects ROT; 14 subjects CON). We found no significant changes (Z>3.0, p<0.01) in premotor cortex BOLD correlations following learning.

Discussion

This work reports an extensive investigation of brain metabolism changes following visuomotor rotation learning. The main finding is that a specific brain region previously activated by task performance and visuomotor learning (Experiment 1) within left premotor cortex shows elevated aerobic glycolysis for several hours following task completion (Experiment 2; Figure 3.7), though no other changes in metabolism or resting BOLD correlations are found (Experiment 3). Since aerobic glycolysis is most closely associated with glutamatergic cycling at the synapse, alterations in resting aerobic glycolysis likely represent alterations in synaptic strength following task performance. These data are consistent with the synaptic homeostasis hypothesis suggesting increased synaptic strength and energy metabolism during wakefulness (Tononi and Cirelli 2003).

Role of aerobic glycolysis

Because our findings are based upon changes in resting brain metabolism, we must first consider the role of ongoing aerobic glycolysis in the brain. Aerobic glycolysis is regionally increased in areas of elevated neuronal activity due to an elevation of glucose metabolism greater than oxygen metabolism (Fox, Raichle et al. 1988). This is the case during periods of transient neuronal activity, as evidenced by task-related PET studies (Baron, Rougemont et al. 1984; Fox, Raichle et al. 1988; Raichle and Mintun 2006), and is also the case in the eyes-closed awake state (Chapter 2). It had initially been assumed that some fraction of glucose, approximately 10%, is metabolized non-

oxidatively in the brain, though it's distribution was unknown (Raichle and Mintun 2006). In Chapter 2 we report that the distribution of aerobic glycolysis in the eyes-closed awake brain is not homogenous, and in fact closely matches brain regions expected to have high levels of functional activity, including the default network and prefrontal cortex bilaterally (Figure 3.6). Given this physiology, an elevation in aerobic glycolysis indicates a concurrent increase in the underlying neuronal activity and synaptic strength of that region.

Investigation of the cellular basis of this response reveals that neuronal activity induces an increase in astrocytic glycolysis in close spatiotemporal apposition to neuronal activity (Kasischke, Vishwasrao et al. 2004). Increased neuronal activity, specifically at glutamatergic synapses, result in an elevation of glutamate in the synaptic cleft. Astrocytes then remove glutamate from the synaptic cleft via a Na^+/glutamate cotransporter that causes an increase in Na^+/K^+ ATPase activity (Pellerin and Magistretti 1996). The energy needed for the pumping action of Na^+/K^+-ATPase is derived from aerobic glycolysis (Pellerin and Magistretti 1996; Magistretti and Chatton 2005). The use of aerobic glycolysis by Na^+/K^+-ATPase is not unique to the astrocyte. It fuels Na^+/K^+-ATPase in all cells that possess this membrane-bound pump (Pellerin and Magistretti 1996) including neurons (Wu, Aoki et al. 1997). This is especially important in subcellular regions of the neuron far removed from the mitochondria, such as the post-synaptic density (PSD) (Wu, Aoki et al. 1997), though the fraction of energy derived from neuronal glycolysis remains unclear (Sheng and Hoogenraad 2007). Aerobic glycolysis provides a rapid source of energy that is utilized by both astrocytes and

neurons to subserve neuronal signaling, the primary usage of energy in the brain (Attwell and Laughlin 2001).

In addition to its role in energy production, aerobic glycolysis provides necessary precursors for anabolic processes in the cell. Glycolytic intermediates are necessary for the production of precursors for RNA and DNA synthesis via the pentose-phosphate pathway (PPP) (Gaitonde, Jones et al. 1987; Larrabee 1989). In the adult brain it is estimated that 5-10% of the glucose consumed may enter the PPP (Gaitonde, Jones et al. 1987). Though a complete understanding of the role of aerobic glycolysis in anabolic processes is lacking, there are several intriguing pieces of data that suggest that aerobic glycolysis levels are closely associated with synaptic density. Extrapolating from data collected during early-life synaptic development in infants, glycolytic flux appears to closely parallel overall synaptic density (Chugani, Phelps et al. 1987; Altman, Perlman et al. 1993) with an overabundance of synapses and aerobic glycolysis in early life that peaks around the age of nine with a subsequent decrease to adult levels during adolescence (Andersen 2003). This association may be due to to an increase in the bioenergetic needs of regions with high synaptic density, or it may be due to the non-energetic and anabolic utilization of glycolytic intermediates. Consistent with the latter hypothesis, flux through the PPP increases following traumatic brain injury, though overall glucose utilization does not change (Dusick, Glenn et al. 2007).

Changes in cellular neurophysiology following learning

We find an increase in aerobic glycolysis in left premotor cortex following visuomotor learning (Figure 3.7). There are several possible explanations for this regional change in brain metabolism.

A regional increase in aerobic glycolysis may be due to a regional increase in glutamatergic activity in the eyes-closed awake state. Aerobic glycolysis is closely associated with glutamatergic flux at the synapse (see discussion above), and a pre-synaptic increase in glutamate release or post-synaptic increase in glutamate flux may partially result in the observed changes in aerobic glycolysis. Since most functional imaging studies focus upon changes in metabolism during task performance, the role of spontaneous glutamatergic flux at the synapse remains to be completely elucidated. There is evidence, though, that learning can cause changes in glutamate receptor concentration and activity.

Learning tasks induce long-term changes in cellular neurophysiology via mechanisms such as long-term potentiation (LTP). Spatial learning tasks that induce LTP are associated with increased extracellular glutamate concentrations (Richter-Levin, Canevari et al. 1995), indicating an elevation in pre-synaptic glutamate release prior to a post-synaptic change in receptor activity and affinity. An elevation in local glutamatergic activity also occurs following experiential learning during wakefulness. Local glucose utilization and cerebral blood flow both increase during wakefulness (Vyazovskiy, Cirelli et al. 2008) in parallel with increases in AMPA receptor density (Vyazovskiy, Cirelli et al. 2008), suggesting that increases in synaptic strength induce changes in aerobic glycolysis, the hypothesis tested directly in this experiment.

The changes in cellular neurophysiology induced by learning remain long following task completion. LTP alters the ultrastructure of the synapse causing an increase in the apposition zones, larger postsynaptic densities (PSD), and enlarged spine profiles (Buchs and Muller 1996). Since aerobic glycolysis supplies the PSD with energy (Wu, Aoki et al. 1997; Sheng and Hoogenraad 2007), an alteration in synaptic structure could also cause a subsequent increase in aerobic glycolysis.

In addition, transient neuronal activity results in the temporary increase of glucose transporter density (GLUT1 and GLUT3) associated with changes in local rates of glucose metabolism (Koehler-Stec, Li et al. 2000). Though increased glucose transporter density can be seen in the first few minutes of task performance, it remains unknown how long these changes persist. A residual increase in glucose transport may result in a net increase in aerobic glycolysis given a constant cerebral blood flow and oxygen metabolism (as was found in our data).

Increased spontaneous glutamatergic neurotransmission, observed as an increase in aerobic glycolysis, following task performance is surprising, though prior studies have observed a replay of neuronal activity following task performance, most often in post-learning sleep (Peigneux, Laureys et al. 2004). Replay of synaptic activity by ensembles of hippocampal cells during REM sleep (Skaggs and McNaughton 1996; Kali and Dayan 2004) occurs, though its role appears limited to sleep. These findings are consistent with our assertion that task performance induces long-term changes in cellular neurophysiology, though we are the first to report, to our knowledge, alterations in activity patterns during wakefulness following task performance.

In addition to supporting increased glutamate activity, it is possible that some of the glucose being metabolized glycolytically is being used to develop precursors for new synapses or alter existing synapses, as often occurs in long-term potentiation (Buchs and Muller 1996; Chen and Tonegawa 1997). Elevation of aerobic glycolysis following task performance may represent an increase in synaptic density in brain regions involved in task performance, consistent with long-term potentiation alterations in post-synaptic NMDA and AMPA receptor density and efficacy (Bashir, Alford et al. 1991; Buchs and Muller 1996). An increase in anabolic utilization of glucose may result in increased density of dendritic spines and remodeling of the post-synaptic density, findings consistent with long-term potentiation and learning. Unfortunately the fraction of glucose used for anabolic processes compared to energy production remains unclear.

Regional changes in aerobic glycolysis

Using a combination of fMRI and PET (Experiment 1 and 2), we report that visuomotor rotation causes altered activity within left premotor cortex during task performance that corresponds to regions with elevated aerobic glycolysis in the post-learning resting state (Figure 3.8).

Premotor cortex activity has been traditionally associated with the planning of motor actions. Its activity is increased during numerous visuomotor and motor tasks transiently (Petersen, van Mier et al. 1998; Halsband and Lange 2006). At the individual neuron level, learning a visuomotor task can alter premotor cortex activity in the monkey (Mitz, Godschalk et al. 1991), signifying a learning-related change in neuronal firing, though it remains unclear how long these changes last following task completion.

Changes in visuospatial information, such as visuomotor rotation, influence premotor cortex activity and cause altered activity within lateral premotor cortex region during task performance (Experiment 1; Figure 3.3). In order for subjects to perform the visuomotor rotation task accurately, they have to integrate visuospatial cues (provided by lateral parietal cortex) with motor and sensory cues (provided by motor cortex) to compute a movement plan and trajectory (Experiment 1) (di Pellegrino and Wise 1993).

Altered activity within premotor cortex likely reflects a change in synaptic activity due to learning. Alternately, the change in resting aerobic glycolysis may be simply due to kinematic effects of prior movements. In order to control for this possible confound, we compared rotation learning with performance of an identical motor task without visuomotor rotation. Subjects had no conscious awareness of the applied visuomotor rotation and performed the identical number of movements, making it unlikely that kinematic change due to hand and arms movements differed between rotation learning and motor control groups. Subjects were more accurate in performance of the motor control task, providing another possible explanation for our task-related differences in metabolism, though our data was collected over the span of three hours and it is unlikely that activity within premotor cortex would differ between rotation learning and motor task participants in this timeframe.

In addition to changes in premotor cortex, performance of a rotation learning task has been previously reported to result in a transient increase in cerebral blood flow and slow wave EEG activity in right parietal cortex (Ghilardi, Ghez et al. 2000; Huber, Ghilardi et al. 2004), though no corollary change in BOLD signal or metabolism was

found in this study (Experiment 1; Experiment 2). There are several possible explanations for these differences.

First, previous studies compared visuomotor rotation to a pre-learned sequence of target stimuli, resulting in minimal alterations in premotor cortex and increases in right parietal cortex, presumably because the control task also utilized premotor cortex for movement planning (Donoghue, Sanes et al. 1998) but did not utilize right parietal cortex for visuospatial integration (Honda, Deiber et al. 1998; Ghilardi, Ghez et al. 2000). Further, these studies were performed in the acute stage of task performance or in post-learning sleep, though practice related reorganization following visuomotor tasks (van Mier, Tempel et al. 1998; Della-Maggiore and McIntosh 2005) result in increased activity in prefrontal and premotor areas and a decrease in primary motor and parietal cortex activity.

Second, changes in aerobic glycolysis within premotor cortex may induce electrical changes in parietal cortex, consistent with prior observations using this task. We performed resting-state functional connectivity analysis on a resting fMRI dataset collected on the same individuals from the PET study (Experiment 3). Connectivity analysis revealed a network of cortical regions correlated in their spontaneous activity to left premotor cortex [-55 3 10], including bilateral premotor, motor, and parietal cortex as well as insula (Figure 3.9). Changes in aerobic glycolysis, reflecting mostly pre-synaptic inputs (Jueptner and Weiller 1995) may induce changes in post-synaptic electrical activity within parietal cortex, as detected via EEG. Consistent with this hypothesis, transcranial magnetic stimulation of functionally connected cortical regions induce alterations in the electrical and BOLD signal in distant locations (Munchau, Bloem et al.

2002; Logothetis 2003; Ruff, Bestmann et al. 2008; Ruff, Blankenburg et al. 2008), indicating parallel changes in activity patterns across functionally coupled regions.

Synaptic Homeostasis Hypothesis

One intriguing explanation for this alteration in energy metabolism in the eyes closed awake state following task performance is provided by the synaptic homeostasis hypothesis. This hypothesis associates wakefulness with synaptic potentiation (Vyazovskiy, Cirelli et al. 2008) and sleep with synaptic depression (Tononi and Cirelli 2003), a homeostatic process that facilitates continual learning and memory through experience while preserving long-term synaptic balance and energy utilization. Supporting data for this hypothesis is provided by evidence that CMRGlu, $CMRO_2$ (Boyle, Scott et al. 1994) and CBF (Boyle, Scott et al. 1994; Braun, Balkin et al. 1997) all increase during wakefulness, but CMRGlu disproportionately so, resulting in putative increases in aerobic glycolysis. We provide the first evidence, to our knowledge, that learning a difficult task is accompanied not only by the expected regional increase in aerobic glycolysis during task performance but also a persistence of this aerobic glycolysis long after the task has been completed.

The human brain has a tremendous capacity to store information. This information, coded at the level of neurons as alterations in synaptic strength and structure, induces regional increases in aerobic glycolysis during task performance (Fox, Raichle et al. 1988; Wu, Aoki et al. 1997; Raichle and Mintun 2006). But, though we no longer are performing the task, residual changes in neurophysiology remain (Buchs and

Muller 1996), though our understanding of these changes at the cellular level remains incomplete.

We posit that brain plasticity induces alterations in synaptic strength and aerobic glycolysis following completion of task performance. These changes in neurophysiology are likely correlated to the degree of synaptic alteration and difficulty of task performance, with overlearned, rote behaviors causing minimal residual changes in aerobic glycolysis while novel, difficult paradigms cause significant changes in resting metabolism. Our data is consistent with this hypothesis, with elevation of aerobic glycolysis following performance of the difficult visuomotor rotation task. In addition, data collected following performance of a difficult cognitive paradigm, the Wisconsin card sorting task, has revealed residual global increases in aerobic glycolysis following task completion, though its regional distribution was not investigated (Madsen, Hasselbalch et al. 1995).

Since changes in synaptic strength have a metabolic cost, there has to be some mechanism whereby the capacity of the brain to store new information is restored. Extrapolating from extant data, given the 20% increase in blood flow and glucose metabolism during a day, the body's total energy demand would double in four days without a process to subsequently decrease energy metabolism. There are several possible mechanisms to account for these changes. The synaptic homeostasis hypothesis suggests that slow-wave sleep may provide the brain an opportunity to downregulate synaptic strength, resulting in decreased aerobic glycolysis. Previous studies have found sleep to have a beneficial effect on performance of cognitive and motor tasks (Jha, Jones et al. 2005; Orban, Rauchs et al. 2006; Gais, Albouy et al. 2007), including the visuomotor

rotation task utilized in this experiment (Huber, Ghilardi et al. 2004). In contrast, an alternative hypothesis would be that synaptic strength decays slowly over time irrespective of sleep, though evidence for this alternate hypothesis is lacking and sleep deprivation experiments suggest that a temporal decay in synaptic strength is unlikely (Braun, Balkin et al. 1997; Yoo, Hu et al. 2007). From these findings, we postulate that the regional increase in aerobic glycolysis that we have described will revert to the region's pre-task levels following a night of sleep allowing for renewed synaptic plasticity, an empirical question that will be addressed in future experiments.

Stability of cerebral blood flow and metabolism

While we find changes in aerobic glycolysis following task performance, we find no corresponding alterations in blood flow, glucose, or oxygen metabolism following task completion. These data suggest that the local-to-global ratio of these metabolic variables is unchanged by task performance, though we cannot discount additional changes in global metabolism (Boyle, Scott et al. 1994; Braun, Balkin et al. 1997). Previous studies have found that overall cerebral blood flow and glucose utilization both decrease by approximately 20% following a night of sleep (Boyle, Scott et al. 1994; Buysse, Nofzinger et al. 2004). We surmise that these global measures of blood flow and metabolism may reflect an integration of regionally specific changes, namely regions with increased activity drive whole-brain alterations. Future studies will have to address the possible role of global changes in cerebral metabolism in addition to the regional changes reported in this experiment. Of note, though, is that even if global metabolism increases over the course of the day, the observed changes in glycolysis would exceed the

global changes, consistent with the interpretation of the data presented herein (Borghammer, Jonsdottir et al. 2008).

Stability of functional connectivity measures

We found no changes in resting BOLD correlations to premotor cortex following visuomotor learning (Experiment 3). There are several possible explanations. First, given the high degree of variance in the spontaneous BOLD signal, this analysis may not have enough power to detect subtle alterations caused by learning. Few studies have found acute changes in resting state networks identified with BOLD correlations within individuals, though long-term training may cause some subtle alterations (Sun, Miller et al. 2007). Networks identified using resting BOLD fluctuations are closely associated with anatomical connectivity, with high correlation between structural diffusion tensor imaging measures and resting BOLD correlations (Greicius, Supekar et al. 2008). Anatomical disconnection of networks does significantly alter resting BOLD correlations (Johnston, Vaishnavi et al. 2008), though learning induced changes may be more subtle. Following parietal stroke, resting BOLD correlations are initially weakened in attentional networks, but these connections are partially restored in parallel to behavioral improvement, though their roles in normal physiology remains unclear (He, Snyder et al. 2007). Longitudinal studies of BOLD connectivity have revealed changes during development with increasing myelination and coupling of functionally separate cortical regions into a cohesive network (Fair, Cohen et al. 2008), though again these changes occur over a period of years and it remains unclear how quickly these changes appear following changes in cellular neurophysiology. Future studies will have to assess the

sensitivity of BOLD correlation analysis to assess changes in brain physiology following intensive learning.

The stability of resting BOLD correlation networks in the span of several hours following learning is reassuring given its increasing use in studying disease pathophysiology. Changes in functional connectivity (Fox and Raichle 2007) found in stroke, Alzheimer's, schizophrenia, and depression likely reflect long-term changes in cellular neurophysiology that are not simply transient task-related effects.

Conclusion

In conclusion, we find changes in resting brain metabolism, specifically aerobic glycolysis, following a brief period of visuomotor learning. These metabolic alterations likely reflect changes in underlying synaptic structure and activity. These findings support the synaptic homeostasis hypothesis, and suggest that regional metabolic alterations may persist in the resting state following task performance. Future studies will determine whether the regional increase in aerobic glycolysis following task performance is subsequently reset after a night of sleep, possibly accounting for some of the beneficial effects of sleep upon task performance.
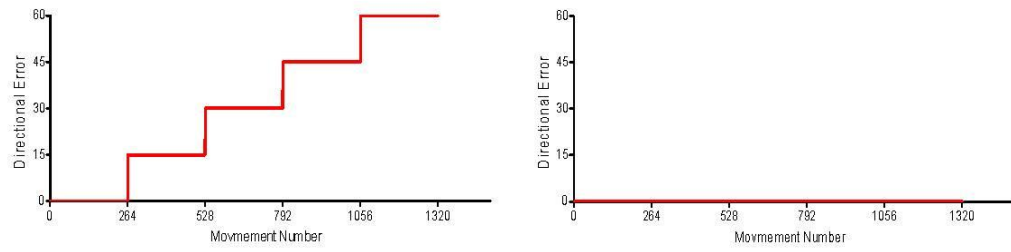
Figure 3.1: Rotation (ROT) and motor control (CON) paradigms used for all experiments.

Subjects performed an equivalent number of movements in both groups either with or without visuomotor rotation.
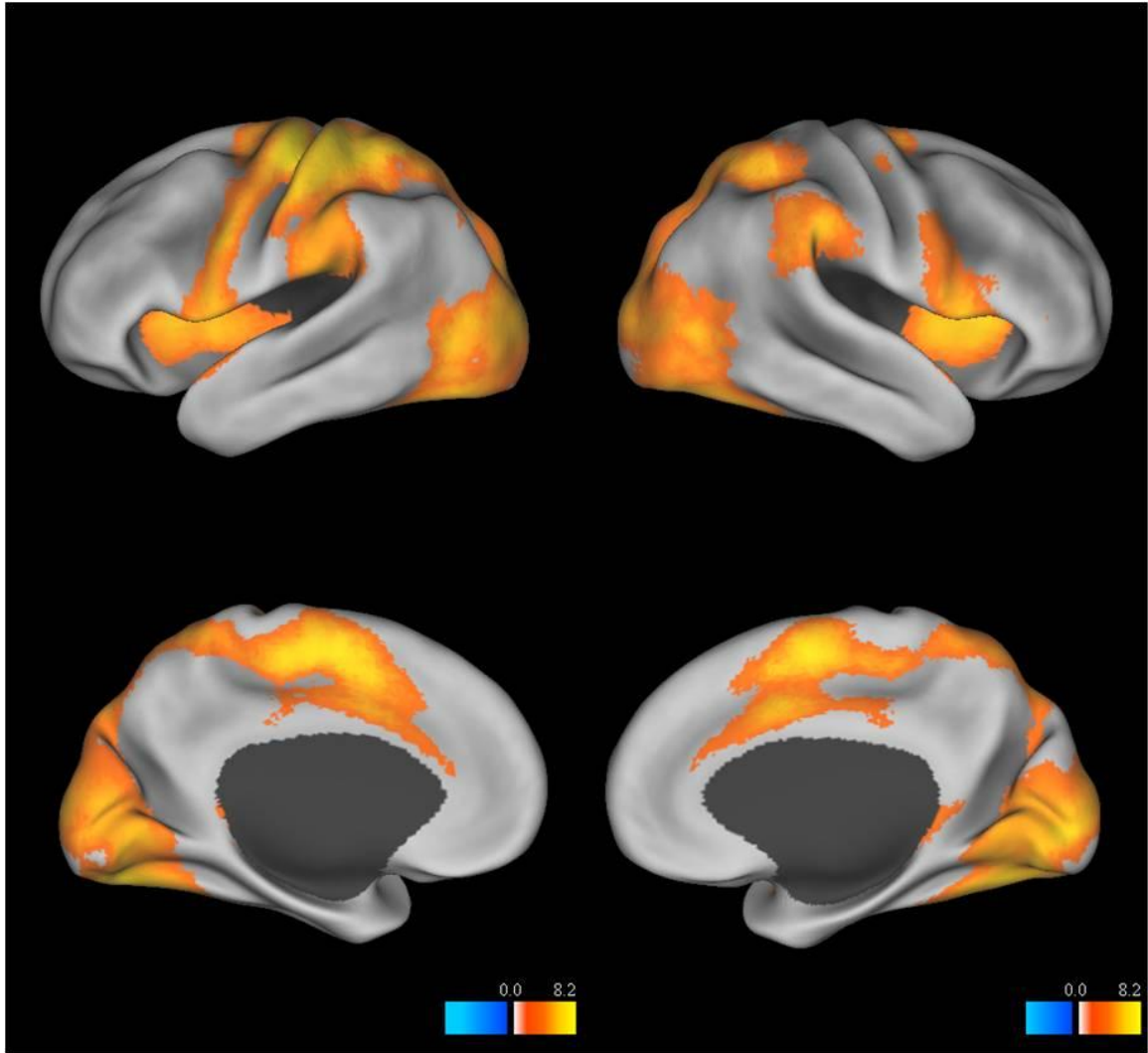
Figure 3.2: Change in BOLD during motor task performance.

Regions with elevated BOLD signal during performance of the motor task (n=28, groupwise *t*-test, Z>3.0, p<0.01, cluster >17, corrected for multiple comparisons).
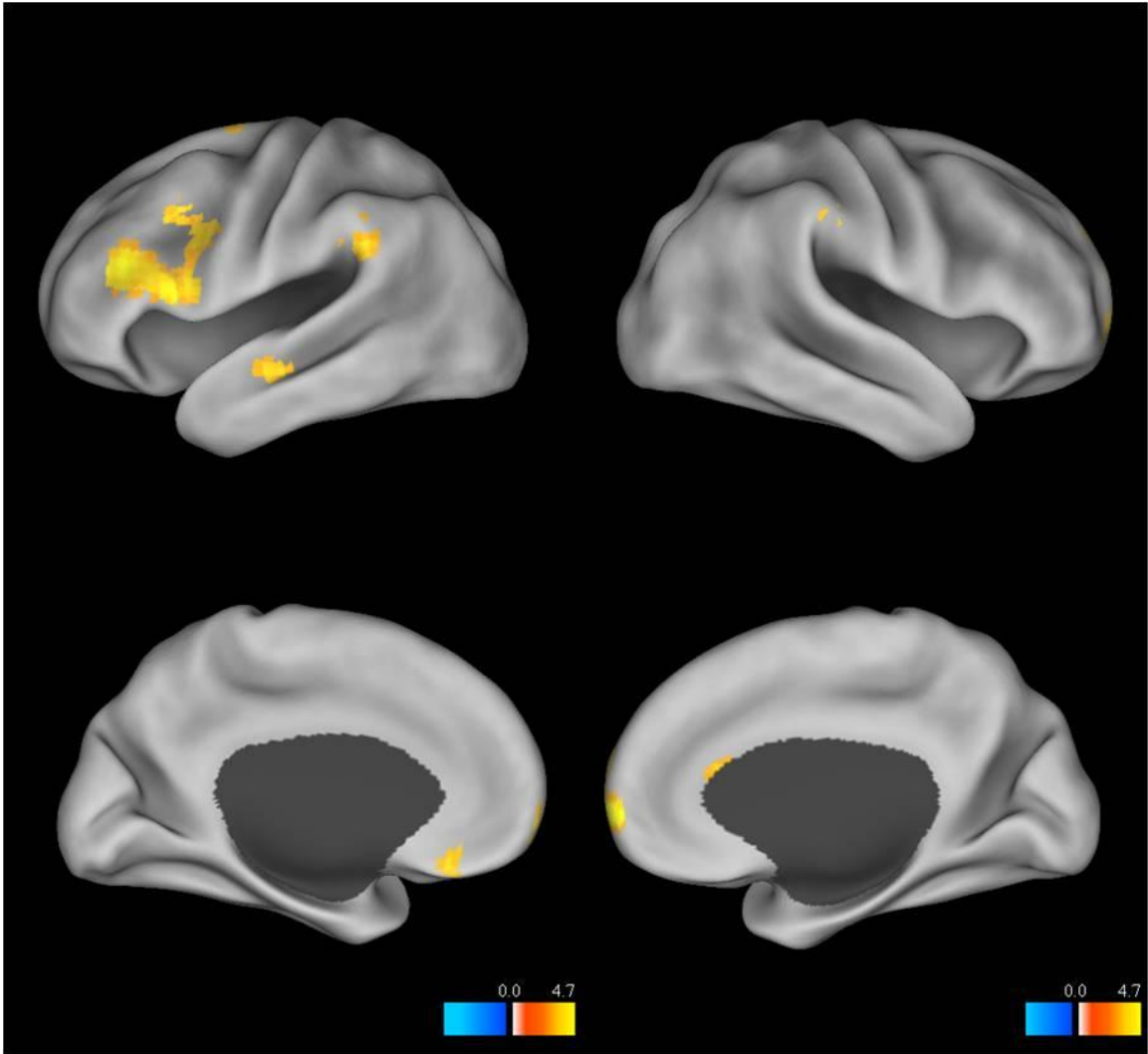
Figure 3.3: Change in BOLD signal following visuomotor rotation.

Regions with altered BOLD signal following visuomotor learning (n=28, task x time x group ANOVA; Z>3.0, p<0.01, cluster >17, corrected for multiple comparisons).

Figure 3.4: Behavioral performance of visuomotor rotation task.

Subjects performed out-and-back reaching movements to circular targets that changed colors at random at 0.93Hz. Performance on the visuomotor rotation task significantly improved ($p<0.05$) both within and across levels of rotation. For visualization purposes, directional error was normalized by the imposed visuomotor rotation.
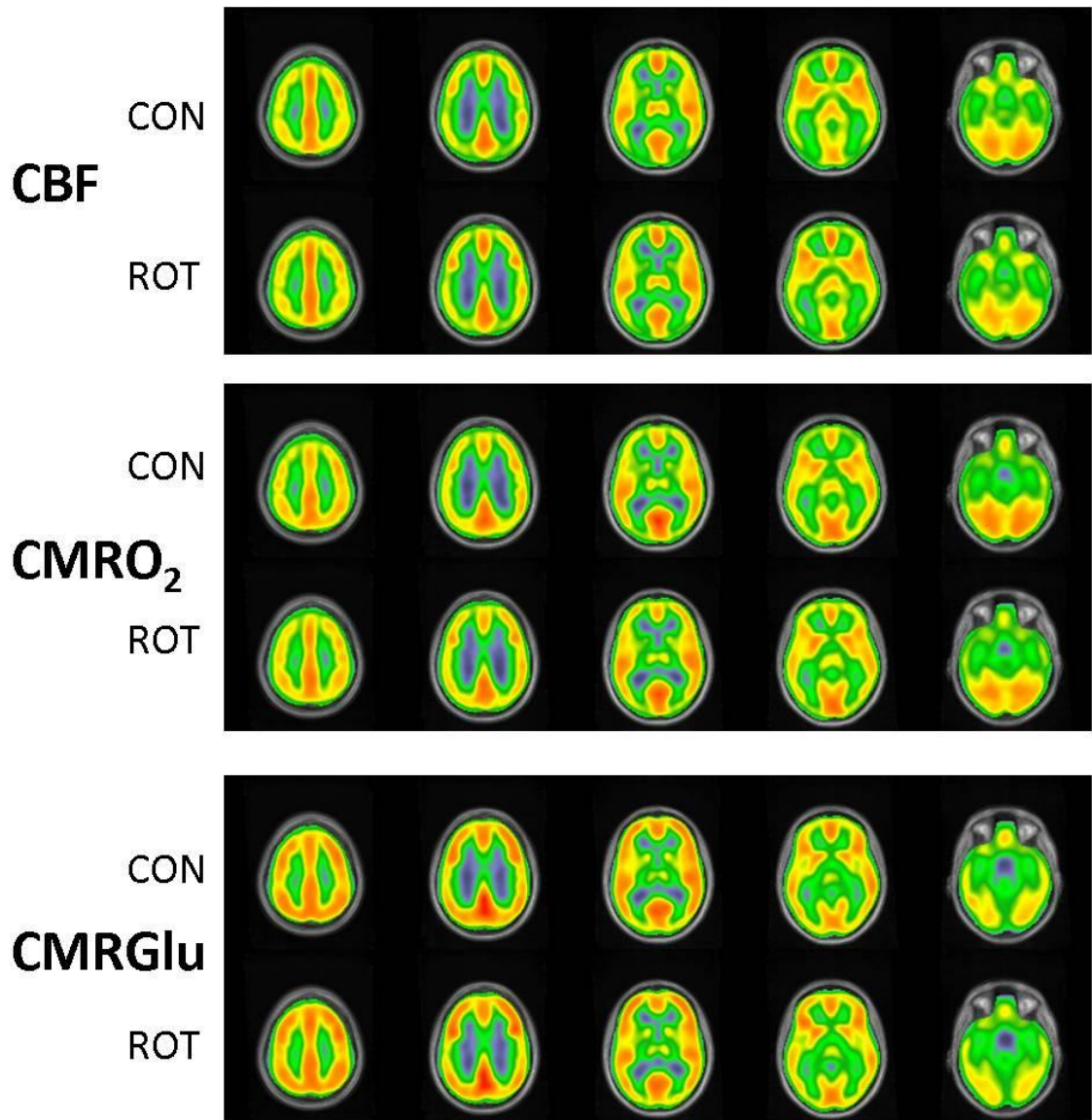
Figure 3.5: Global maps of cerebral blood flow and metabolism in rotation learning (ROT) and motor control (CON) subjects prior to task performance.
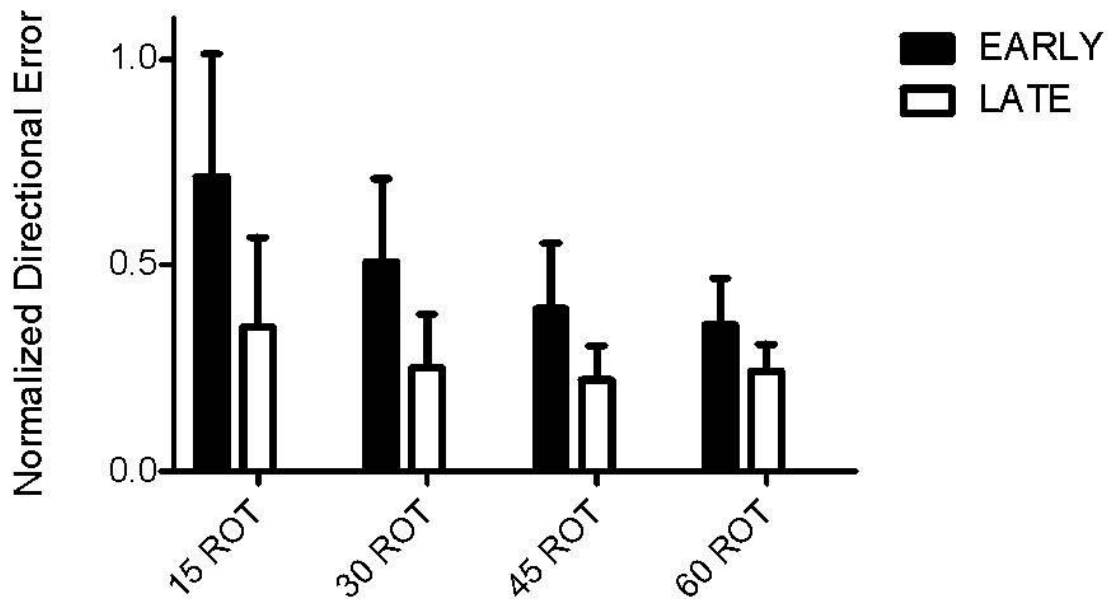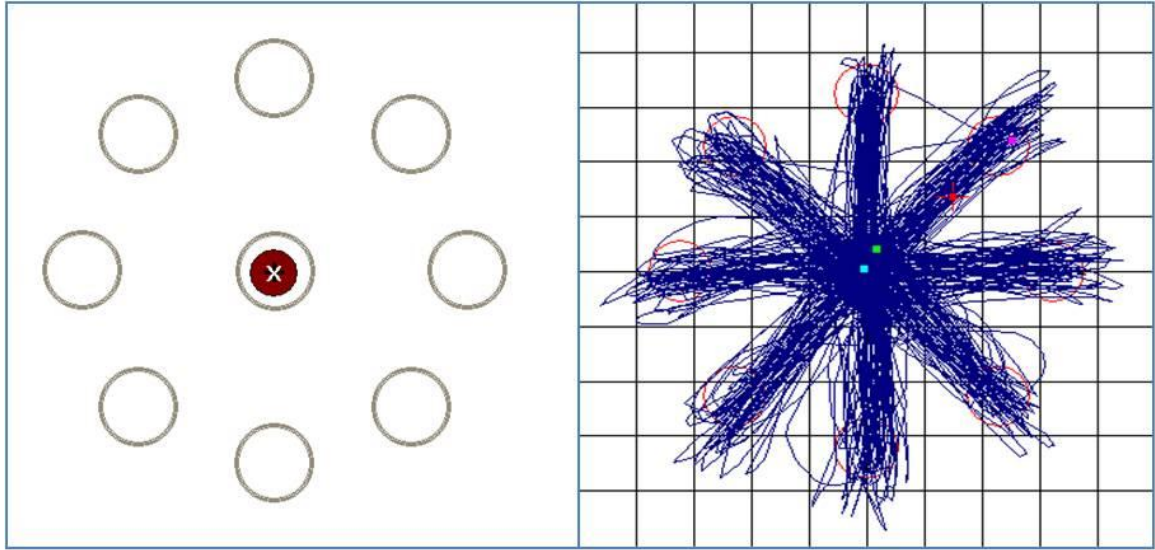
Average maps of cerebral blood flow (Upper; CBF), oxygen consumption (Middle; CMRO$_2$), and glucose consumption (Lower; CMRGlu) were computed using data collected in the initial (pre-task) eyes-closed awake state and averaged across 18 subjects. Because we were interested in regional changes, the whole brain mean was set to 1.0. Note the large deviations in oxygen and glucose consumption across the brain, most prominently between gray and white matter. Despite regional variations, CMRO$_2$, CMRGlu and CBF generally are matched across most of the brain. Of note, the regional distribution of metabolic variables was not significantly different in the pre-task state between the two groups.
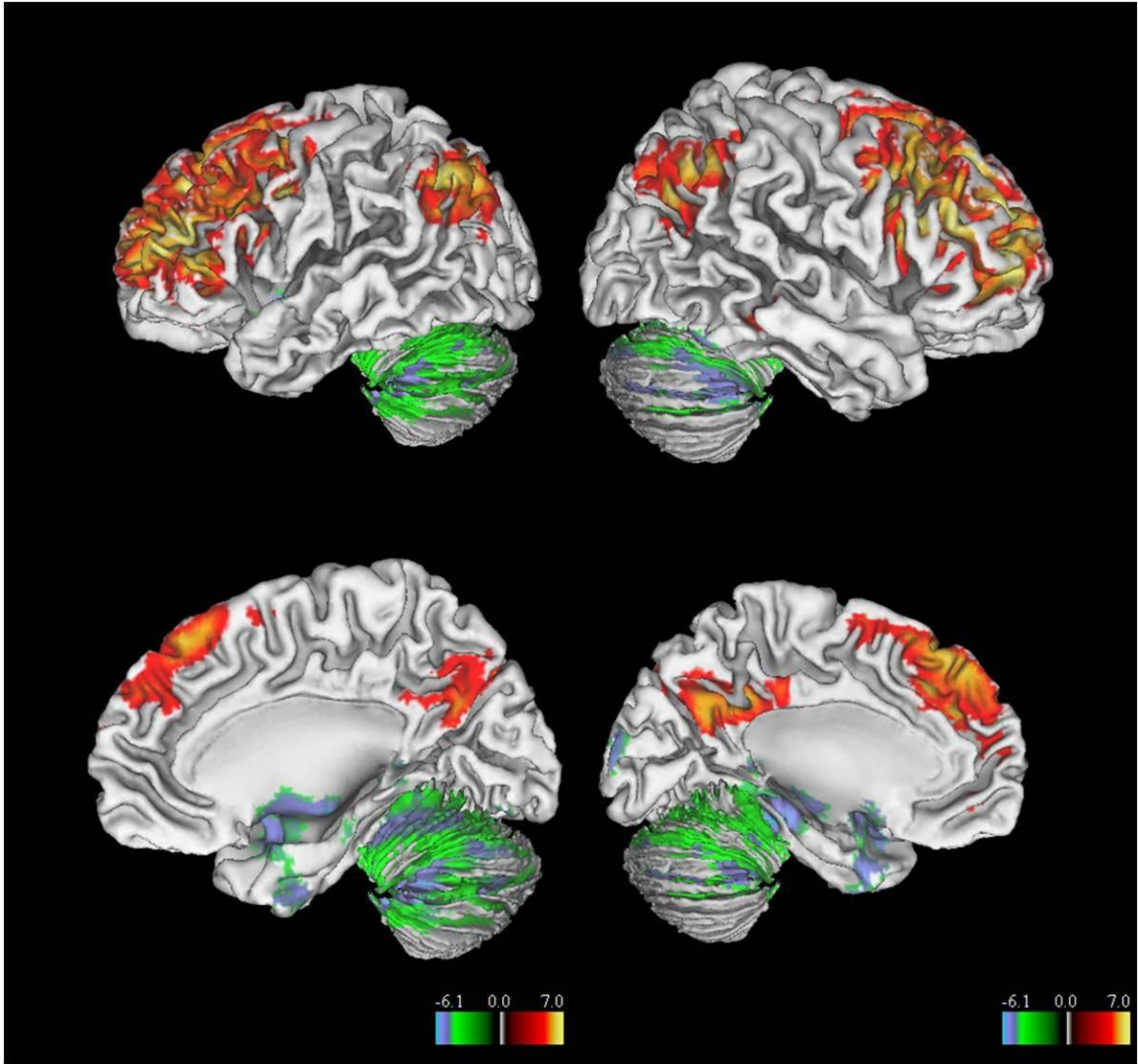
Figure 3.6: Elevated aerobic glycolysis.

Regions of the brain are shown with aerobic glycolysis (Glycolytic Index; GI) significantly elevated compared to the line of regression (n=18, groupwise t-test, |Z|>4.4, p<0.0001, cluster size >99).
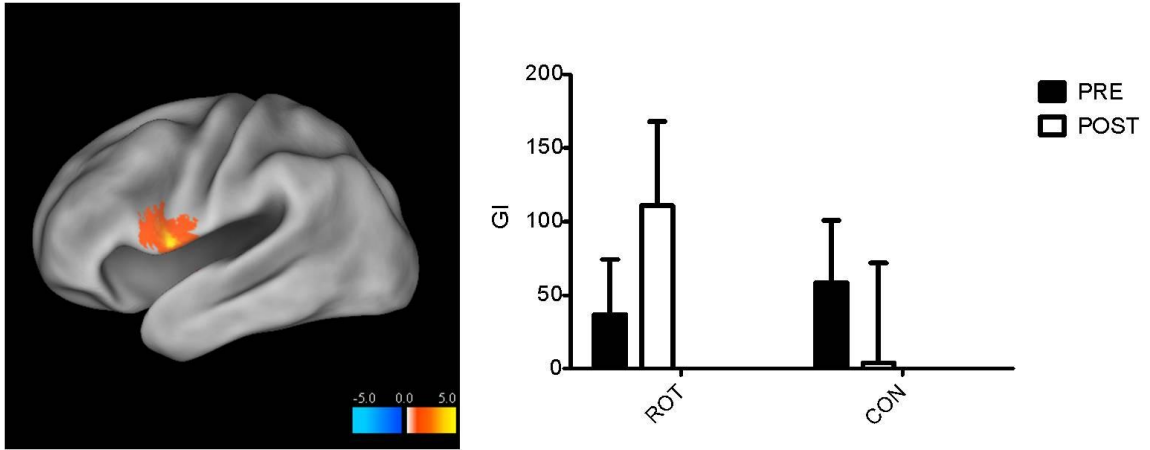
Figure 3.7: Residual increase in aerobic glycolysis in the resting state after task completion.

Significant increase in glycolysis (GI) within left premotor cortex following visuomotor rotation. Repeated measures t-test (n=18, repeated measures t-test, Z>4.4, p<0.001, cluster size >99).

fMRI during task   Δ fMRI rotation learning   Δresting glycolysis   Overlap
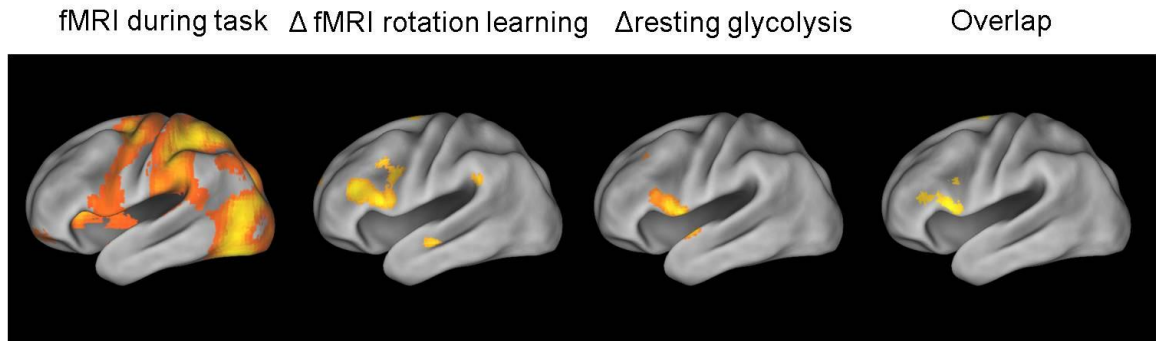
Figure 3.8: Conjunction analysis between visuomotor rotation fMRI and resting aerobic glycolysis.

(a): Regions with elevated BOLD signal during performance of the motor task (n=28, groupwise *t*-test, Z>3.0, p<0.01, cluster >17, corrected for multiple comparisons). (b): Regions with altered BOLD signal following visuomotor learning (task x time x group; Z>3.0, p<0.01, cluster >17, corrected for multiple comparisons). (c): Regions with elevated aerobic glycolysis following visuomotor rotation (n=18, repeated measures t-test, Z>4.4, p<0.00001, cluster >99, corrected for multiple comparisons. (d): Intersection of voxels showing significantly elevated GI following visuomotor learning and elevated BOLD during task performance and altered BOLD during visuomotor rotation.
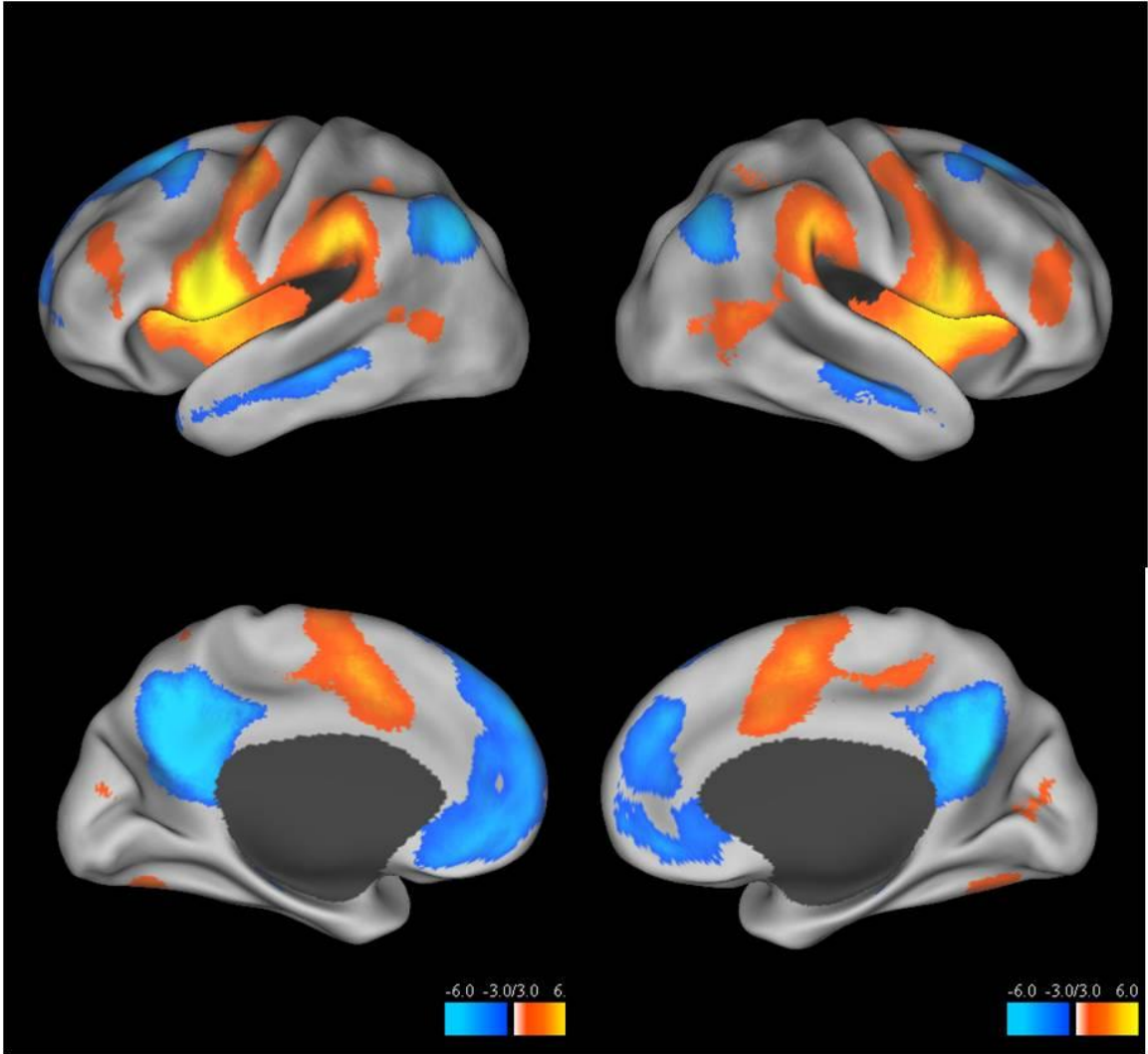
Figure 3.9: Resting BOLD correlation mapping with left premotor cortex seed.

Functional connectivity analysis (n=18, groupwise *t*-test, Z>3.0, p<0.01, cluster >17, corrected for multiple comparisons) using a 6mm radius spherical seed region placed in left premotor cortex [-55 3 10].

Chapter 4: Aerobic glycolysis is elevated in cortical networks with balanced excitation and inhibition

Abstract

Neuronal activity results in a regional increase in cerebral blood flow and glucose metabolism disproportionate to the increase in oxygen metabolism, resulting in local increases in aerobic glycolysis. In the eyes closed resting state, the brain continues to metabolize energy inhomogeneously across the brain reflecting ongoing neuronal activity. The relationship between cerebral energy utilization and local neurochemistry remains unclear, though it has been assumed that excitatory neurotransmission predominates in the energetic cost of brain function. In order to assess the correlation between cerebral metabolism and neurochemistry, we compared resting positron emission tomography data from 33 healthy young adults studied in the eyes-closed awake state with postmortem autoradiography data from two older neurologically normal adults. Cerebral blood flow, glucose, and oxygen metabolism were negatively correlated with excitatory neurotransmitter receptor density while oxygen extraction fraction was positively correlated with inhibitory receptor density. Aerobic glycolysis was nonlinearly correlated to the ratio of excitation to inhibition (E/I) and was highest in regions of balanced E/I. Brain regions with high levels of aerobic glycolysis in the resting state, including the default network, differ in their underlying neurochemistry, suggesting that in addition to differential response to stimuli, cortical networks also differ in their subcellular constituents. Our results provide an important bridge between distributed

brain networks revealed using functional neuroimaging and their underlying neurochemistry.

Introduction

The human brain uses energy to support neuronal activity, primarily associated with the input and output of neurons at the neuronal synapse (Attwell and Laughlin 2001). In the adult human brain, most of this energy is provided by the oxidation of glucose to carbon dioxide and water (Sokoloff 1977). However, following transient increases in neuronal activity, glucose utilization increases more than oxygen consumption, resulting in an elevation in aerobic glycolysis (Fox, Raichle et al. 1988). The cellular processes reliant upon aerobic glycolysis include astrocytic Na^+/K^+ ATPase associated with the cycling of glutamate from the synaptic cleft (Pellerin and Magistretti 1994; Pellerin and Magistretti 1996). But in addition to transient task related alterations in energy metabolism, the brain continues to utilize energy while at rest (Raichle and Mintun 2006). In fact, for many years researchers have known some fraction of glucose is used for purposes other than providing substrate for oxidative phosphorylation (Raichle, Posner et al. 1970; Madsen, Hasselbalch et al. 1995), though its role has remained unclear.

The relationship between cerebral energy utilization and the underlying neurochemical processes at the synapse have largely been unexplored to date. It is assumed that since glutamatergic neurotransmission predominates in the brain, most cerebral energy utilization is devoted to excitatory neurotransmission (Sibson, Dhankhar

97

et al. 1998; Attwell and Laughlin 2001), though inhibitory and neuromodulatory neurotransmitters may also have an energetic cost (Patel, de Graaf et al. 2005; Buzsaki, Kaila et al. 2007).

We hypothesized those cortical regions with a high density of glutamatergic receptors would have high metabolic rates, specifically high levels of glucose metabolism, cerebral blood flow, and aerobic glycolysis. To test this hypothesis, we compared resting positron emission tomography data from 33 healthy young adults studied in the eyes-closed awake state with postmortem autoradiography data from two older neurologically normal adults.

Methods

Positron Emission Tomography

Participants

Positron emission tomography (PET) was performed in thirty-three healthy, right-handed neurologically normal participants (19 women) aged 20 to 33 years (mean 25.4 ± 2.6) recruited from the Washington University community. Subjects were excluded if they had contraindications to MRI, history of mental illness, possible pregnancy, or medication use that could interfere with brain function. All experiments were approved by the Human Research Protection Office (HRPO) and Radioactive Drug Research Committee (RDRC) at Washington University in St. Louis. Written informed consent was provided by all participants.

Image Acquisition

Structural MRI: MRI scans were obtained in all subjects to guide anatomical localization. High-resolution structural images were acquired using a 3D sagittal T1-weighted MPRAGE on a Siemens (Siemens, Erlangen, Germany) 3T Allegra [TE=3.93ms, TR=1900ms, TI=1100ms, flip angle=20°, 256x256 acquisition matrix, 160 slices, 1x1x1 mm voxels] or 1.5T Sonata scanner [TE=3.93ms, TR=1900ms, TI=1100ms, flip angle =15°, 224x256 acquisition matrix, 160 slices, 1x1x1 mm voxels].

PET Scanning: Studies were performed using a Siemens model 961 ECAT EXACT HR 47 PET scanner (Siemens/CTI, Knoxville, TN) with 47 slices encompassing an axial field of view of 15cm. Transverse resolution was 3.8-5.0 mm FWHM and axial resolution was 4.7-5.7 mm full width at half maximum (FWHM). Attenuation data was obtained using ^{68}Ge-^{68}Ga rotating rod sources to enable quantitative reconstruction of subsequent emission scans. Emission data were obtained in the 2D mode (inter-slice septa extended). All PET data was reconstructed using a ramp filter (approximately 6mm FWHM) and then blurred to 12 mm FWHM. Subject head movement during scanning was restricted by a thermoplastic mask. All PET images were acquired in the eyes-closed waking state. No specific instructions were given regarding cognitive activity during scanning other than to remain awake.

All subjects underwent a single PET session including one FDG scan (to measure CMRGlu) and either one (13 subjects) or two (20 subjects) replicate sets of three ^{15}O scans to measure CBV, CBF, and CMRO$_2$, respectively. In subjects with two replicates of ^{15}O scans, CBV, CBF, and CMRO$_2$, values were averaged for data analysis.

PET Measurement of Glucose Metabolism: ^{18}F-fluorodeoxygluse (FDG) uptake and trapping was used to image CMRGlu(Fox, Raichle et al. 1988). Measurements of

CMRGlu were performed after slow intravenous injection of 5mCi of $[^{18}F]$ FDG. Dynamic acquisition of PET emission data continued for 60 minutes with 25 5-sec frames, 9 20-sec frames, 10 1-min frames, and 9 5-min frames. Venous samples for plasma glucose determination were obtained just before and at the mid-point of the scan.

$[^{15}O]$tracer PET scans: 120 second dynamic scans comprised of 2 second frames that began with tracer injection (or inhalation) (Raichle, Martin et al. 1983; Mintun, Raichle et al. 1984). With this method, the optimum 40 second scan was created from summation of the appropriate frames. By reconstructing all frames and then creating a whole brain time-activity curve, the onset of activity in the brain could be judged exactly. **CBF Scan:** Distribution of CBF was measured with a 40-sec emission image (derived from a 120 second dynamic scan) after rapid injection of 50 mCi $[^{15}O]$water in saline (Raichle, Martin et al. 1983). **CBV Scan:** Distribution of CBV was measured with a 5-min emission scan beginning 2 min after brief inhalation of 75mCi of $[^{15}O]$carbon monoxide in room air (Martin, Powers et al. 1987). **$CMRO_2$ Scan:** Distribution of $CMRO_2$ was measured with a 40-sec emission scan (derived from a 120 second dynamic scan) after brief inhalation of 60 mCi of $[^{15}O]$oxygen in room air (Mintun, Raichle et al. 1984).

General PET Data Analysis:

Preprocessing: For each subject, measures of CBF, CBV, $CMRO_2$, and CMRGlu were aligned to each other and then to the subject's MPRAGE. The re-aligned data was then transformed to Talairach space (Lancaster, Glass et al. 1995) using in-house software and scaled to a whole-brain mean of one (local-to-global ratio (Raichle, MacLeod et al. 2001)).

Glycolytic Index: In order to quantitatively assess aerobic glycolysis, we performed a linear regression of CMRGlu on $CMRO_2$. The residuals were scaled by 1000 to produce the glycolytic index (GI). GI represents glucose consumption above or below that predicted by oxygen consumption.

PET statistics: To combine results across subjects, we computed a general linear model (GLM) which contained metabolic data for $CMRO_2$, CMRGlu, CBF, CBV, OEF, OGI, and GI for each subject.

Surface mapping: Volumetric statistical results were projected onto the cortical surface of the PALS B12 (population-average landmark and surface-based) atlas by multifiducial mapping (Van Essen 2005). Surface mapping was performed using Caret v5.512 [http://brainmap.wustl.edu/caret].

Brodmann Regions: Brodmann regions were extracted from the PALS B12 atlas (Caret v5.512). Values for $CMRO_2$, CMRGlu, CBF, CBV, OEF, OGI, and GI were extracted for each Brodmann region in the brain (41 regions for each hemisphere) from the general linear model (GLM) computed for each subject.

Receptor density measurements

Participants: Neurotransmitter receptor density was assessed in two neurologically normal postmortem human brains using quantitative autoradiography (Eickhoff, Schleicher et al. 2007).

Autoradiography: Briefly, excitatory receptor density was assessed by measurement of AMPA ([^{3}H]AMPA), Kainate ([^{3}H]Kainate), and NMDA ([^{3}H]MK801). Inhibitory

receptor density was assessed by measurement of GABA$_A$ ([^{3}H]Muscimol and [^{3}H]Flumazenil) and GABA$_B$ ([^{3}H]CGP).

Excitatory/Inhibitory receptor ratio: A ratio was computed of excitatory to inhibitory receptor density and scaled to a whole brain mean of one (E/I > 1, greater excitation; E/I < 1, greater inhibition).

Correlation statistics: Pair-wise correlations were computed over regions corresponding to Brodmann areas defined using Caret software (Van Essen 2005)on relative metabolic measures averaged over subjects and neurotransmitter receptor density (weighted Pearson's product-moment correlation, 35 df, α=0.05).

Results

We compared positron emission tomography (PET) data (cerebral blood flow, oxygen metabolism, glucose metabolism, oxygen extraction fraction, and aerobic glycolysis) from 33 young neurologically normal subjects with postmortem autoradiography data (excitatory, inhibitory, and excitatory/inhibitory receptor density) from two neurologically normal older individuals. Data was compared in a standardized Talaraich space using 37 pre-defined regions of interest comprising of Brodmann regions on the cortical surface from the Caret atlas (Table 4.1).

Excitatory receptor density was negatively correlated to cerebral blood flow (CBF; r= -0.348, p<0.05), cerebral metabolic rate of oxygen (CMRO$_2$; r= -0.509, p<0.01), cerebral metabolic rate of glucose (CMRGlu; r= -0.470, p<0.01) and oxygen extraction fraction (OEF; r= -0.423, p<0.01) (Figure 4.1). In contrast, inhibitory receptor

density was positively correlated to OEF (r=0.406, P<0.05), though no significant correlations were found with CBF, $CMRO_2$, or CMRGlu (Figure 4.2)

The ratio of excitatory to inhibitory receptors (E/I) was negatively correlated to CBF (r= -0.332, p<0.05), $CMRO_2$ (r= -0.608. p<0.001), CMRGlu (r = -0.537, p<0.001), and OEF (r = -0.641, p<0.001) (Figure 4.3). The ratio of excitation to inhibition (E/I), though, was not linearly correlated to the amount of aerobic glycolysis (glycolytic index, GI). Surprisingly, regions with a balanced density of excitatory and inhibitory receptors had the highest glycolysis and regions with either excessive excitatory or inhibitory receptor density had low GI (quadratic r=0.727, p<0.001) (Figure 4.4).

Discussion

We have assessed regional differences in cortical receptor density in postmortem human brain and found significant correlations to resting cerebral metabolism from a separate group of individuals. Our results can be summarized in three main findings. First, cortical regions with a higher density of AMPA, Kainate, and NMDA receptors have lower metabolic rates (CBF, $CMRO_2$, CMRGlu). Second, cortical regions with higher density of $GABA_A$ and $GABA_B$ have a higher oxygen extraction fraction. Third, aerobic glycolysis is highest in cortical regions with a balanced ratio of excitatory and inhibitory receptors.

Our results stand in sharp contrast with a hypothesized positive correlation between excitatory receptor density and metabolism that underlies most estimates of cerebral energy utilization (Sibson, Dhankhar et al. 1998; Ames 2000; Attwell and Laughlin 2001). One possible explanation for this unexpected finding is that receptor

density may be an inaccurate reflection of ongoing excitatory activity. Ineffectual or silent synapses exist in the developing nervous system, suggesting that some glutamatergic receptors may be inactive without appropriate modulatory priming (Renger, Egles et al. 2001). This hypothesis, though, is inconsistent with a wide range of evidence suggesting a correlation between receptor density and neuronal activity (Kennedy 2000; Eickhoff, Schleicher et al. 2007; Sheng and Hoogenraad 2007). In addition, increased neuronal activity following long-term potentiation is associated with an increase in glutamatergic receptor density (Buchs and Muller 1996; Jacob, Moss et al. 2008), suggesting that receptor density may be a reasonable surrogate measure for neuronal activity. Elevation of excitatory neurotransmission in epileptiform cortex is associated with focal increases in cerebral blood flow (Kahane, Merlet et al. 1999) and significant increases in the density of AMPA and NMDA mRNA (Mathern, Pretorius et al. 1997). These data suggest that the observed negative correlation between cerebral metabolism and excitatory receptor density likely reflects neuronal physiology.

An alternate explanation of these data is that cortical regions with a disproportionately higher density of glutamatergic receptors may, in fact, utilize less energy than regions that have to compensate for inhibitory tone at the dendrite. If we assume that all cortical regions have similar levels of excitability, cortical regions with greater inhibitory receptor density require greater pre-synaptic firing in order to induce a postsynaptic response. Though we assume that the post-synaptic response is the main energetic cost in the brain, spiking activity itself is only a minor contributor to total energy consumption (Ames 2000; Attwell and Laughlin 2001). Increased fluctuations of the postsynaptic membrane potential in cortical regions with inhibitory tone may be

104

responsible for these observed correlations. Previous modeling studies have estimated the cost of inhibitory neurotransmission to reflect approximately 10-15% of total cerebral energy consumption (Shulman, Rothman et al. 2004; Patel, de Graaf et al. 2005; Buzsaki, Kaila et al. 2007). This estimation of energy cost is likely an underestimate as it does not account for the compensatory excitatory neurotransmission required to counteract inhibitory input to the postsynaptic neuron (Buzsaki, Kaila et al. 2007). Brain regions with higher levels of inhibitory receptor density (lower E/I) may therefore require increased blood flow and energy metabolism in order for an equivalent neuronal response (synaptic output). Unfortunately, direct data to support this hypothesis is lacking as the energetic costs of the integration of numerous excitatory and inhibitory inputs at the dendrite remains unknown.

Our finding of a positive correlation between inhibitory receptor density and oxygen extraction fraction suggests that postsynaptic GABAergic activity may primarily induce increases in oxidative metabolism. The OEF is relatively homogenous across the brain, though an elevation in visual cortex has been previously reported (Lebrun-Grandie, Baron et al. 1983; Raichle, MacLeod et al. 2001) and is paralleled by disproportionate inhibitory receptor density. Visual cortex receives significant excitatory inputs from the LGN, though local horizontal inhibitory circuits are vital for development and maintenance of receptor field properties (Gabbott and Somogyi 1986). These data indicate that cortical regions with high inhibitory tone are likely to increase oxygen extraction before inducing changes in blood flow to increase oxygen supply.

In contrast to other metabolic measures, aerobic glycolysis is highest in regions with a balanced ratio between excitation and inhibition (E/I) (Figure 4.4). The role of

glycolysis is most closely associated with astrocytic uptake and cycling of glutamate (Pellerin and Magistretti 1996; Voutsinos-Porche, Bonvento et al. 2003; Kasischke, Vishwasrao et al. 2004). The discrepancy between the CMRGlu and aerobic glycolysis as it relates to neurochemistry warrants further discussion. While CMRGlu primarily reflects neuronal energy utilization (since most glucose is fated for complete oxidation associated with neuronal membrane potential fluctuations), aerobic glycolysis reflects astrocytic energy utilization (primarily due to glutamate cycling). Regions with balanced E/I have elevations in aerobic glycolysis disproportionate to its elevation in CMRGlu (which is highest in regions with low E/I) indicating an unexpected shift in the fate of glucose depending on the neurochemical profile of the region. We unfortunately do not have a complete explanation for this finding. A balanced E/I suggests that cortical regions may receive significant excitatory and inhibitory inputs that must by integrated at the dendrite in order to compute the postsynaptic response. These regions likely have greater glutamate flux than regions with high concentrations of either excitatory or inhibitory receptors alone due to the presence of local inhibitory feedback circuits preventing postsynaptic firing. Future studies will have to assess the concentration of glutamate in the synaptic cleft directly in relation to local neurochemistry.

Conversely, an alternate explanation for the observed E/I: aerobic glycolysis correlation is that regions with balanced E/I are utilizing a larger fraction of glucose for non-energetic or anabolic processes. Glucose is a source of carbon fragments needed for production of DNA and RNA via the pentose phosphate pathway (Gaitonde, Jones et al. 1987). Cortical regions with balanced E/I may require greater membrane turnover and undergo greater oxidative stress as a result. In addition to producing five-carbon

fragments, the pentose phosphate shunt also produces NADPH that may help compensate for local oxidative stress (Palmer 1999). These findings are surprising and merit further investigation using in vitro and modeling experiments.

Our data indicates that in addition to their differential response to stimuli, cortical networks differ in their innate neurochemical profile (Figure 4.5). The brain can be subdivided into functional units by clustering of Brodmann regions in Figure 4.4. Regions with high levels of inhibition (low E/I) and low levels of glycolysis include visual cortex (BA17/18/19). In contrast, the default and cognitive control networks (Raichle, MacLeod et al. 2001; Dosenbach, Fair et al. 2007; Buckner, Andrews-Hanna et al. 2008) have a balanced distribution of excitatory and inhibitory receptors and high levels of glycolysis. Sensory regions including primary motor and somatosensory cortex (BA1/2/3/4) have a similar balanced distribution of excitatory and inhibitory receptors, but minimal elevation in glycolysis. Temporal lobe, including primary auditory cortex, hippocampus, and parahippocampal gyrus, has predominantly excitatory receptor density and has low levels of aerobic glycolysis. These correlations indicate that cortical networks differ innately in their energy utilization independent of task state.

A partial explanation for the relationship between aerobic glycolysis and E/I may be provided by investigation of neuronal development. At birth, the brain is primarily glycolytic as the enzymes necessary for complete oxidation metabolism are not produced until several weeks postnatal (Chugani, Phelps et al. 1987; Altman, Perlman et al. 1993; Powers, Rosenbaum et al. 1998). But aerobic glycolysis actually continues to increase in the infant brain long after birth and peak at the age of six in parallel to increases in synaptic density. Since aerobic glycolysis is most closely associated with glutamate flux

(Pellerin and Magistretti 1996), this longitudinal progression may reflect an increase in excitatory neurotransmission, consistent with structural imaging data suggesting an increase in postsynaptic density in infancy followed by synaptic pruning (Larsen, Bonde Larsen et al. 2006). What remains unknown is whether inhibitory receptors follow a similar longitudinal trajectory. There is considerable postnatal alteration in neurotransmitter receptor density in early life with alterations in both NMDA and GABA receptor density seen in the first decade of life in monkeys (Shaw, Cameron et al. 1991; Lewis 1997; Andersen 2003), similar to the trajectory of glucose metabolism. The present data suggest that all cortical regions may initially have a balanced ratio of excitation to inhibition and be highly glycolytic at birth, but during postnatal development, these cortical regions may specialize to predominantly inhibitory or excitatory receptor profiles with a concomitant reduction in their utilization of aerobic glycolysis. Future studies will have to determine to what extent changes in cerebral metabolism can be accounted for by changes in local receptor density.

In conclusion, we provide evidence that cerebral blood flow, glucose, and oxygen metabolism are negatively correlated with excitatory neurotransmitter receptor density while oxygen extraction fraction is positively correlated with inhibitory receptor density. Aerobic glycolysis is nonlinearly correlated to the ratio of excitation to inhibition (E/I) and is highest in regions of balanced E/I. While a complete explanation of these findings remains to be found, we believe that inhibitory neurotransmission is likely to account for a larger fraction of energy utilization than heretofore realized. We also find that in addition to a differential response to stimuli, cortical networks also differ in their

subcellular constituents. Future in vivo and modeling studies are needed to define the

role of excitatory and inhibitory receptor function in cerebral energy utilization.
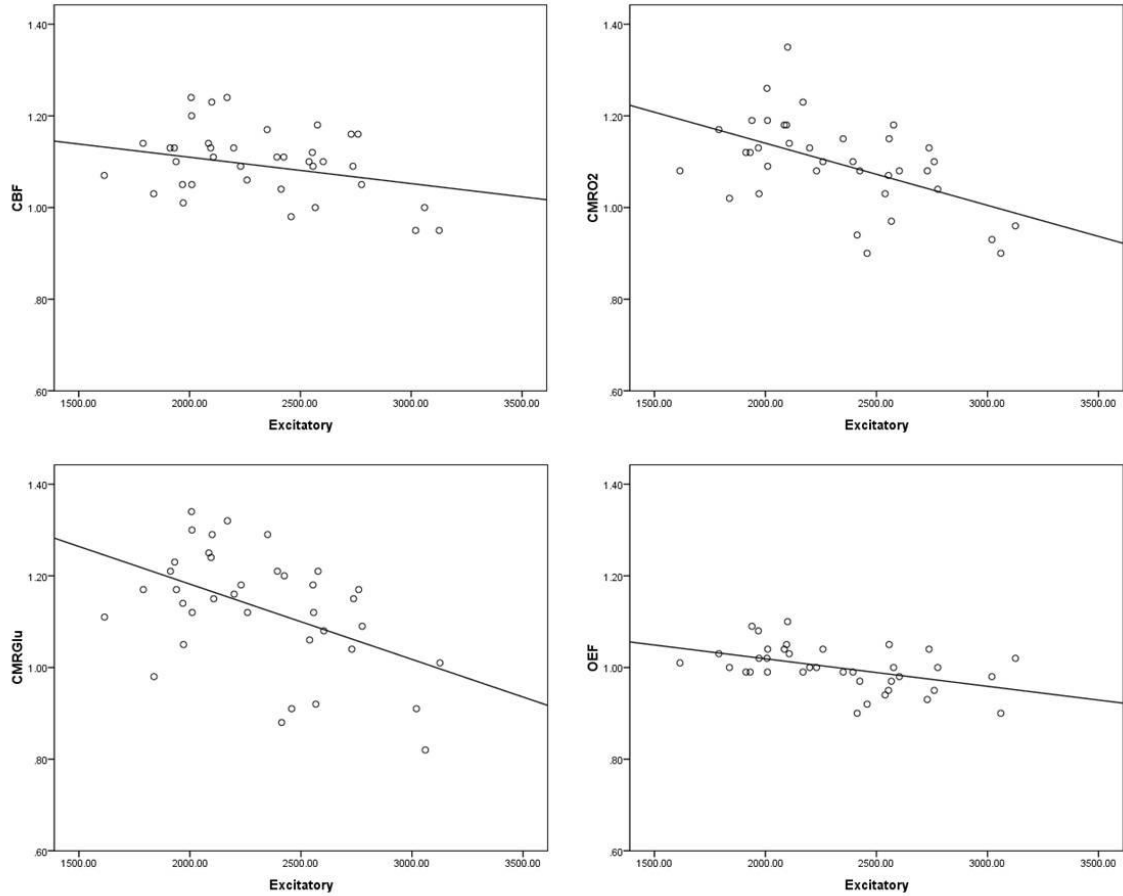
Figure 4.1: Correlation between excitatory receptor density and cerebral metabolism across cortical Brodmann regions.

Average cerebral blood flow (CBF; upper left), oxygen consumption (CMRO2; upper right), glucose consumption (CMRGlu; lower left), and oxygen extraction fraction (OEF; lower right).
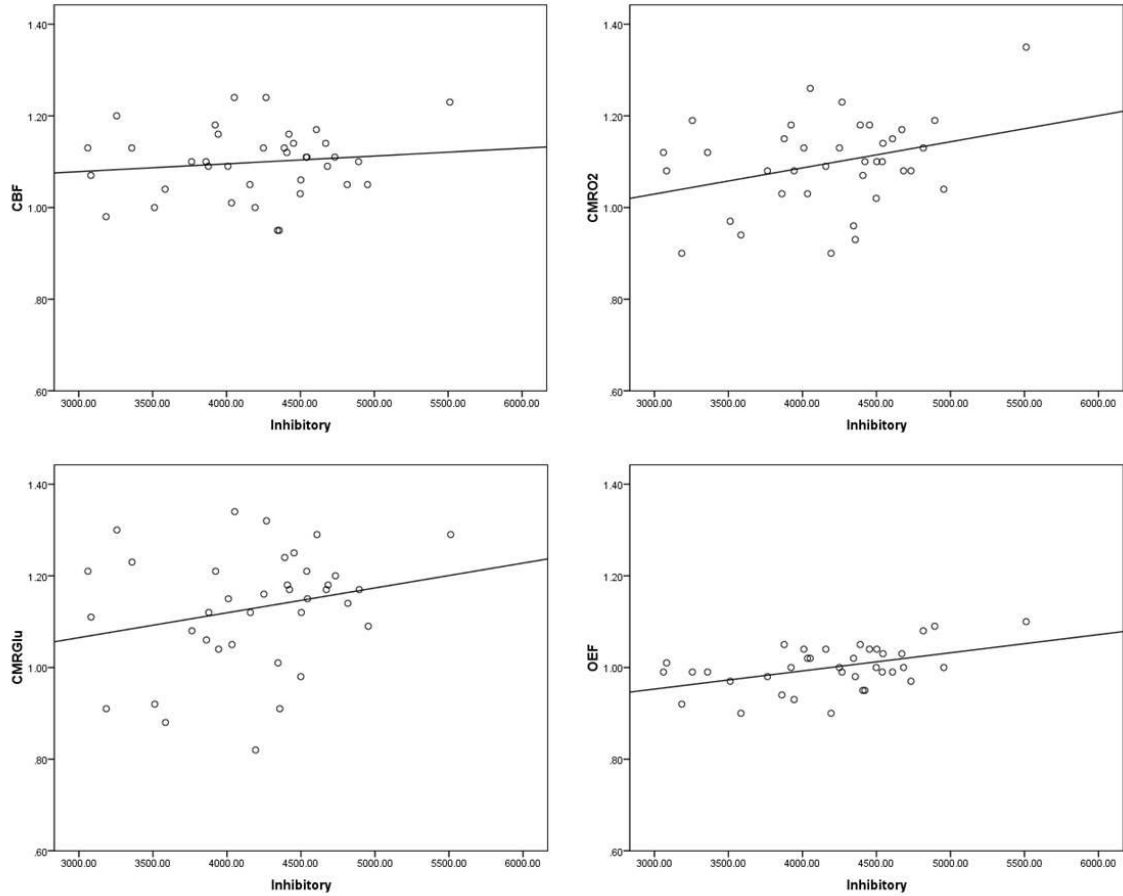
Figure 4.2: Correlation between inhibitory receptor density and cerebral metabolism across cortical Brodmann regions.

Average cerebral blood flow (CBF; upper left), oxygen consumption (CMRO2; upper right), glucose consumption (CMRGlu; lower left), and oxygen extraction fraction (OEF; lower right).
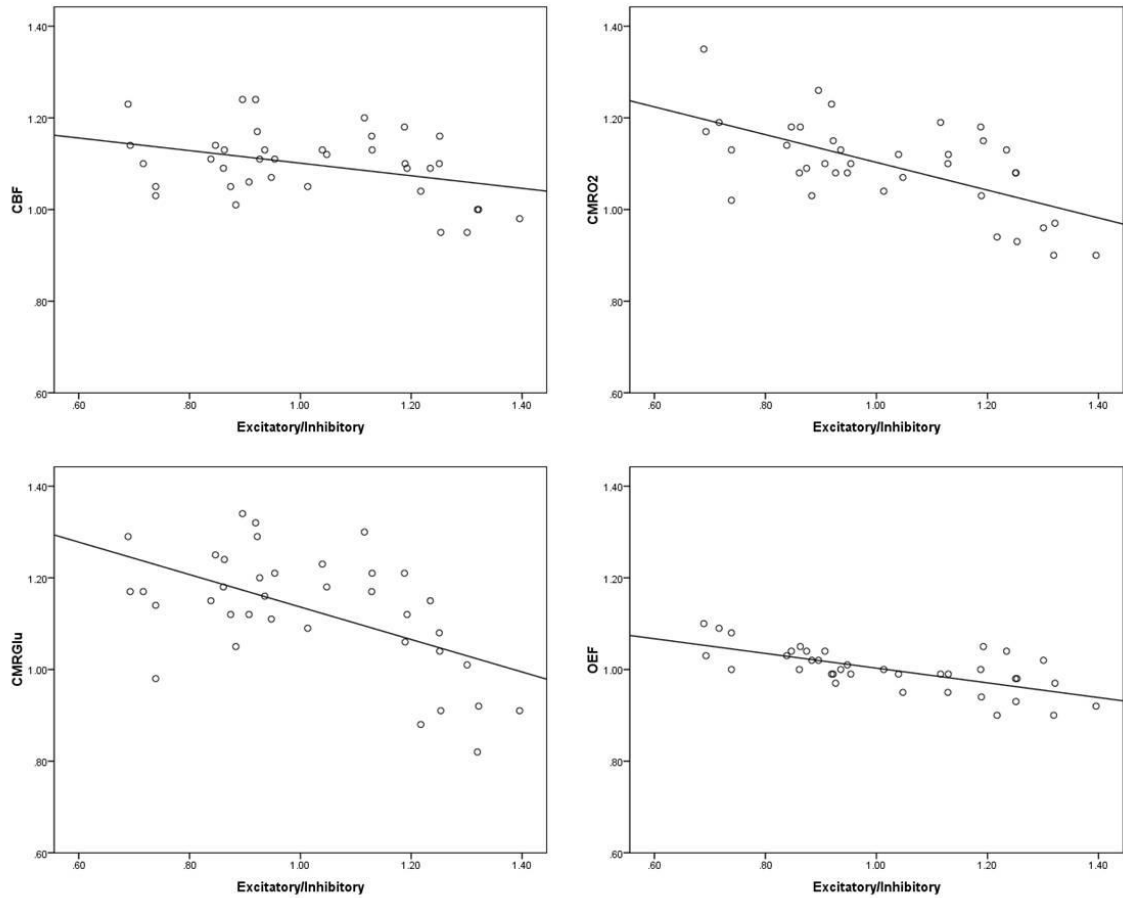
Figure 4.3: Correlation between excitatory/inhibitory (E/I) receptor density and cerebral metabolism across cortical Brodmann regions.

Average cerebral blood flow (CBF; upper left), oxygen consumption (CMRO2; upper right), glucose consumption (CMRGlu; lower left), and oxygen extraction fraction (OEF; lower right).
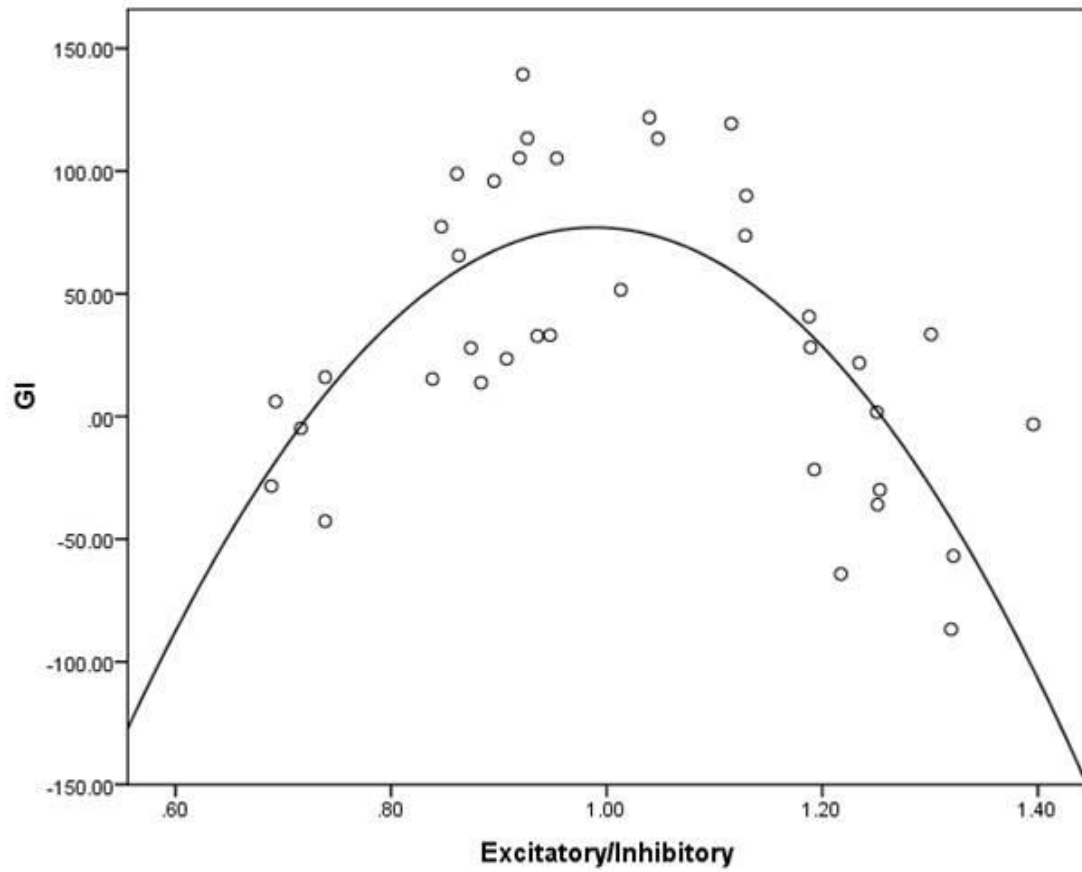
Figure 4.4: Correlation between excitatory/inhibitory (E/I) receptor density and aerobic glycolysis (GI).
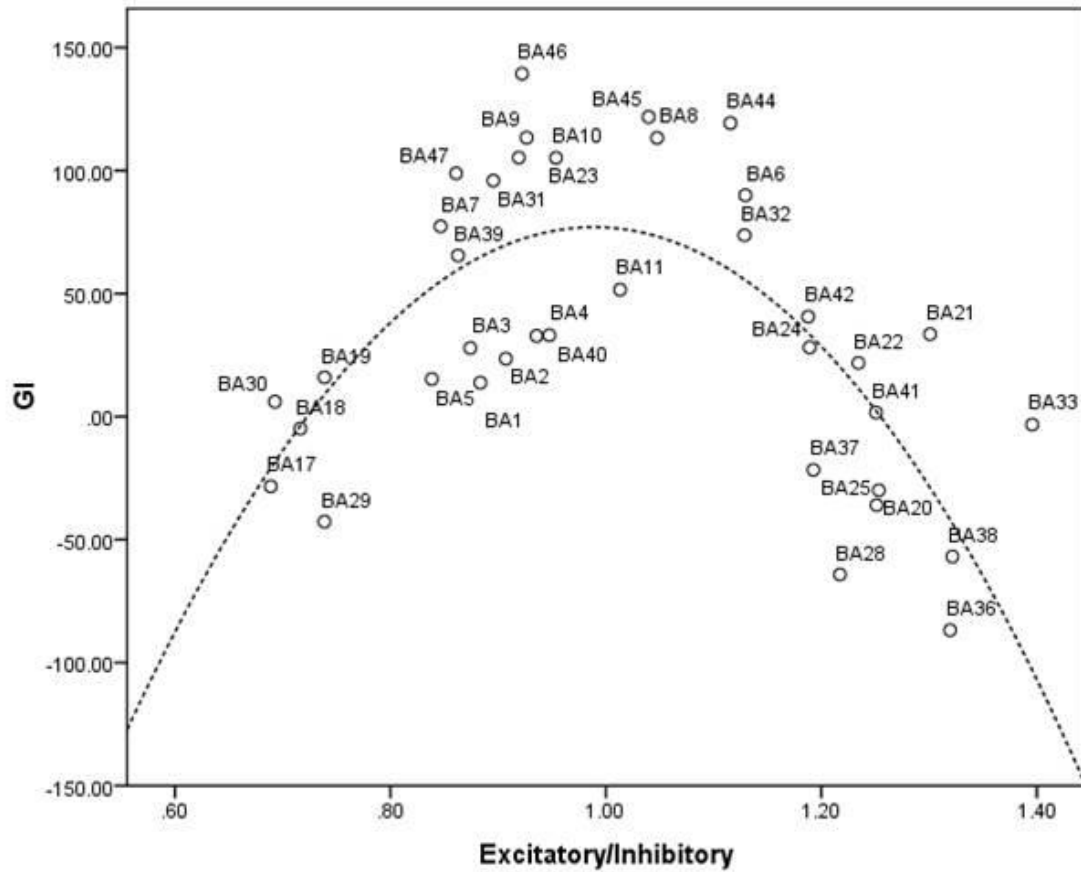
Figure 4.5: Correlation between excitatory/inhibitory (E/I) receptor density and aerobic glycolysis (GI) labeled by Brodmann regions.

Note that primary visual cortex has low E/I, default network and primary sensorimotor cortex has balanced E/I and temporal lobe and hippocampus has elevated E/I. In conjunction with aerobic glycolysis, several distinct cortical networks can be readily ascertained by clustering regions on the GI x E/I axis.

AVERAGE	Voxels	GI	OEF	CBF	CMRO2	CMRGlu	Excitatory	Inhibitory	EI	AMPA	Kainate	NMDA	GABAA	GABAB	BZ
BROD.01	1212	13.77	1.02	1.01	1.03	1.05	1971	4034	0.846	398	567	1006	1560	1954	2600
BROD.02	1401	23.51	1.04	1.06	1.10	1.12	2259	4503	0.886	451	598	1210	1670	2280	2775
BROD.03	895	27.88	1.04	1.05	1.09	1.12	2010	4158	0.828	384	546	1081	1670	1988	2870
BROD.04	3594	33.08	1.01	1.07	1.08	1.11	1615	3082	0.936	351	445	819	1082	1563	1956
BROD.05	857	15.27	1.03	1.11	1.14	1.15	2107	4544	0.811	434	520	1154	1622	2159	3148
BROD.06	2912	89.95	0.99	1.13	1.12	1.21	1912	3061	1.112	379	548	985	1178	1637	1670
BROD.07	2721	77.35	1.04	1.14	1.18	1.25	2085	4453	0.794	549	435	1102	1867	2121	2797
BROD.08	1593	113.27	0.95	1.12	1.07	1.18	2554	4409	1.125	618	669	1267	1284	2627	2279
BROD.09	2086	113.38	0.97	1.11	1.08	1.20	2425	4733	1.002	597	730	1098	1286	2782	2616
BROD.10	2176	105.17	0.99	1.11	1.10	1.21	2394	4539	0.996	669	687	1038	1383	2547	2601
BROD.11	2700	51.61	1.00	1.05	1.04	1.09	2776	4955	1.079	795	761	1220	1444	2883	2699
BROD.17	1458	-28.39	1.10	1.23	1.35	1.29	2100	5612	0.608	495	269	1336	2553	2198	4074
BROD.18	2797	-4.85	1.09	1.10	1.19	1.17	1939	4894	0.653	461	267	1211	2059	2063	3603
BROD.19	4125	15.99	1.08	1.05	1.13	1.14	1968	4817	0.678	514	288	1166	2049	2122	3340
BROD.20	2268	-29.93	0.98	0.95	0.93	0.91	3020	4357	1.334	640	1279	1101	1511	2772	1659
BROD.21	1118	33.49	1.02	0.95	0.96	1.01	3126	4345	1.337	633	1349	1144	1692	2682	1634
BROD.22	3173	21.79	1.04	1.09	1.13	1.15	2737	4010	1.290	536	1161	1040	1419	2454	1692
BROD.23	626	105.27	0.99	1.24	1.23	1.32	2169	4267	0.881	483	478	1208	1603	2028	2875
BROD.24	1632	28.17	0.94	1.10	1.03	1.06	2539	3861	1.230	704	559	1277	1228	2155	2184
BROD.25	292	-35.97	0.93	1.16	1.08	1.04	2729	3944	1.252	733	601	1395	1427	2139	2182
BROD.28	251	-64.19	0.90	1.04	0.94	0.88	2413	3585	1.251	671	854	888	1142	1958	2111
BROD.29	74	-42.71	1.00	1.03	1.02	0.98	1838	4499	0.690	372	378	1088	1852	2075	2995
BROD.30	186	6.07	1.03	1.14	1.17	1.17	1790	4672	0.677	362	371	1057	1562	2202	3377
BROD.31	831	95.92	1.02	1.24	1.26	1.34	2007	4053	0.845	465	366	1176	1801	2082	2140
BROD.32	1298	73.71	0.95	1.16	1.10	1.17	2760	4422	1.199	828	675	1257	1245	2509	2581
BROD.33	226	-3.22	0.92	0.98	0.90	0.91	2458	3185	1.355	694	468	1296	1215	1612	1930
BROD.36	493	-86.76	0.90	1.00	0.90	0.82	3060	4194	1.435	631	1307	1122	1387	2754	1492
BROD.37	2156	-21.68	1.05	1.09	1.15	1.12	2557	3877	1.231	527	774	1256	1282	2198	2076
BROD.38	1641	-56.87	0.97	1.00	0.97	0.92	2567	3512	1.277	686	465	1416	1426	1830	1938
BROD.39	1314	65.48	1.05	1.13	1.18	1.24	2095	4391	0.814	384	533	1179	1723	2032	2994
BROD.40	1463	32.78	1.00	1.13	1.13	1.16	2199	4250	0.900	484	551	1165	1510	1959	3071
BROD.41	452	1.71	0.98	1.10	1.08	1.08	2603	3764	1.216	483	1130	990	1627	2104	1692
BROD.42	812	40.65	1.00	1.18	1.18	1.21	2577	3923	1.203	484	1090	1003	1520	2315	1696
BROD.44	763	119.31	0.99	1.20	1.19	1.30	2009	3257	1.027	513	521	975	1478	1550	1935
BROD.45	465	121.81	0.99	1.13	1.12	1.23	1931	3359	0.981	516	419	996	1450	1686	1895
BROD.46	950	139.37	0.99	1.17	1.15	1.29	2350	4608	0.950	601	668	1081	1451	2522	2721
BROD.47	284	98.87	1.00	1.09	1.08	1.18	2230	4683	0.889	652	576	1002	1535	2641	2549

Table 4.1: Metabolism (average; N=33) and neurochemistry (average; N=2) for each Brodmann region in the brain.

Regions from Caret atlas. GI, glycolytic index; OEF, oxygen extraction fraction; CBF, cerebral blood flow; CMRO2, cerebral metabolic rate of oxygen; CMRGlu, cerebral metabolic rate of glucose.

Chapter 5: Conclusion and future directions

This thesis set out to investigate the regional distribution and functional role of aerobic glycolysis in the resting human brain. This thesis presents several functional and methodological insights into resting brain physiology and provides a new framework by which researchers can understand diseases of the brain.

The first experiment, *Regional distribution of aerobic glycolysis in the human brain* (Chapter 2), demonstrates that aerobic glycolysis is not homogenous across the cortex. Brain regions known to have high levels of functional activity, including the default and cognitive control networks, have elevated glycolysis in eyes-closed rest. We also find that the distribution of aerobic glycolysis does not completely mirror the pattern of glucose utilization. For example, some cortical regions have high levels of glucose and oxygen metabolism (including visual cortex), but they have minimal aerobic glycolysis. These data also indicate that aerobic glycolysis may be a more direct marker of neuronal activity than glucose utilization or oxygen consumption alone.

The second experiment, *Resting brain metabolism is modified by task performance: metabolic plasticity of the brain* (Chapter 3), provides evidence that aerobic glycolysis is elevated regionally following performance of a rotational learning task. These data provide supporting evidence to our hypothesis that local changes in cortical physiology cause changes in resting brain metabolism. Aerobic glycolysis is increased in left premotor cortex for several hours following after task completion. This premotor cortex region is activated acutely during motor task performance and alters its activity

during visuomotor learning. These data provide new insights into the mechanisms of learning and raise questions about the mechanisms of synaptic homeostasis.

The final experiment, *Aerobic glycolysis is elevated in cortical networks with balanced excitation and inhibition* (Chapter 4), provides evidence that the distribution of aerobic glycolysis is closely related to the underlying neurochemistry of the cortex. Brain regions with elevated glycolysis also have a balanced distribution of excitatory and inhibitory neurotransmitter receptors, suggesting an association between synaptic plasticity and aerobic glycolysis. Further, we find a surprising negative correlation between excitatory receptor density and cerebral blood flow, glucose, and oxygen metabolism.

Significance of findings

The findings emerging from this work provide several important contributions. First, we provide the first evidence, to our knowledge, that aerobic glycolysis is elevated within two widely distributed cortical networks during eyes-closed rest, the default and cognitive control networks.

The default network is known to be involved in self-referential thought and mind wandering, among other putative roles (Gusnard and Raichle 2001; Raichle, MacLeod et al. 2001; Buckner, Andrews-Hanna et al. 2008). Cerebral blood flow within the default network decreases during performance of goal-directed tasks, suggesting indirectly that this network has a high level of functional activity in the resting state (Shulman, Corbetta et al. 1997). We provide evidence that neuronal activity within this distributed network is

in fact elevated during eyes-closed rest, though we did not investigate the network's behavioral function.

More surprising, though, is the detection of elevated aerobic glycolysis within another distributed cortical network that includes the anterior cingulate, dorsolateral prefrontal cortex, and anterior parietal cortex known as the cognitive control network. This cortical system is associated with transient task-related activity during switching of cognitive sets, for example at the onset and offset of task performance (Braver and Barch 2006; Dosenbach, Fair et al. 2007; Dosenbach, Fair et al. 2008; Fair, Cohen et al. 2008). But this network has not been identified using traditional functional neuroimaging techniques to have high levels of resting functional activity. This may be because task-related functional neuroimaging experiments rely upon comparison between two states, for example an 'active' task state and a 'passive' rest or visual fixation state. Any differences between these two states are assessed (via subtraction) and functions are attributed to regional differences. These data suggest that this network has a high level of resting activity that does not decrease, unlike the default network. This theory is supported by several pieces of evidence. The putative role for this cortical network is to assess changes in brain state (Fox, Snyder et al. 2005). In order to accurately assess block transitions, this region (or some corollary region) needs to continuously observe the external world to compare prior and current behavioral inputs to accurately track transitions, a function that may be associated with error detection signals arising from anterior cingulate (Dosenbach, Fair et al. 2007). In this context, high levels of activity within this network may reflect its continuous activation in eyes-closed rest and other task-related states. This network can be seen as meta-network directing other brain

regions to increase or decrease their activity in response to task set. While direct evidence for this is not at hand, our data provides the first evidence that functional activity may be maintained in these cortical regions at rest. The activity of this network will have to be assessed during various task states for confirmation.

The cortical networks identified with high levels of glycolysis in eyes-closed rest also significantly overlap with brain regions identified by other neuroimaging studies in diseases of consciousness. Experiments performed by Steven Laureys and colleagues assessed subjects with varying degrees of impairment in consciousness, including sleep, coma, locked in syndrome, and persistent vegetative state (Laureys, Perrin et al. 2005; Boly, Phillips et al. 2008; Boly, Phillips et al. 2008). They found consistent decreases in glucose metabolism within a widely distributed network of cortical regions that closely resemble those with elevated glycolysis in the resting state (M. Boly, personal communication). While overlap between these networks does not imply causation, it is intriguing that regions with high glycolysis while at rest would also be impaired in disorders of consciousness. Consciousness transcends moment to moment changes in neuronal activity and likely involves widely distributed cortical and thalamocortical networks (Tononi 2004; Boly, Phillips et al. 2008). Consciousness likely requires ongoing neuronal activity for its maintenance, though there is considerable disagreement about the magnitude of activity and energy metabolism necessary (Tononi 2004; Laureys 2005). Some fraction of the brain's ongoing neuronal activity is likely to be devoted to activities related to consciousness, though. Much research has focused on the role of the default network and activity within this network has been found to correlate to loss of consciousness, though there remains considerable debate about this issue (Boly, Phillips

et al. 2008; Greicius, Kiviniemi et al. 2008). So have we identified a 'network' for consciousness? Maybe. But it is just as likely that some small fraction of the cortical or subcortical regions with elevated glycolysis is responsible for processes associated with consciousness and a majority of the observed network is instead involved in other processes. Future work will have to test this hypothesis by assessing aerobic glycolysis in patients with disorders of consciousness.

The presence of widely distributed networks with elevated glycolysis in itself may not be completely surprising given evidence that the ongoing activity of the brain is responsible for 95% of the brain's energy utilization (Raichle and Mintun 2006). But concurrent evidence from Chapter 4 reveals that these cortical networks not only differ in their response to stimulation, but also differ in their innate neurochemical profile. Regions with elevated glycolysis also have a balanced ratio of excitatory and inhibitory (glutamtergic:GABAergic) postsynaptic receptors. This has several important implications.

Regions with elevated glycolysis can be identified by their neurochemistry without regard to their functional activity. Neurochemistry data was collected from a separate group of subjects postmortem. This suggests that the activities performed by the default and cognitive control networks may lead to long-term changes in cellular neurochemistry. One theory to explain this finding would be that inhibitory and excitatory neurotransmission are in competition with each other. Increased synaptic strength results in an increase in excitatory receptor density, but competing inputs also result in elevated inhibition. There is considerable evidence that most synaptic connections are highly local, with only a small fraction of inputs from distant cortical

regions. In the visual cortex, less than 5% of the inputs to V1 are from the LGN, though these inputs may be highly efficacious and drive cellular activity (Felleman and Van Essen 1991). Visual cortex actually has a low ratio of excitation to inhibition and low levels of aerobic glycolysis, suggesting that local inhibitory circuits predominate. Conversely, medial temporal lobe, including the hippocampus, has a high ratio of excitation to inhibition and low levels of aerobic glycolysis. These regions are highly interconnected with large numbers of glutamatergic cells, consistent with our findings (Wieraszko 1982; Ackermann, Finch et al. 1984; Cervos-Navarro and Diemer 1991; Eid, Williamson et al. 2008).

In Chapter 3 we provide evidence that regional aerobic glycolysis is elevated in the resting state following task completion. We confirm and expand upon the work of Madsen and colleagues who initially observed an increase in global resting aerobic glycolysis following completion of the Wisconsin card sorting task in humans (Madsen, Hasselbalch et al. 1995).

These data suggest that local changes in cellular activity, particularly associated with learning, change resting brain metabolism. We postulate that learning may alter brain metabolism by altering the balance of excitatory to inhibitory receptors in the postsynaptic membrane. While direct evidence for this is lacking in our data, synaptic efficacy is predominantly increased by alteration of the postsynaptic density by increases in receptor density or alteration in the binding potential of neurotransmitters to their respective binding sites. Previous studies have assumed that this functional adaptation (e.g. learning) is achieved via an increase in excitatory receptors without alteration in inhibitory receptor density. An increase in both excitatory and inhibitory receptor density

may increase the specificity of neuronal signaling, providing an alternate approach to induce specific and efficacious synaptic transmission.

Our data provides several other insights about brain function. The resting brain cannot be considered a clean slate upon which researchers simply add an experimental manipulation. The human brain is highly dependent on prior activity and experiences. In this framework, simple exposure to information can alter the brain's response to a future repetition of this information. This is consistent with the known decrease in neuronal activity after repeated practice of simple cognitive and motor tasks (Raichle, Fiez et al. 1994; Petersen, van Mier et al. 1998). Experiences cause identifiable metabolic (and presumably neurochemical if seen in context of data from Chapter 4) changes in cortical regions that are only transiently activated. This finding raises several intriguing questions.

First, what is the cellular mechanism responsible for these changes? Increased aerobic glycolysis may reflect increased spontaneous glutamate flux, closely associated with astrocytic Na^+/K^+ ATPase in cellular models (Pellerin and Magistretti 1994; Pellerin and Magistretti 1996). Residual increases in glycolysis may reflect increased utilization of glucose for anabolic processes (Gaitonde, Jones et al. 1987). Unfortunately, we are unable to detect the fraction of glucose that enters the pentose phosphate shunt or directly image glutamate flux in vivo at this time.

Second, what is the timeframe of these changes? We only measured a single time point following task completion (spanning 2.5 hours of eyes-closed rest). There has to be some mechanism whereby this elevation in synaptic strength and energy metabolism is remediated. This may occur via slow wave sleep as suggested by the synaptic

homeostasis hypothesis or fade over time regardless of sleep (Tononi and Cirelli 2003). Sleep appears to be a convenient time for synaptic downregulation given the decrease in transcription of proteins involved in energy metabolism and excitatory neurotransmission in this state (Cirelli and Tononi 2000; Tononi and Cirelli 2001). At this time we cannot differentiate between these two possible outcomes.

Third, to what extent can these changes in metabolism accurately reflect prior activity patterns? With a relatively simple motor learning paradigm, we detect increased aerobic glycolysis hours following task completion. Could a similar approach be taken to determine if a subject has been performing another difficult activity whose transient functional activity pattern is known? If this approach could be expanded to other tasks and behaviors, this method could provide a putative 'mind-reader' or 'lie-detector' type role. It appears unlikely that this approach (at least with PET) would have the spatial and temporal resolution to accurately reflect prior activity patterns, though that remains to be investigated experimentally.

Future experiments

These data provide several new avenues for future research. First, future studies will have to evaluate the fate of glucose beyond the production of ATP. An energy-centric view of glucose utilization is unable to account for regional elevations of aerobic glycolysis and its residual increases following learning. We postulate that protein synthesis and DNA replication may be increased regionally following learning, reflecting the fate of increased aerobic glycolysis. New techniques will have to be developed to

assess cellular processes such as the pentose phosphate shunt in vivo. We are severely limited in our ability to define cellular processes at the human cortical level beyond simple measures of energy metabolism and a few select neurotransmitters (GABA and dopamine predominantly) at this time. Development of new radioligands and replication in animal models of such experiments will be necessary to determine the cellular processes implicated in aerobic glycolysis.

To follow up on the learning related changes in glycolysis found in this thesis, a series of experiments will have to be performed to assess the role of sleep in synaptic homeostasis. First, in order to confirm that the decreases in blood flow and glucose utilization that have been reported following sleep (Boyle, Scott et al. 1994; Braun, Balkin et al. 1997) are actually due to changes in aerobic glycolysis and not oxidative phosphorylation, aerobic glycolysis will have be assessed both before and immediately after sleep in a single group of subjects. Though such experiments are logistically difficult, they can and should be performed to determine the role of sleep in resetting cerebral metabolism. These experiments can provide important insights into the beneficial effect of sleep on various behaviors and provide a new avenue to assess sleep disorders and memory.

In addition, a series of experiments should be performed to assess the longitudinal progression of the observed increases in aerobic glycolysis following learning. It appears unlikely that increases in aerobic glycolysis could be maintained for long periods of time simply because that would be energetically inefficient. These changes may slowly decay or an active process such as slow wave sleep may mediate their subsequent decrease. A control condition comparing learning before and after sleep with slow wave sleep

deprivation would further provide insight into the distinct sleep processes necessary for maintenance of synaptic homeostasis.

Implications for disease pathophysiology

We report an elevation in aerobic glycolysis in widely distributed cortical networks during eyes-closed rest. Surprisingly, these networks have also been implicated as regions of high amyloid deposition in Alzheimer's disease (Buckner, Snyder et al. 2005). Though initial studies focused upon the default network, binding of the amyloid-specific PET ligand Pittsburgh Compound B (PIB) is better correlated to the network identified in Chapter 2 (Vlassenko et al., unpublished observation). There are several possible implications. First, aerobic glycolysis may predispose cortical regions for development of amyloid plaques, though an exact mechanism is unknown. Since Alzheimer's is a neurodegenerative disease that strikes late in life, a lifetime of aerobic glycolysis could result in local changes in cellular physiology that predispose for amyloid deposition. One intriguing possibility is that glutamate flux itself may be involved with amyloid deposition. Recent studies have found that amyloid deposition is accelerated following posttranslational modification with pyroglutamate, a cyclized form of glutamate (Schilling, Zeitschel et al. 2008). Since aerobic glycolysis is associated with glutamate flux, it is possible that a lifetime of glutamate flux within the default and cognitive control system (or the repeated activation and deactivation of these networks) may predispose the cellular cyclization of glutamate via glutaminyl cyclase. Future studies will have to investigate the cellular linkages between aerobic glycolysis and

amyloid deposition. Other possible mechanisms linking these two phenomenons include membrane turnover processes, already implicated in amyloid deposition in animal models and recently in humans (Brody, Magnoni et al. 2008; Cirrito, Kang et al. 2008). Since the default and cognitive control networks are sites of high levels of synaptic plasticity, amyloid may accumulate in these regions as a byproduct of neuronal signaling (Cirrito, Kang et al. 2008). Given the spatial correlation between the regional distribution of amyloid deposition and aerobic glycolysis, this research may open a new avenue of research to understand the pathophysiology of Alzheimer's disease.

Conclusion

Aerobic glycolysis is a functionally relevant marker of neuronal activity that is modulated by prior transient task performance and reflects unique cellular neurochemistry. The research presented here provides some insight into the functional role of aerobic glycolysis in the resting human brain.

Bibliography

Ackermann, R. F., D. M. Finch, et al. (1984). "Increased glucose metabolism during long-duration recurrent inhibition of hippocampal pyramidal cells." J Neurosci **4**(1): 251-64.

Altman, D. I., J. M. Perlman, et al. (1993). "Cerebral oxygen metabolism in newborns." Pediatrics **92**(1): 99-104.

Ames, A., 3rd (2000). "CNS energy metabolism as related to function." Brain Res Brain Res Rev **34**(1-2): 42-68.

Andersen, S. L. (2003). "Trajectories of brain development: point of vulnerability or window of opportunity?" Neurosci Biobehav Rev **27**(1-2): 3-18.

Attwell, D. and C. Iadecola (2002). "The neural basis of functional brain imaging signals." Trends in Neuroscience **25**: 621-625.

Attwell, D. and S. B. Laughlin (2001). "An energy budget for signaling in the grey matter of the brain." J Cereb Blood Flow Metab **21**(10): 1133-45.

Baron, J. C., D. Rougemont, et al. (1984). "Local interrelationships of cerebral oxygen consumption and glucose utilization in normal subjects and in ischemic stroke patients: a positron tomography study." J Cereb Blood Flow Metab **4**(2): 140-9.

Bashir, Z. I., S. Alford, et al. (1991). "Long-term potentiation of NMDA receptor-mediated synaptic transmission in the hippocampus." Nature **349**(6305): 156-8.

Bergersen, L. H., P. J. Magistretti, et al. (2005). "Selective postsynaptic co-localization of MCT2 with AMPA receptor GluR2/3 subunits at excitatory synapses exhibiting AMPA receptor trafficking." Cereb Cortex **15**(4): 361-70.

Blomqvist, G., R. J. Seitz, et al. (1994). "Regional cerebral oxidative and total glucose consumption during rest and activation studied with positron emission tomography." Acta Physiol Scand **151**(1): 29-43.

Boly, M., C. Phillips, et al. (2008). "Consciousness and cerebral baseline activity fluctuations." Hum Brain Mapp **29**(7): 868-74.

Boly, M., C. Phillips, et al. (2008). "Intrinsic brain activity in altered states of consciousness: how conscious is the default mode of brain function?" Ann N Y Acad Sci **1129**: 119-29.

Borghammer, P., K. Y. Jonsdottir, et al. (2008). "Normalization in PET group comparison studies--the importance of a valid reference region." Neuroimage **40**(2): 529-40.

Boyle, P. J., J. C. Scott, et al. (1994). "Diminished brain glucose metabolism is a significant determinant for falling rates of systemic glucose utilization during sleep in normal humans." J Clin Invest **93**(2): 529-35.

Braun, A. R., T. J. Balkin, et al. (1997). "Regional cerebral blood flow throughout the sleep-wake cycle. An H2(15)O PET study." Brain **120 (Pt 7)**: 1173-97.

Braver, T. S. and D. M. Barch (2006). "Extracting core components of cognitive control." Trends Cogn Sci **10**(12): 529-32.

Brody, D. L., S. Magnoni, et al. (2008). "Amyloid-beta dynamics correlate with neurological status in the injured human brain." Science **321**(5893): 1221-4.

Brown, A. M. (2004). "Brain glycogen re-awakened." J Neurochem **89**(3): 537-52.

Buchs, P. A. and D. Muller (1996). "Induction of long-term potentiation is associated with major ultrastructural changes of activated synapses." Proc Natl Acad Sci U S A **93**(15): 8040-5.

Buckner, R. L., J. R. Andrews-Hanna, et al. (2008). "The Brain's Default Network: Anatomy, Function, and Relevance to Disease." Ann N Y Acad Sci **1124**: 1-38.

Buckner, R. L., A. Z. Snyder, et al. (2005). "Molecular, structural, and functional characterization of Alzheimer's disease: evidence for a relationship between default activity, amyloid, and memory." J Neurosci **25**(34): 7709-17.

Buysse, D. J., E. A. Nofzinger, et al. (2004). "Regional brain glucose metabolism during morning and evening wakefulness in humans: preliminary findings." Sleep **27**(7): 1245-54.

Buzsaki, G., K. Kaila, et al. (2007). "Inhibition and brain work." Neuron **56**(5): 771-83.

Cerdan, S., T. B. Rodrigues, et al. (2006). "The redox switch/redox coupling hypothesis." Neurochem Int **48**(6-7): 523-30.

Cervos-Navarro, J. and N. H. Diemer (1991). "Selective vulnerability in brain hypoxia." Crit Rev Neurobiol **6**(3): 149-82.

Chatton, J. Y., L. Pellerin, et al. (2003). "GABA uptake into astrocytes is not associated with significant metabolic cost: implications for brain imaging of inhibitory transmission." Proc Natl Acad Sci U S A **100**(21): 12456-61.

Chen, C. and S. Tonegawa (1997). "Molecular genetic analysis of synaptic plasticity, activity-dependent neural development, learning, and memory in the mammalian brain." Annu Rev Neurosci **20**: 157-84.

Chugani, H. T., M. E. Phelps, et al. (1987). "Positron emission tomography study of human brain functional development." <u>Ann Neurol</u> **22**(4): 487-97.

Cirelli, C. and G. Tononi (2000). "Gene expression in the brain across the sleep-waking cycle." <u>Brain Res</u> **885**(2): 303-21.

Cirrito, J. R., J. E. Kang, et al. (2008). "Endocytosis is required for synaptic activity-dependent release of amyloid-beta in vivo." <u>Neuron</u> **58**(1): 42-51.

Damoiseaux, J. S., S. A. Rombouts, et al. (2006). "Consistent resting-state networks across healthy subjects." <u>Proc Natl Acad Sci U S A</u> **103**(37): 13848-53.

DeBerardinis, R. J., A. Mancuso, et al. (2007). "Beyond aerobic glycolysis: transformed cells can engage in glutamine metabolism that exceeds the requirement for protein and nucleotide synthesis." <u>Proc Natl Acad Sci U S A</u> **104**(49): 19345-50.

Della-Maggiore, V. and A. R. McIntosh (2005). "Time course of changes in brain activity and functional connectivity associated with long-term adaptation to a rotational transformation." <u>J Neurophysiol</u> **93**(4): 2254-62.

di Pellegrino, G. and S. P. Wise (1993). "Visuospatial versus visuomotor activity in the premotor and prefrontal cortex of a primate." <u>J Neurosci</u> **13**(3): 1227-43.

Donoghue, J. P., J. N. Sanes, et al. (1998). "Neural discharge and local field potential oscillations in primate motor cortex during voluntary movements." <u>J Neurophysiol</u> **79**(1): 159-73.

Dosenbach, N. U., D. A. Fair, et al. (2008). "A dual-networks architecture of top-down control." <u>Trends Cogn Sci</u> **12**(3): 99-105.

Dosenbach, N. U., D. A. Fair, et al. (2007). "Distinct brain networks for adaptive and stable task control in humans." <u>Proc Natl Acad Sci U S A</u> **104**(26): 11073-8.

Dusick, J. R., T. C. Glenn, et al. (2007). "Increased pentose phosphate pathway flux after clinical traumatic brain injury: a [1,2-13C2]glucose labeling study in humans." J Cereb Blood Flow Metab **27**(9): 1593-602.

Eickhoff, S. B., A. Schleicher, et al. (2007). "Analysis of neurotransmitter receptor distribution patterns in the cerebral cortex." Neuroimage **34**(4): 1317-30.

Eid, T., A. Williamson, et al. (2008). "Glutamate and astrocytes--key players in human mesial temporal lobe epilepsy?" Epilepsia **49 Suppl 2**: 42-52.

Fair, D. A., A. L. Cohen, et al. (2008). "The maturing architecture of the brain's default network." Proc Natl Acad Sci U S A **105**(10): 4028-32.

Felleman, D. J. and D. C. Van Essen (1991). "Distributed hierarchical processing in the primate cerebral cortex." Cereb Cortex **1**(1): 1-47.

Forman, S. D., J. D. Cohen, et al. (1995). "Improved assessment of significant activation in functional magnetic resonance imaging (fMRI): use of a cluster-size threshold." Magn Reson Med **33**(5): 636-47.

Fox, M. D. and M. E. Raichle (2007). "Spontaneous fluctuations in brain activity observed with functional magnetic resonance imaging." Nat Rev Neurosci **8**(9): 700-11.

Fox, M. D., A. Z. Snyder, et al. (2005). "Transient BOLD responses at block transitions." Neuroimage **28**(4): 956-66.

Fox, M. D., A. Z. Snyder, et al. (2005). "The human brain is intrinsically organized into dynamic, anticorrelated functional networks." Proc Natl Acad Sci U S A **102**(27): 9673-8.

Fox, P. T. and M. E. Raichle (1986). "Focal physiological uncoupling of cerebral blood flow and oxidative metabolism during somatosensory stimulation in human subjects." Proc Natl Acad Sci U S A **83**(4): 1140-4.

Fox, P. T., M. E. Raichle, et al. (1988). "Nonoxidative glucose consumption during focal physiologic neural activity." Science **241**(4864): 462-4.

Frick, A., J. Magee, et al. (2004). "LTP is accompanied by an enhanced local excitability of pyramidal neuron dendrites." Nat Neurosci **7**(2): 126-35.

Frick, A., J. Magee, et al. (2004). "LTP is accompanied by an enhanced local excitability of pyramidal neuron dendrites." Nature Neuroscience **7**: 126-135.

Gabbott, P. L. and P. Somogyi (1986). "Quantitative distribution of GABA-immunoreactive neurons in the visual cortex (area 17) of the cat." Exp Brain Res **61**(2): 323-31.

Gage, F. H., G. Kempermann, et al. (1998). "Multipotent progenitor cells in the adult dentate gyrus." J Neurobiol **36**(2): 249-66.

Gais, S., G. Albouy, et al. (2007). "Sleep transforms the cerebral trace of declarative memories." Proc Natl Acad Sci U S A **104**(47): 18778-83.

Gaitonde, M. K., J. Jones, et al. (1987). "Metabolism of glucose into glutamate via the hexose monophosphate shunt and its inhibition by 6-aminonicotinamide in rat brain in vivo." Proc R Soc Lond B Biol Sci **231**(1262): 71-90.

Ghandour, M. S., G. Vincendon, et al. (1980). "Astrocyte and oligodendrocyte distribution in adult rat cerebellum: an immunohistological study." J Neurocytol **9**(5): 637-46.

Ghilardi, M., C. Ghez, et al. (2000). "Patterns of regional brain activation associated with different forms of motor learning." Brain Res **871**(1): 127-45.

Ghilardi, M. F., D. Eidelberg, et al. (2003). "The differential effect of PD and normal aging on early explicit sequence learning." Neurology **60**(8): 1313-9.

Gjedde, A. and S. Marrett (2001). "Glycolysis in neurons, not astrocytes, delays oxidative metabolism of human visual cortex during sustained checkerboard stimulation in vivo." J Cereb Blood Flow Metab **21**(12): 1384-92.

Greicius, M. D., V. Kiviniemi, et al. (2008). "Persistent default-mode network connectivity during light sedation." Hum Brain Mapp.

Greicius, M. D., K. Supekar, et al. (2008). "Resting-State Functional Connectivity Reflects Structural Connectivity in the Default Mode Network." Cereb Cortex.

Gruol, D. L. and C. L. Franklin (1987). "Morphological and physiological differentiation of Purkinje neurons in cultures of rat cerebellum." J Neurosci **7**(5): 1271-93.

Gusnard, D. A. and M. E. Raichle (2001). "Searching for a baseline: functional imaging and the resting human brain." Nat Rev Neurosci **2**(10): 685-94.

Halsband, U. and R. K. Lange (2006). "Motor learning in man: a review of functional and clinical studies." J Physiol Paris **99**(4-6): 414-24.

Hatazawa, J., M. Ito, et al. (1988). "Measurement of the ratio of cerebral oxygen consumption to glucose utilization by positron emission tomography: its consistency with the values determined by the Kety-Schmidt method in normal volunteers." J Cereb Blood Flow Metab **8**(3): 426-32.

He, B. J., A. Z. Snyder, et al. (2007). "Breakdown of functional connectivity in frontoparietal networks underlies behavioral deficits in spatial neglect." Neuron **53**(6): 905-18.

Honda, M., M. P. Deiber, et al. (1998). "Dynamic cortical involvement in implicit and explicit motor sequence learning. A PET study." Brain **121 (Pt 11)**: 2159-73.

Huang, Z. J., G. Di Cristo, et al. (2007). "Development of GABA innervation in the cerebral and cerebellar cortices." Nat Rev Neurosci **8**(9): 673-86.

Huber, R., M. F. Ghilardi, et al. (2004). "Local sleep and learning." Nature **430**(6995): 78-81.

Jacob, T. C., S. J. Moss, et al. (2008). "GABA(A) receptor trafficking and its role in the dynamic modulation of neuronal inhibition." Nat Rev Neurosci **9**(5): 331-43.

Jha, S. K., B. E. Jones, et al. (2005). "Sleep-dependent plasticity requires cortical activity." J Neurosci **25**(40): 9266-74.

Johnston, J. M., S. N. Vaishnavi, et al. (2008). "Loss of resting interhemispheric functional connectivity after complete section of the corpus callosum." J Neurosci **28**(25): 6453-8.

Jueptner, M. and C. Weiller (1995). "Review: does measurement of regional cerebral blood flow reflect synaptic activity? Implications for PET and fMRI." Neuroimage **2**(2): 148-56.

Kahane, P., I. Merlet, et al. (1999). "An H(2) (15)O-PET study of cerebral blood flow changes during focal epileptic discharges induced by intracerebral electrical stimulation." Brain **122 (Pt 10)**: 1851-65.

Kali, S. and P. Dayan (2004). "Off-line replay maintains declarative memories in a model of hippocampal-neocortical interactions." Nat Neurosci **7**(3): 286-94.

Kasischke, K. A., H. D. Vishwasrao, et al. (2004). "Neural activity triggers neuronal oxidative metabolism followed by astrocytic glycolysis." Science **305**(5680): 99-103.

Kennedy, M. B. (2000). "Signal-processing machines at the postsynaptic density." Science **290**(5492): 750-4.

Kennedy, M. J. and M. D. Ehlers (2006). "Organelles and trafficking machinery for postsynaptic plasticity." Annu Rev Neurosci **29**: 325-62.

Koehler-Stec, E. M., K. Li, et al. (2000). "Cerebral glucose utilization and glucose transporter expression: response to water deprivation and restoration." J Cereb Blood Flow Metab **20**(1): 192-200.

Krakauer, J. W., Z. M. Pine, et al. (2000). "Learning of visuomotor transformations for vectorial planning of reaching trajectories." J Neurosci **20**(23): 8916-24.

Kudrimoti, H. S., C. A. Barnes, et al. (1999). "Reactivation of hippocampal cell assemblies: effects of behavioral state, experience, and EEG dynamics." J Neurosci **19**(10): 4090-101.

Lancaster, J. L., T. G. Glass, et al. (1995). "A modality-independent approach to spatial normalization of tomographic images of the human brain." Hum Brain Mapp **3**: 209-223.

Larrabee, M. G. (1989). "The pentose cycle (hexose monophosphate shunt). Rigorous evaluation of limits to the flux from glucose using 14CO2 data, with applications to peripheral ganglia of chicken embryos." J Biol Chem **264**(27): 15875-9.

Larsen, C. C., K. Bonde Larsen, et al. (2006). "Total number of cells in the human newborn telencephalic wall." Neuroscience **139**(3): 999-1003.

Laureys, S. (2005). "The neural correlate of (un)awareness: lessons from the vegetative state." Trends Cogn Sci **9**(12): 556-9.

Laureys, S., F. Perrin, et al. (2005). "Residual cognitive function in comatose, vegetative and minimally conscious states." Curr Opin Neurol **18**(6): 726-33.

Lauritzen, M. (2001). "Relationship of spikes, synaptic activity and local changes of cerebral blood flow." Journal of Cerebral Blood Flow and Metabolism **21**: 1367-1383.

Lauritzen, M. and L. Gold (2003). "Brain function and neurophysiological correlates of signals used in functional neuroimaging." Journal of Neuroscience **23**: 3972-3980.

Lebrun-Grandie, P., J. C. Baron, et al. (1983). "Coupling between regional blood flow and oxygen utilization in the normal human brain. A study with positron tomography and oxygen 15." Arch Neurol **40**(4): 230-6.

Lewis, D. A. (1997). "Development of the prefrontal cortex during adolescence: insights into vulnerable neural circuits in schizophrenia." Neuropsychopharmacology **16**(6): 385-98.

Li, Y., P. Nowotny, et al. (2004). "Association of late-onset Alzheimer's disease with genetic variation in multiple members of the GAPD gene family." Proc Natl Acad Sci U S A **101**(44): 15688-93.

Logothetis, N. K. (2003). "The underpinnings of the BOLD functional magnetic resonance imaging signal." J Neurosci **23**(10): 3963-71.

Logothetis, N. K., J. Pauls, et al. (2001). "Neurophysiological investigation of the basis of the fMRI signal." <u>Nature</u> **412**(6843): 150-7.

Louie, K. and M. A. Wilson (2001). "Temporally structured replay of awake hippocampal ensemble activity during rapid eye movement sleep." <u>Neuron</u> **29**(1): 145-56.

Lynch, M. A. (2004). "Long-term potentiation and memory." <u>Physiological Reviews</u> **84**: 87-136.

Madsen, P. L., S. G. Hasselbalch, et al. (1995). "Persistent resetting of the cerebral oxygen/glucose uptake ratio by brain activation: evidence obtained with the Kety-Schmidt technique." <u>J Cereb Blood Flow Metab</u> **15**(3): 485-91.

Magistretti, P. J. and J. Y. Chatton (2005). "Relationship between L-glutamate-regulated intracellular Na+ dynamics and ATP hydrolysis in astrocytes." <u>J Neural Transm</u> **112**(1): 77-85.

Magistretti, P. J. and L. Pellerin (1999). "Cellular mechanisms of brain energy metabolism and their relevance to functional brain imaging." <u>Philos Trans R Soc Lond B Biol Sci</u> **354**(1387): 1155-63.

Mao, B. Q., F. Hamzei-Sichani, et al. (2001). "Dynamics of spontaneous activity in neocortical slices." <u>Neuron</u> **32**(5): 883-98.

Marder, E. and J. M. Goaillard (2006). "Variability, compensation and homeostasis in neuron and network function." <u>Nat Rev Neurosci</u> **7**(7): 563-74.

Marshall, L., H. Helgadottir, et al. (2006). "Boosting slow oscillations during sleep potentiates memory." <u>Nature</u> **444**(7119): 610-3.

Martin, S. J., P. D. Grimwood, et al. (2000). "Synaptic plasticity and memory: an evaluation of the hypothesis." <u>Annu Rev Neurosci</u> **23**: 649-711.

Martin, S. J., P. D. Grimwood, et al. (2000). "Synaptic plasticity and memory: an evaluation of the hypothesis." <u>Annual Review of Neuroscience</u> **23**: 649-711.

Martin, W. R., W. J. Powers, et al. (1987). "Cerebral blood volume measured with inhaled C15O and positron emission tomography." <u>Journal of Cerebral Blood Flow & Metabolism</u> **7**(4): 421-6.

Mathern, G. W., J. K. Pretorius, et al. (1997). "Human hippocampal AMPA and NMDA mRNA levels in temporal lobe epilepsy patients." <u>Brain</u> **120 (Pt 11)**: 1937-59.

McAvoy, M. P., J. M. Ollinger, et al. (2001). "Cluster size thresholds for assessment of significant activation in fMRI." <u>Neuroimage</u> **13**: S198.

Mintun, M., A. G. Vlassenko, et al. (2002). "Time-related increase of oxygen utilization in continuously activated human visual cortex." <u>Neuroimage</u> **16**: 531-537.

Mintun, M. A., P. T. Fox, et al. (1989). "A highly accurate method of localizing regions of neuronal activation in the human brain with positron emission tomography." <u>J Cereb Blood Flow Metab</u> **9**(1): 96-103.

Mintun, M. A., M. E. Raichle, et al. (1984). "Brain oxygen utilization measured with O-15 radiotracers and positron emission tomography." <u>J Nucl Med</u> **25**(2): 177-87.

Mintun, M. A., A. G. Vlassenko, et al. (2004). "Increased lactate/pyruvate ratio augments blood flow in physiologically activated human brain." <u>Proc Natl Acad Sci U S A</u> **101**(2): 659-64.

Mitz, A. R., M. Godschalk, et al. (1991). "Learning-dependent neuronal activity in the premotor cortex: activity during the acquisition of conditional motor associations." J Neurosci **11**(6): 1855-72.

Munchau, A., B. R. Bloem, et al. (2002). "Functional connectivity of human premotor and motor cortex explored with repetitive transcranial magnetic stimulation." J Neurosci **22**(2): 554-61.

Orban, P., G. Rauchs, et al. (2006). "Sleep after spatial learning promotes covert reorganization of brain activity." Proc Natl Acad Sci U S A **103**(18): 7124-9.

Palmer, A. M. (1999). "The activity of the pentose phosphate pathway is increased in response to oxidative stress in Alzheimer's disease." J Neural Transm **106**(3-4): 317-28.

Patel, A. B., R. A. de Graaf, et al. (2005). "The contribution of GABA to glutamate/glutamine cycling and energy metabolism in the rat cortex in vivo." Proc Natl Acad Sci U S A **102**(15): 5588-93.

Peigneux, P., S. Laureys, et al. (2004). "Are spatial memories strengthened in the human hippocampus during slow wave sleep?" Neuron **44**(3): 535-45.

Pellerin, L. and P. J. Magistretti (1994). "Glutamate uptake into astrocytes stimulates aerobic glycolysis: a mechanism coupling neuronal activity to glucose utilization." Proc Natl Acad Sci U S A **91**(22): 10625-9.

Pellerin, L. and P. J. Magistretti (1996). "Excitatory amino acids stimulate aerobic glycolysis in astrocytes via an activation of the Na+/K+ ATPase." Dev Neurosci **18**(5-6): 336-42.

Pelvig, D. P., H. Pakkenberg, et al. (2007). "Neocortical glial cell numbers in human brains." <u>Neurobiol Aging</u>.

Petersen, S. E., H. van Mier, et al. (1998). "The effects of practice on the functional anatomy of task performance." <u>Proc Natl Acad Sci U S A</u> **95**(3): 853-60.

Petzold, G. C., D. F. Albeanu, et al. (2008). "Coupling of neural activity to blood flow in olfactory glomeruli is mediated by astrocytic pathways." <u>Neuron</u> **58**(6): 897-910.

Phelps, M. E., S. C. Huang, et al. (1979). "Tomographic measurement of local cerebral glucose metabolic rate in humans with (F-18)2-fluoro-2-deoxy-D-glucose: validation of method." <u>Ann Neurol</u> **6**(5): 371-88.

Powers, W. J., J. L. Rosenbaum, et al. (1998). "Cerebral glucose transport and metabolism in preterm human infants." <u>J Cereb Blood Flow Metab</u> **18**(6): 632-8.

Powers, W. J., T. O. Videen, et al. (2007). "Selective defect of in vivo glycolysis in early Huntington's disease striatum." <u>Proc Natl Acad Sci U S A</u> **104**(8): 2945-9.

Raichle, M. E. (2006). "Neuroscience. The brain's dark energy." <u>Science</u> **314**(5803): 1249-50.

Raichle, M. E., J. A. Fiez, et al. (1994). "Practice-related changes in human brain functional anatomy during nonmotor learning." <u>Cereb Cortex</u> **4**(1): 8-26.

Raichle, M. E., A. M. MacLeod, et al. (2001). "A default mode of brain function." <u>Proc Natl Acad Sci U S A</u> **98**(2): 676-82.

Raichle, M. E., W. R. Martin, et al. (1983). "Brain blood flow measured with intravenous H2(15)O. II. Implementation and validation." <u>J Nucl Med</u> **24**(9): 790-8.

Raichle, M. E. and M. A. Mintun (2006). "Brain work and brain imaging." <u>Annu Rev Neurosci</u> **29**: 449-76.

Raichle, M. E., J. B. Posner, et al. (1970). "Cerebral blood flow during and after hyperventilation." <u>Arch Neurol</u> **23**(5): 394-403.

Renger, J. J., C. Egles, et al. (2001). "A developmental switch in neurotransmitter flux enhances synaptic efficacy by affecting AMPA receptor activation." <u>Neuron</u> **29**(2): 469-84.

Ribeiro, S., D. Gervasoni, et al. (2004). "Long-lasting novelty-induced neuronal reverberation during slow-wave sleep in multiple forebrain areas." <u>PLoS Biol</u> **2**(1): E24.

Richter-Levin, G., L. Canevari, et al. (1995). "Long-term potentiation and glutamate release in the dentate gyrus: links to spatial learning." <u>Behav Brain Res</u> **66**(1-2): 37-40.

Ruff, C. C., S. Bestmann, et al. (2008). "Distinct causal influences of parietal versus frontal areas on human visual cortex: evidence from concurrent TMS-fMRI." <u>Cereb Cortex</u> **18**(4): 817-27.

Ruff, C. C., F. Blankenburg, et al. (2008). "Hemispheric Differences in Frontal and Parietal Influences on the Human Occipital Cortex: Direct Confirmation with Concurrent TMS-fMRI." <u>J Cogn Neurosci</u>.

Schilling, S., U. Zeitschel, et al. (2008). "Glutaminyl cyclase inhibition attenuates pyroglutamate Abeta and Alzheimer's disease-like pathology." <u>Nat Med</u> **14**(10): 1106-11.

Schwartz, W. J., C. B. Smith, et al. (1979). "Metabolic mapping of functional activity in the hypothalamo-neurohypophysial system of the rat." <u>Science</u> **205**(4407): 723-5.

Settergren, G., B. S. Lindblad, et al. (1976). "Cerebral blood flow and exchange of oxygen, glucose, ketone bodies, lactate, pyruvate and amino acids in infants." Acta Paediatr Scand **65**(3): 343-53.

Shamoto, H. and H. T. Chugani (1997). "Glucose metabolism in the human cerebellum: an analysis of crossed cerebellar diaschisis in children with unilateral cerebral injury." J Child Neurol **12**(7): 407-14.

Shaw, C., L. Cameron, et al. (1991). "Pre- and postnatal development of GABA receptors in Macaca monkey visual cortex." J Neurosci **11**(12): 3943-59.

Sheng, M. and C. C. Hoogenraad (2007). "The postsynaptic architecture of excitatory synapses: a more quantitative view." Annu Rev Biochem **76**: 823-47.

Shulman, G. L., M. Corbetta, et al. (1997). "Top-down modulation of early sensory cortex." Cereb Cortex **7**(3): 193-206.

Shulman, R. G., D. L. Rothman, et al. (2004). "Energetic basis of brain activity: implications for neuroimaging." Trends Neurosci **27**(8): 489-95.

Sibson, N. R., A. Dhankhar, et al. (1997). "In vivo 13C NMR measurements of cerebral glutamine synthesis as evidence for glutamate-glutamine cycling." Proc Natl Acad Sci U S A **94**(6): 2699-704.

Sibson, N. R., A. Dhankhar, et al. (1998). "Stoichiometric coupling of brain glucose metabolism and glutamatergic neuronal activity." Proc Natl Acad Sci U S A **95**(1): 316-21.

Siesjo, B. K. (1978). Brain Energy Metabolism. New York, John Wiley & Sons.

Siesjo, B. K. and F. Plum (1971). "Cerebral energy metabolism in normoxia and in hypoxia." Acta Anaesthesiol Scand Suppl **45**: 81-101.

Simpson, J. R., Jr., A. Z. Snyder, et al. (2001). "Emotion-induced changes in human medial prefrontal cortex: I. During cognitive task performance." Proc Natl Acad Sci U S A **98**(2): 683-7.

Skaggs, W. E. and B. L. McNaughton (1996). "Replay of neuronal firing sequences in rat hippocampus during sleep following spatial experience." Science **271**(5257): 1870-3.

Sokoloff, L. (1977). "Relation between physiological function and energy metabolism in the central nervous system." J Neurochem **29**(1): 13-26.

Sun, F. T., L. M. Miller, et al. (2007). "Functional connectivity of cortical networks involved in bimanual motor sequence learning." Cereb Cortex **17**(5): 1227-34.

Tononi, G. (2004). "An information integration theory of consciousness." BMC Neurosci **5**(1): 42.

Tononi, G. and C. Cirelli (2001). "Modulation of brain gene expression during sleep and wakefulness: a review of recent findings." Neuropsychopharmacology **25**(5 Suppl): S28-35.

Tononi, G. and C. Cirelli (2003). "Sleep and synaptic homeostasis: a hypothesis." Brain Res Bull **62**(2): 143-50.

Tononi, G. and C. Cirelli (2006). "Sleep function and synaptic homeostasis." Sleep Med Rev **10**(1): 49-62.

Ungerleider, L. G., J. Doyon, et al. (2002). "Imaging brain plasticity during motor skill learning." Neurobiol Learn Mem **78**(3): 553-64.

Van Essen, D. C. (2005). "A Population-Average, Landmark- and Surface-based (PALS) atlas of human cerebral cortex." Neuroimage **28**(3): 635-62.

van Mier, H., L. W. Tempel, et al. (1998). "Changes in brain activity during motor learning measured with PET: effects of hand of performance and practice." J Neurophysiol **80**(4): 2177-99.

Vincent, J. L., I. Kahn, et al. (2008). "Evidence for a Frontoparietal Control System Revealed by Intrinsic Functional Connectivity." J Neurophysiol.

Vincent, J. L., A. Z. Snyder, et al. (2006). "Coherent spontaneous activity identifies a hippocampal-parietal memory network." J Neurophysiol **96**(6): 3517-31.

Vlassenko, A. G., M. M. Rundle, et al. (2006). "Human brain glucose metabolism may evolve during activation: findings from a modified FDG PET paradigm." Neuroimage **33**(4): 1036-41.

Vlassenko, A. G., M. M. Rundle, et al. (2006). "Regulation of blood flow in activated human brain by cytosolic NADH/NAD+ ratio." Proc Natl Acad Sci U S A **103**(6): 1964-9.

Voutsinos-Porche, B., G. Bonvento, et al. (2003). "Glial glutamate transporters mediate a functional metabolic crosstalk between neurons and astrocytes in the mouse developing cortex." Neuron **37**(2): 275-86.

Vyazovskiy, V. V., C. Cirelli, et al. (2008). "Molecular and electrophysiological evidence for net synaptic potentiation in wake and depression in sleep." Nat Neurosci **11**(2): 200-8.

Vyazovskiy, V. V., C. Cirelli, et al. (2008). "Cortical metabolic rates as measured by 2-deoxyglucose-uptake are increased after waking and decreased after sleep in mice." Brain Res Bull **75**(5): 591-7.

Wieraszko, A. (1982). "Changes in the hippocampal slices energy metabolism following stimulation and long-term potentiation of Schaffer collaterals-pyramidal cell synapses tested with the 2-deoxyglucose technique." Brain Res **237**(2): 449-57.

Wu, K., C. Aoki, et al. (1997). "The synthesis of ATP by glycolytic enzymes in the postsynaptic density and the effect of endogenously generated nitric oxide." Proc Natl Acad Sci U S A **94**(24): 13273-8.

Yoo, S. S., P. T. Hu, et al. (2007). "A deficit in the ability to form new human memories without sleep." Nat Neurosci **10**(3): 385-92.

Zach, N., N. Kanarek, et al. (2005). "Segregation between acquisition and long-term memory in sensorimotor learning." Eur J Neurosci **22**(9): 2357-62.